International Journal of Heat and Mass Transfer 128 (2019) 892–933

Contents lists available at ScienceDirect

International Journal of Heat and Mass Transfer

journal homepage: www.elsevier.com/locate/ijhmt

Review

Review of pool boiling enhancement by surface modification

Gangtao Liang [a,b], Issam Mudawar [b,*]

[a] Key Laboratory of Ocean Energy Utilization and Energy Conservation of Ministry of Education, School of Energy and Power Engineering, Dalian University of Technology, Dalian 116024, China
[b] Purdue University Boiling and Two-Phase Flow Laboratory (PU-BTPFL), School of Mechanical Engineering, 585 Purdue Mall, West Lafayette, IN 47907, USA

ARTICLE INFO

Article history:
Received 18 June 2018
Received in revised form 3 September 2018
Accepted 6 September 2018
Available online 21 September 2018

Keywords:
Pool boiling
Enhancement
Surface modification
Heat transfer coefficient
Critical heat flux (CHF)

ABSTRACT

This paper provides a comprehensive review of published articles addressing passive enhancement of pool boiling using surface modification techniques. They include macroscale, microscale, and nanoscale surfaces, as well as multiscale (hybrid-scale), and hybrid-wettability techniques. Different enhancement methods are assessed in terms of underlying fluid routing mechanisms and ability to achieve three distinct heat transfer goals: eliminating incipient boiling hysteresis, increasing nucleate boiling heat transfer coefficient, and ameliorating critical heat flux (CHF), especially for inert dielectric coolants that are both highly wetting and possess relatively poor thermophysical properties. While different enhancement scales are shown to provide different degrees of success in achieving the three goals, it is shown that both microscale and nanoscale surface features are susceptible to blockage, resulting in deterioration of the enhancement over time. This review also points to scarcity of sufficiently sized databases for a given enhancement scheme in terms of fluid type, surface material, size, and orientation, enhancement shape, pattern, and scale, and operating pressure. This renders available findings less-than-adequate tools for design of practical cooling systems.

Contents

* Corresponding author.
E-mail address: mudawar@ecn.purdue.edu (I. Mudawar).
URL: https://engineering.purdue.edu/BTPFL (I. Mudawar).

https://doi.org/10.1016/j.ijheatmasstransfer.2018.09.026
0017-9310/

Nomenclature

A	area
A^+	area fraction
B	dimensionless parameter
C	compensating factor
d	diameter
g	gravitational acceleration
H	channel height
h	heat transfer coefficient
h_{fg}	latent heat of vaporization
K	fitting factor
k	thermal conductivity
k_m	thermal conductivity of porous matrix
P_r	reduced pressure
q''	surface heat flux
r	bubble radius; pore radius
r^+	non-dimensional roughness
R_a	average surface roughness
S	area factor
S_m	mean spacing between surface peaks
T	temperature
ΔT_i	superheat at boiling incipience, $T_i - T_{sat}$
ΔT_{sat}	surface superheat, $T_w - T_{sat}$
u_c	capillary velocity
V''	wicked volume flux
v_{fg}	specific volume difference
W	wicking coefficient
Wi	wicking number

Greek symbols

α	contact angle
α_m	modified contact angle
α_{rec}	receding contact angle
β	geometrical factor
δ	gap width; coating thickness
ε	volumetric porosity
θ	cavity cone angle; surface orientation angle
λ_c	critical wavelength
μ	viscosity
φ	solid fraction
ρ	density
σ	surface tension

Subscripts

b	boiling
CHF	critical heat flux
f	liquid
g	vapor
i	incipience
nc	natural convection
p	particle
sat	saturation
$unconf$	unconfined
w	surface

1. Introduction

1.1. Two-phase cooling solutions

1.1.1. Background and applications

Performance of devices in many applications is becoming increasingly dependent on the ability to dissipate large amounts of heat while maintaining material temperatures below prescribed limits. These include supercomputers, computer data centers, hybrid vehicle power electronics, heat exchangers for hydrogen storage, advanced radar, X-ray medical equipment, aircraft, satellite and spacecraft avionics, and laser and microwave directed energy weapons, collectively categorized as relatively *low-temperature* applications [1–4]. But high heat dissipation is also encountered in *high-temperature* applications, including air-fuel heat exchangers for high-Mach aircraft engines, fusion reactor blankets, particle accelerator targets, magnetohydrodynamic (MHD) electrode walls, and rocket nozzles [1–4]. They also include quenching of metal alloy parts from very high temperatures to achieve optimum alloy microstructure and superior mechanical properties [5,6]. Rapid developments in both the low-temperature and high-temperature applications have greatly exasperated heat dissipation at device, module and system levels, which is a key reason behind recent efforts to develop better cooling schemes, especially for the low-temperature applications.

An early popular scheme to tackle the increases in heat dissipation, especially for electronic and power devices, is use of air-cooled heat sink attachments. With time, there have been many efforts to enhance the performance of these heat sinks, including use of fans incorporated into the heat sink itself and improving conductivity of interface materials. But, because of poor thermal transport properties of air, these improvements fell short of the ability to tackle increases in heat dissipation from modern devices. And, by the early 1980s, aggressive miniaturization of electronic components within high performance devices rendered air-cooled heat sinks virtually obsolete, causing a drastic shift to cooling schemes utilizing single-phase dielectric liquids. With their superior thermophysical properties compared to air, these liquids were better able to capture the dissipated heat in the form of a rise in the coolant's sensible heat.

However, by the mid-1980s, heat dissipation in many electronic and power devices began to cross the 100 W/cm^2 threshold, exceeding the capabilities of most single-phase liquid cooling schemes. Since then, cooling system developers have shifted focus to two-phase cooling schemes. With their ability to capitalize upon the coolant's sensible as well as latent heat, two-phase schemes offer the ability to dissipate far greater amounts of heat while simultaneously maintaining acceptably low device temperatures. Fig. 1 compares ranges of heat transfer coefficients attainable with different fluids and cooling schemes.

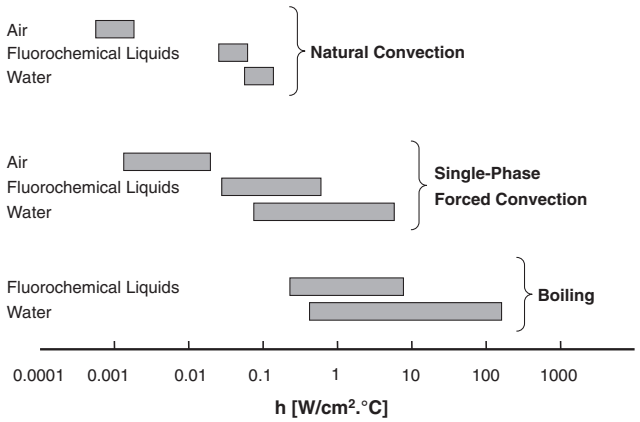

Fig. 1. Ranges of heat transfer coefficients attainable for different coolants with natural convection, single-phase liquid forced convection, and boiling. Adapted from Mudawar [1].

1.1.2. Two-phase cooling schemes

To date, several two-phase cooling schemes have been recommended for high heat flux removal. And developing fundamental understanding of the phase change mechanisms and practical implementation of these schemes have been two primary goals of studies at the Purdue University Boiling and Two-Phase Flow Laboratory (PU-BTPFL) dating back to 1984. These schemes can be grouped into *passive*, *semi-passive*, and *active* categories, depending on the manner in which the coolant is supplied to the heat-dissipating surface.

Passive two-phase cooling schemes rely on buoyancy-driven pool boiling. Fig. 2 shows a schematic of a typical pool boiling *thermosyphon*, wherein heat-dissipating modules submerged in a liquid pool release the heat via nucleate boiling. This system relies entirely on buoyancy to maintain coolant motion within a closed chamber, where vapor produced by the boiling rises to the top portion of the chamber, condenses upon the surfaces of an air-cooled or liquid-cooled condenser, and the condensed liquid drips back to the liquid pool below. Proponents of pool boiling point to several advantages: passive fluid circulation, simplicity of construction, ease of fabrication and sealing, maintenance-free operation, and absence of pump-induced fluid pulsation [7].

Semi-passive two-phase cooling schemes rely in part on buoyancy, but require a relatively small pump to assist coolant circulation. The most common variety of these schemes involves cooling with the aid of a gravity-driven (falling) liquid film from an elevated plenum, and relying on buoyancy to drive the vapor upwards, where it condenses into liquid in the plenum [9–11]. The primary purpose of the small pump is to maintain steady level of liquid in the inlet plenum. While semi-passive schemes do offer certain cooling benefits, their advantages relative to thermosyphons are somewhat limited.

Active two-phase cooling schemes rely on a pump to tackle coolant circulation within the thermal management system. They include channel flow boiling [12–14], mini/micro-channel heat sinks [15,16], jet-impingement [17,18], and spray cooling [19–21]. They also include hybrid cooling schemes, which combine the merits of two or more active cooling schemes in pursuit of performance superior to those of the individual schemes [22,23]. However, the need for a large pump, complex plumbing and flow control, and high cost are all key concerns when considering implementation of any active cooling scheme.

1.2. Problems associated with dielectric fluorochemical coolants

1.2.1. Poor thermophysical properties

Early liquid thermal management systems used water in a variety of 'indirect cooling' schemes, where the heat dissipating device is attached to a thermally conducting substrate that is subjected to the water cooling, buffering the device from any water contact. Here, thermal cooling performance is greatly influenced by thermal resistance between the device and substrate. Examples of indirect water cooling include situations involving extremely high heat fluxes, such as fusion reactor blankets [24,25] and X-ray devices [26].

Clearly, better cooling may be realized with 'direct cooling' (also termed immersion cooling), where the device is subjected directly to the coolant, thereby eliminating the thermal conduction resis-

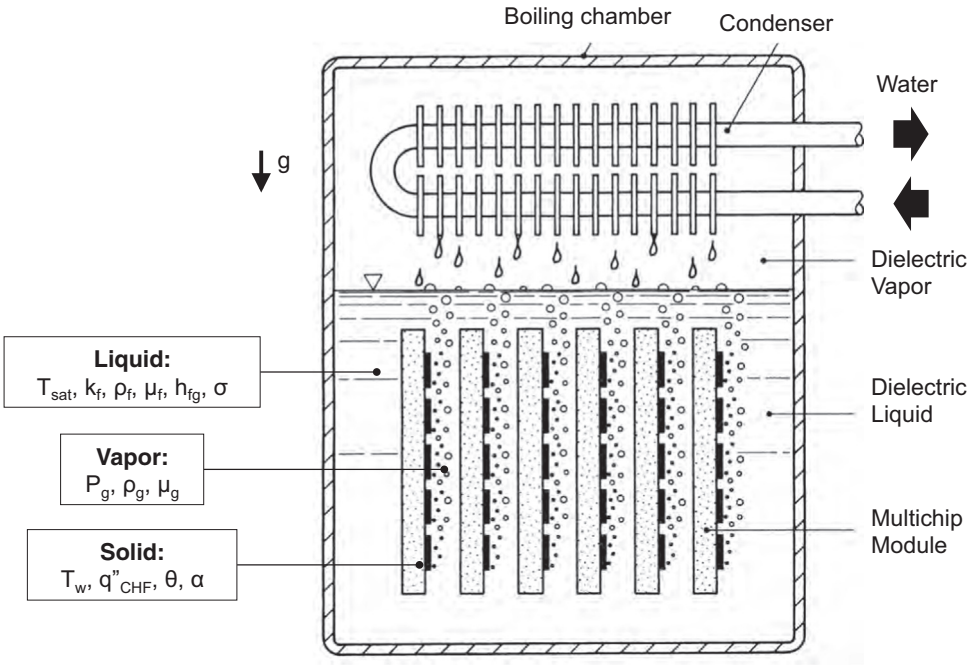

Fig. 2. Schematic of typical buoyancy-driven pool boiling thermosyphon, and system nomenclature. Adapted from Anderson and Mudawar [8].

tance. However, for current carrying electronic and power devices, the coolant in a direct cooling configuration must be both inert and dielectric. This implies that, despite its superior thermophysical properties, water cannot be used in these situations because of poor dielectric properties.

Acceptable coolants must be dielectric, inert, stable, non-flammable, and non-reactive. While Freon type refrigerants do possess these properties and have been used in the past in direct cooling situations, most are presently banned from use because of environmental concerns. Alternatives include 3 M company's 'Fluorinert' and 'Novec' fluids, which provide superior environmental properties (especially the Novec series), and are therefore highly favored for direct cooling of electronic and power devices. However, these fluids are not without shortcomings. Key among those are relatively poor thermophysical properties, high air solubility, and extremely small contact angle. Lacking the attractive thermophysical properties of water, these fluids necessitate the use of surface enhancement techniques to meet the cooling requirements of modern electronic devices. High air solubility (*e.g.,* 48% by volume at 1 atm and 25 °C for 3 M's FC-72) [27] can result in artificial boiling incipience at temperatures well below saturation temperature of the pure fluid [28,29]. These coolants must therefore be thoroughly deaerated before being charged into a tightly sealed cooling system. And very small contact angles (typically below 10°) contribute to irregularities in boiling initiation and high tendency for leaks.

1.2.2. Difficulty in initiating nucleate boiling

The surface temperature required to initiate nucleate boiling is often determined by performing a force balance for a spherical bubble forming at a surface cavity, and relating fluid pressure to fluid temperature using the Clausius-Clapeyron equation,

$$\Delta T_i = T_i - T_{sat} = \frac{T_{sat}\upsilon_{fg}}{h_{fg}}\frac{2\sigma}{r}, \tag{1}$$

where T_i, T_{sat}, and r are the incipient boiling surface temperature, saturation temperature, and bubble radius, respectively. Most popular incipience theories, such as those of Hsu [30], Han and Griffith [31], and Davis and Anderson [32], are based on the assumptions of (1) existence of a relatively large vapor embryo within the cavity, and (2) that bubble radius at the mouth of the cavity is equal or proportional to the cavity radius. According to Eq. (1), this implies that the superheat required to induce bubble growth and release from a particular cavity is inversely proportional to the cavity radius. However, for dielectric fluorochemicals, very small contact angle causes appreciable penetration of liquid deep into the cavity, allowing initial capture of only a small embryo whose radius is much smaller than that of the cavity. This implies that the radius that needs to be employed in Eq. (1) should be that of the small embryo, which results in an incipience superheat much larger than predicted using the cavity radius [29]. An important factor influencing formation and size of initial embryo is the relative between the magnitude of effective cone angle, θ, of the cavity and contact angle, α. Fig. 3 shows three possible scenarios related to embryo capture as bulk liquid attempts to replenish a cavity. Combination of a relatively wide-angle cavity and smaller contact angle ($\theta > \alpha$), Fig. 3(a), causes the liquid to 'flood' the cavity, preventing formation of a vapor embryo. Fig. 3(b) shows capture of a relatively large embryo for $\theta < \alpha$ in relatively large contact angle fluids such as water. On the other hand, Fig. 3(c) depicts the capture of a very small embryo for $\theta < \alpha$ in very small contact angle fluids such as dielectric fluorochemicals. Growth of a very small embryo as depicted in Fig. 3(c) requires much higher superheat than predicted according to Eq. (1) using the cavity radius. For example, Reeber and Frieser [33] reported that nucleation in FC-72 did not begin even with a surface temperature 46 °C higher than saturation temperature. You et al. [34] examined the boiling incipience for FC-72 and R-113 on sputtered surfaces of various materials with cavities on the order of 1 μm. Based on measured incipience superheats of 18–51 °C for FC-72 and 43–75 °C for R-113, and using the bubble growth criterion in Eq. (1), they estimated embryo radii of 0.024–0.15 μm for FC-72, and 0.022–0.077 μm for R-113, much smaller than cavity radius. Hence, estimating boiling incipience temperature for highly wetting fluids requires determination of distribution of embryo sizes rather than those of surface features [8].

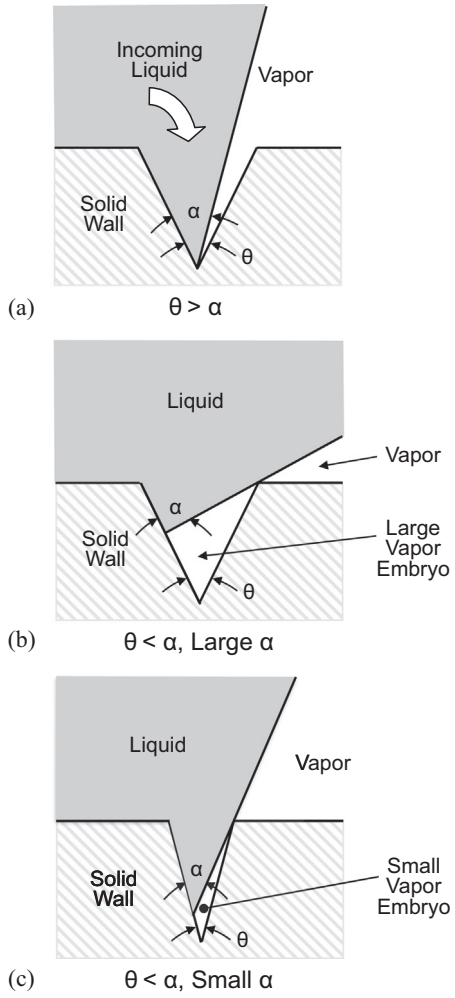

Fig. 3. Different vapor embryo capture patterns: (a) no vapor embryo for $\theta > \alpha$, (b) large embryo for $\theta < \alpha$ and relatively large α, and (c) small embryo for $\theta < \alpha$ and small α.

1.2.3. Incipience excursion (overshoot) and temperature drop, and incipience hysteresis

As discussed in the previous section, boiling incipience in low contact angle fluorochemicals is delayed to high surface superheats. But once incipience takes effect, this excess superheat is quickly dissipated by vigorous boiling. Additionally, bubble growth from one cavity can extend into neighboring ones, activating those cavities as well, and causing the boiling to spread rapidly over a large portion of the heated surface. These effects cause rapid transition from relative poor heat transfer dominated by natural convection in liquid just prior to boiling incipience, to highly effective nucleate boiling. The outcome of this transition is a sudden drastic decrease in surface temperature as shown in Fig. 4. The large superheat required to initiate the boiling process when increasing the surface heat flux (heating mode) is commonly referred to as 'incipience excursion' or 'incipience overshoot,' and the ensuing temperature drop immediately following incipience as 'incipience temperature drop'. Notice how decreasing the wall heat flux (cooling mode) results in nucleate boiling characteristics virtually identical to those of the heating mode at both high fluxes corresponding to fully developed boiling, and very low heat fluxes associated with liquid natural convection. However, the excursion region is fully bypassed during the cooling mode, which is why differences between heating and cooling modes are described as 'incipience hysteresis.' One reason for lack of excursion during the

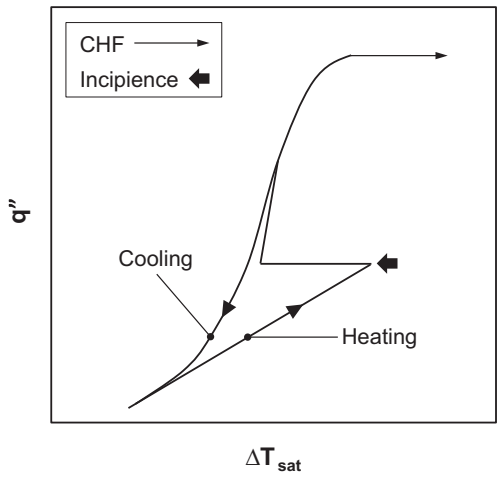

Fig. 4. Schematic of incipience overshoot and temperature drop, and incipience hysteresis encountered with small contact angle dielectric fluorochemical coolants.

cooling mode is abundance of vapor from the fully developed nucleate boiling region, which serves to provide larger vapor embryos in active cavities and activate neighboring initially inactive cavities [35]. These phenomena have been reported by many investigators [29,36–39], who cautioned against their damaging effects for temperature sensitive devices. Potential damage to these devices is encountered in two different ways, first due to surface overheating just prior to incipience, and immediately following incipience due to the large temperature drop; the latter may induce 'thermal shock' to the device. It should be noted that these incipience effects are observed with both bare and enhanced surfaces. Following is a more detailed look into the surface temperature drop immediately following incipience.

Clearly, the large temperature drop that accompanies boiling incipience of low contact angle coolants is the product of the large, rapid change in heat transfer coefficient as the heat transfer mode transitions from natural convection to nucleate boiling. For a small, fairly isothermal surface undergoing both natural convection and nucleate boiling over separate areas A_{nc} and A_b, respectively, total heat transfer is the net result of both heat transfer modes,

$$\frac{q''}{\Delta T_{sat}} = h\ A = h_{nc}A_{nc} + h_bA_b, \tag{2}$$

where h is the overall heat transfer coefficient, and h_{nc} and h_b are the heat transfer coefficients associated with natural convection and nucleate boiling, respectively. By defining the boiling area fraction as $A^+ = A_b/A$, the heat transfer coefficient can be expressed as

$$h = h_{nc}\left(1 - A^+\right) + h_bA^+. \tag{3}$$

Notice in Eq. (3) how as A^+ grows gradually toward unity (fully developed nucleate boiling region), the overall heat transfer coefficient h will likewise increase to the value of h_b. The transient increase in A^+ upon incipience is influenced by surface size and pattern of boiling activation. Small heaters incur large jumps in A^+ since the area influenced by boiling from a single site can occupy a significant fraction of the surface area [8]. Rapid patterns of activation (*e.g.,* due to surface orientation or surface enhancement) can cause large swings in A^+ and therefore result in considerable temperature drop.

Another contributor to the magnitude of incipience temperature drop is conduction within the heating surface. Foil heaters, such as those used by Park and Bergles [40], allow little conduction across the heat transfer surface. Consequently, temperature drop is

highly localized, and the large change in local heat transfer coefficient is sensed as a large temperature fallback. In contrast, thick heaters allow significant conduction within the heating surface, which dampens localized effects of activation of a few surface cavities. Rapid activation of the entire surface may still induce a measurable temperature drop, but thermal shock is damped by increased thermal capacitance for thick heaters.

1.2.4. Low critical heat flux

Another obvious limitation for pool boiling in dielectric fluids is relatively low critical heat flux (CHF). This is readily apparent when comparing CHF from a bare surface in a fluorochemical to that in water at atmospheric pressure. According to the Zuber model [41–43], CHF for saturated pool boiling in water is 110.4 W/cm^2, whereas that for FC-72 is only 15.24 W/cm^2. Inferior CHF for FC-72 is a direct result of the relatively poor thermophysical properties of FC-72, especially latent heat of vaporization and surface tension. Given the safety requirement of maintaining heat flux below 70% of CHF [44], the upper operational limit for device heat flux is reduced even further. Low CHF is especially problematic for compact electronic cooling systems employing a small boiler. Here, confining walls of the small boiler may interrupt liquid replenishment of the heating surface during vigorous boiling, thereby compromising CHF even further.

1.3. Enhancement techniques and challenges

1.3.1. Major techniques for boiling enhancement

Methodologies that have been proposed to improve nucleate boiling heat transfer can be classified into two major groups: *active* and *passive* [45]. The active techniques require external power, and include mechanical mixing, surface and/or liquid rotation, vibration, suction or injection, and addition of external electrostatic or magnetic fields, all of which have been proven effective at intensifying heat transfer [46]. However, active enhancement techniques are costly and difficult to implement in compact cooling enclosures, such as those used for electronics cooling. In contrast, passive techniques require no direct application of external power, and include modifying coolant properties and/or surface roughness and shape, or using finned surface attachments to increase surface area.

Compared to flow boiling, pool boiling offers few heat transfer enhancement options. Increasing flow velocity in flow boiling improves both single-phase and two-phase heat transfer and postpones CHF by sweeping bubbles away from the surface before they coalesce into an insulating vapor blanket [47]. In pool boiling, however, relatively weak fluid motion is induced by natural convection prior to the onset of boiling and, thereafter, by buoyancy and bubble agitation. Unfortunately, the induced flow cannot be easily controlled. Therefore, attempts at enhancing pool boiling performance are limited mostly to two major methodologies: (a) modifying the fluid itself and/or operating conditions (*e.g.,* saturation pressure and subcooling), and (b) modifying the heating surface. Surface modification can be achieved on a variety of scales: 'macroscale,' 'microscale,' and 'nanoscale,' which are aimed at increasing heat transfer area, increasing nucleation site density, and improving capillary wicking effects, respectively. There are also 'hybrid-scale' methods that combine the cooling merits of different surface modification scales in pursuit of superior cooling performance.

1.3.2. Operational limits for temperature-sensitive devices

Temperature-sensitive devices such as electronic and power devices impose stringent operational limits to implementing a thermal management system employing pool boiling. Most important among these limits are (1) maximum operating temperature (*e.g.,* 125 °C for current high performance electronic and power devices, imposed by both materials and reliability concerns), and (2) CHF. Fig. 5 illustrates how the boiling system must be configured to meet both limits. Shown first are boiling characteristics for a bare (unenhanced) surface, where neither limit is met. Also shown are characteristics for an enhanced albeit unacceptable surface, where, despite superior CHF, maximum surface temperature is exceeded at the maximum operating heat flux. A third case is also shown, where both temperature and CHF limits are properly met. To achieve the desired cooling performance indicated by the third case, it is desired to reduce wall superheat and increase CHF simultaneously.

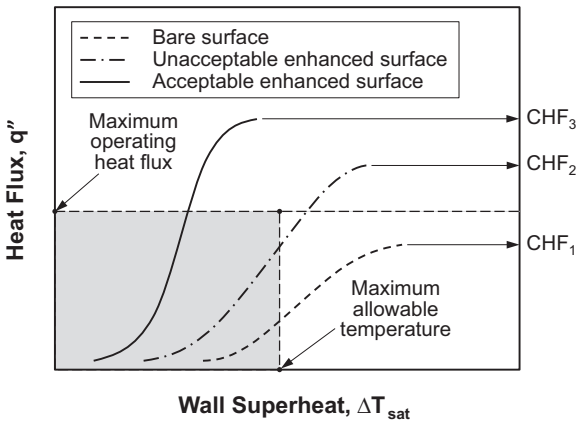

Fig. 5. Optimum enhancement of boiling performance for temperature sensitive devices.

One application where pool boiling might benefit from surface enhancement is thermal management in space systems. Absence of gravity is known to greatly compromise cooling effectiveness by triggering CHF at unusually low heat fluxes [48–51]. Without significant additional enhancement, pool boiling is unlikely to become a viable cooling option for these applications. Here, use of structured surfaces might aid in both increasing surface area and breakup of large coalescent vapor bubbles, thereby ameliorating CHF.

Aside from meeting the two above operational limits, boiling enhancement is employed to achieve other goals as well. Overall, pool boiling enhancement is used to achieve one or more of the following goals: (a) initiating nucleate boiling at lower surface temperature, (b) reducing and/or eliminating incipience temperature excursion, especially for low contact angle coolants, (c) reducing surface temperature (*i.e.*, increasing the heat transfer coefficient associated with nucleate boiling), and (d) increasing CHF to accommodate higher surface heat fluxes.

1.4. Prior reviews on pool boiling enhancement

Several review articles have been published in the past, which address boiling heat transfer enhancement by means of surface modification. These articles either address enhancement of pool boiling along with other heat transfer modes, or are dedicated entirely to pool boiling. Examples of the first category include works by Bergles and co-workers documenting 508 papers and reports [45] and 59 U.S. patents [52] relating to both pool boiling and flow boiling prior to 1980. Bhavnani et al. [53] and Shojaeian and Koşar [54] also reviewed enhancement literature related to both pool and flow boiling using micro/nanostructured surfaces. McCarthy et al. [55], Kim et al. [56], and Attinger et al. [57] published review articles addressing practical concerns with boiling enhancement, including both materials and methods used to fabricate micro/nanostructured surfaces. Examples of reviews

dedicated entirely to pool boiling enhancement include an article by Honda and Wei [58] addressing surface microstructures developed prior to 2004 to improve cooling performance for electronic devices. Lu and Kandlikar [59] reviewed pool boiling enhancement using nanoscale surface modification techniques, and follow-up work by Patil and Kandlikar [60] reviewed techniques for manufacturing porous surfaces for pool boiling applications. A recent article by Mori and Utaka [61] reviewed techniques that have been used to enhance pool boiling CHF, but did not address enhancement of heat transfer coefficient within the nucleate boiling region.

1.5. Objectives of present review

The present paper is a follow-up to a series of reviews by the present authors addressing several fundamental two-phase mechanisms, including fluid mechanics of liquid drop impact on a liquid film [62] and on a heated wall [63], spray cooling in single-phase regime, nucleate boiling regime, and CHF [4], and in high temperature boiling regimes and quenching applications [5], mechanisms and models of pool boiling CHF [64], and pool boiling enhancement techniques using additives and nanofluids [65].

The present review is intended to provide a very comprehensive assessment of passive pool boiling heat transfer enhancement using surface modification. Included are potential problems associated with cooling temperature sensitive electronic and power devices and key challenges for pool boiling enhancement. Key topics discussed are boiling enhancement at different surface modification scales, including *macroscale*, *microscale*, and *nanoscale*, with feature sizes larger than 1 mm, in the range of 1–1000 μm, and smaller than 1 μm, respectively. Also included are *hybrid-scale* enhancement methods, which combine two or more of the enhancement scales just mentioned. Each of the topics presented also includes description of fabricating techniques used in the surface modification. This paper also discusses novel concepts for separating liquid and vapor paths, and pumpless cooling loops. The review is concluded with recommendations concerning future work that is needed to address poorly understood mechanisms or contradictory findings. It should be noted that this review is limited to surface enhancement applied to planner heat dissipating surfaces, and excludes tubular surfaces.

2. System-related influences on nucleate pool boiling other than surface enhancement

2.1. Roles of surface orientation and boiling confinement

Aside from addressing the benefits of surface enhancement on nucleate pool boiling, it is vital to isolate the important influences of system-related constraints on nucleate pool boiling. Designing a cooling package often dictates placing the heat-dissipating device in mostly vertical or horizontal orientations; choice of orientation is based not only on heat transfer considerations but practical packaging concerns as well. Aside from surface orientation, cooling systems in the vast majority of modern applications favor highly compact, lightweight packaging, often causing appreciable constraints on allowable overall size of boiling chamber and/or fluid space around the heat-dissipating device. It is therefore important to explore the effects of both surface orientation and boiling confinement on nucleate boiling performance for bare surfaces, given their potentially important influences on cooling performance for enhanced surfaces as well. Summarized below is a review of published works concerning boiling confinement for vertical surfaces, followed by a similar review for horizontal (upward-facing) surfaces. Presented in this section are findings concerning mostly bare surfaces.

2.2. Boiling confinement for vertical surfaces

Several investigators have reported the enhancement benefits of nucleate pool boiling along a vertically oriented heating surface in a narrow fluid gap [66–69]. These benefits have been attributed mostly to sweeping effects caused by buoyancy, which assist bubble detachment from the vertical surface. However, a potential drawback of reducing the gap width is degradation in CHF [66,70].

Bonjour and Lallemand [71] proposed three distinct regimes for boiling of R-113 in narrow space between two vertical surfaces: nucleate boiling with isolated deformed bubbles, boiling with coalescing bubbles, and partial dryout, which were demarcated with respect to reduced heat flux, defined as the ratio of heat flux to CHF. They achieved measurable heat transfer performance with the first two regimes and degradation with the third. Similar regime classification was suggested by Yao and Chang [72], who employed Bond number to distinguish boiling regimes for R-113, acetone, and water. Fujita et al. [73] reported that the boiling heat transfer coefficient for water first increases with increasing gap width and reaches maximum value before beginning to decrease with further increases in the gap width. Xia et al. [70] showed that the boiling heat transfer coefficient for R-113 increases with decreasing channel gap width and/or increasing channel height at low and moderate heat fluxes, but this trend reverses at high heat fluxes.

Rops et al. [74] reported improvement in the nucleate boiling heat transfer coefficient for water as the liquid pool diameter was decreased from 15 to 4.5 mm, which they attributed to improved fluid circulation, but pool depth and confining wall material had only minor effects on performance.

Geisler and Bar-Cohen [66] investigated pool boiling of FC-72 from a vertical heating surface with coolant confined in a rectangular channel between two vertical plates, and found test heater material to have significant influence on nucleate boiling heat transfer. However, CHF, q''_{CHF}, was independent of the heater material, and influenced rather by ratio of channel height H to gap width δ.

$$\frac{q''_{CHF}}{q''_{CHF,unconf}} = \left[1 + 1.08\times10^{-4}\left(\frac{\rho_f}{\rho_g}\right)^{1.343P_r^{0.252}}\left(\frac{H}{\delta}\right)^{1.517}\right]^{-1} \tag{4}$$

where $q''_{CHF,unconf}$ is CHF corresponding to unconfined boiling, and P_r reduced pressure (ratio of operating pressure to critical pressure). Monde et al. [75] and Bonjour and Lallemand [76] arrived at somewhat similar observations and recommended CHF correlations similar in form to that of Eq. (4).

A major factor contributing to CHF deterioration in confined spaces is blockage of the path of replenishment liquid by upward-moving vapor. Mukherjee and Mudawar [77] investigated boiling from a vertical heating surface mounted into a small boiling section along one of two parallel channel walls, allowing for variations in gap width and use of both bare and enhanced surfaces. But unlike conventional pool boiling thermosyphons, they were able to separate the path of vapor produced along the heating surface from that of replenishment liquid by using a 'pumpless cooling loop' consisting of two vertical parallel tubes connected together at the bottom and sharing a single reservoir atop, as shown in Fig. 6 (a). This system was configured to induce unidirectional (clockwise) coolant motion by capitalizing upon large fluid density differences between the heavier liquid in the 'cold tube' to the right and lighter two-phase mixture in the 'hot tube' to the left. Substantial non-equilibrium in hydrostatic pressure between the two tubes drew liquid downwards through the cold tube as the two-phase mixture was released upwards in the hot tube. By completely isolating the path of replenishment liquid from that of

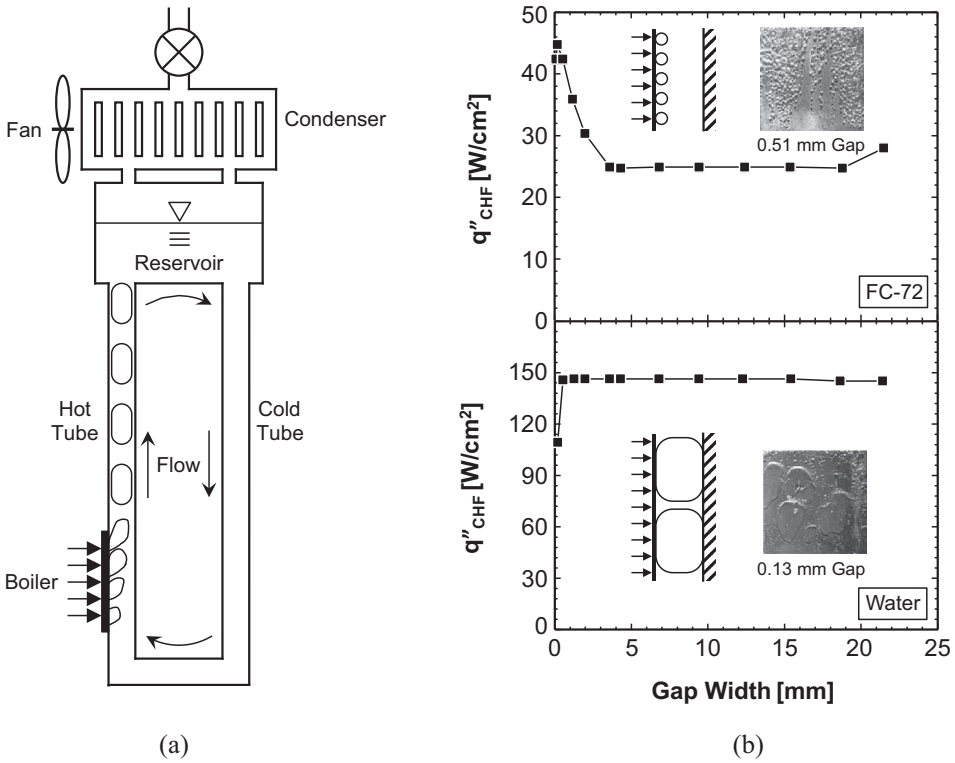

Fig. 6. (a) Pumpless cooling loop concept, and (b) variation of flat surface CHF with gap width. Adapted from Mukherjee and Mudawar [78].

vapor exiting the boiler, Mukherjee and Mudawar showed the cooling performance of this pumpless loop is far more superior to that of conventional pool boiling thermosyphons in several respects. First, it served to completely eliminate the incipience excursion commonly encountered with low contact angle dielectric fluids. Second, it offered 'smart' performance features, being able to increase velocity of liquid entering at the bottom of the hot tube as more vapor was produced in the hot tube, thereby improving cooling performance with increasing heat flux in the boiling section. They also investigated the influence of boiler gap width on CHF for both FC-72 and water. For both fluids, CHF showed little dependence on gap width for large gaps as shown in Fig. 6(b). However, decreasing the gap width below 3.56 mm produced a substantial rise in CHF for FC-72 due to increased flow velocity. On the other hand, CHF for water was fairly insensitive to gap width down to 0.51 mm, below which it began to decrease sharply. These opposite trends were attributed to the much smaller surface tension of FC-72 compared to that for water influencing relative bubble size for the two fluids. For FC-72, very small bubbles could easily pass through very narrow gaps, while, for water, much larger bubbles cause appreciable obstruction to liquid replenishment in narrow gaps. Mukherjee and Mudawar performed follow-up study [78] to investigate CHF for FC-72 from a flat heating surface as well as surfaces with 'micro-channel' (0.2-mm vertical rectangular fins) and 'mini-channel' (1.98-mm vertical rectangular fins) enhancement for different gap widths. Using the pumpless loop concept, they achieved 4.5, 5.9, and 5.7-fold enhancement in CHF with flat, micro-channel, and mini-channel surfaces, respectively, compared to boiling from a flat surface in an unconfined liquid pool.

2.3. Boiling in confined spaces for horizontal surfaces

Other investigations addressed pool boiling in a narrow space between two horizontal surfaces. Misale et al. [79] found that the effect of confinement on heat transfer coefficient for HFE-7100 was insignificant for Bond numbers greater than unity and superheats below 9 °C. Otherwise, the heat transfer coefficient increased with decreasing gap width in the range 0.5–3.5 mm. Stutz et al. [80] observed somewhat similar trends with n-pentane, and attributed the heat transfer enhancement to evaporation of a thin liquid film trapped between squeezed bubbles and the heating surface. However, CHF for HFE-7100 always deteriorated compared to unconfined boiling, the reduction of which was alleviated when the narrow space was orientated vertically [81]. It should be noted that the three studies just mentioned involved heating from the lower horizontal surface. On the other hand, Passos et al. [82–84] and Cardoso et al. [85] examined heating from the upper surface. For gap widths ranging from 0.1 to 13 mm, they found that decreasing gap width enhanced nucleate boiling heat transfer for saturated boiling of both FC-72 and FC-87 at relatively low heat fluxes of less than 4.5 W/cm^2, but degraded heat transfer for subcooled boiling. The enhancement was attributed to strong influence of lateral release of large bubbles that helped draw cold liquid into the boiling gap, and to pulsating movement of bubbles before departure, as shown in Fig. 7.

3. Macro-finned surfaces

Fabricating multiple rectangular or square fins on the heating surface is a popular means to improving boiling heat transfer. While the obvious merit of such is increased heat transfer area, the primary challenge here is optimizing fin size and spacing in pursuit of optimal cooling performance. Klein and Westwater [86] showed that a 1.57-mm spacing between fins was wide enough to allow fins to act independently of each other. This value happens to be near the bubble departure diameter for common liquids in nucleate pool boiling. Rainey and You [87] reported that boiling heat transfer performance for FC-72 from surfaces having

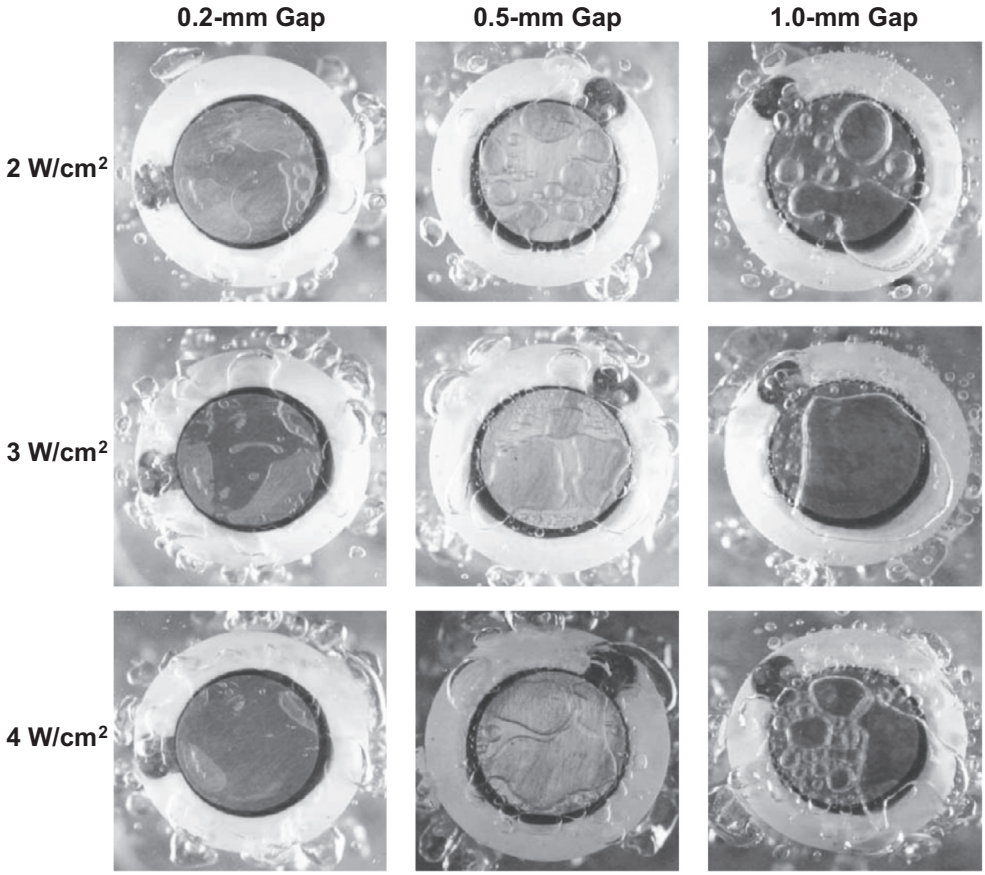

Fig. 7. Images of nucleate boiling of FC-72 in horizontally confined space for different gap widths and heat fluxes. Adapted from Passos et al. [84].

1-mm wide fins with 1-mm spacing was significantly enhanced with increasing fin height up to about 5 mm, above which fin tip temperature became too low to sustain boiling, which reduced the 'effective' boiling area and provided no additional heat transfer enhancement. Parker and El-Genk [88] reported somewhat similar trends for HFE-7100 from a surface with 3-mm wide fins with 4-mm spacing and fin heights up to 5 mm. Yu and Lu [89] examined boiling enhancement with FC-72 for fins having 1-mm width, 0.5 to 2-mm spacings, and heights from 0.5 to 4 mm, and showed that closer and taller fins provided superior nucleate boiling performance and greater CHF. They also observed that boiling was initiated at the fin tip and then spread to the fin root despite higher temperature at the root.

Aside from geometrical parameters, Guglielmini et al. [90,91] and Abuaf et al. [92] showed that boiling heat transfer enhancement for finned surfaces was also influenced by heat flux range, surface orientation, and pressure. Using commercial GEWA surfaces, Ayub and Bergles [93] found that fin spacing for maximum heat transfer enhancement was fluid dependent. Zhong et al. [94] reported that a finned surface having square fins with 1-mm width and spacing, and 2-mm height, yielded 200% enhancement in CHF for water compared to a plain surface for all surface orientations from vertical to downward-facing. Chan et al. [95] reported that optimal boiling enhancement for finned surfaces was achieved by balancing several factors, including active nucleation site density, vapor flow resistance, natural convection, film evaporation, liquid superheat, heat transfer area, bubble coalescence, and liquid reflux resistance.

Since many electronic and power devices cannot accommodate enhancement features that are formed into the surface itself, Reed and Mudawar [96] investigated the use of a 1.27-cm diameter and 1.6-cm long copper cylinder that was pressed at low pressure against the heating surface. They were able to achieve CHF values for FC-72 as high as 85 W/cm^2, a four-fold increase compared to a bare surface. Improved performance with the pressed-on fin was attributed to the small crevice between the boiling surface and fin base, which could be penetrated by highly-wetting fluids, allowing the boiling to commence more easily and spread more evenly with increasing base heat flux than with a soldered-on fin, as shown in Fig. 8(a). Furthermore, they found that nucleate boiling performance was independent of heating surface orientation. Follow-up study by Reed and Mudawar [35] examined the heat transfer enhancement achieved by gently pressing a single copper fin with a spherical base or multiple small metal spheres against the heat transfer surface in order to generate zero-angle artificial nucleation sites as shown in Fig. 8(b). This arrangement was shown to provide multiple advantages, including improved vapor embryo capture, low temperature boiling incipience, and reduction or elimination of the incipience excursion.

Kim and Garimella [97] adopted a similar concept by placing free particles on the heating surface, and bubble nucleation took place preferentially at narrow cavities formed between the particles and surface. The particles tested ranged in size from tens of nanometers to 13 mm. For water, best improvement in boiling heat transfer coefficient (115%) was achieved with a mixture of free particle with diameters ranging from 3 and 6 mm. Follow-up study by Kim et al. [98] showed very different optimum particle size for FC-72. Given poor thermophysical properties (and small contact angle) for FC-72 compared to those for water, millimeter-sized particles produced little enhancement in FC-72. Instead, optimum particle size and weight for FC-72 where 10 μm and 0.2 g, respectively, which enhanced the nucleate boiling heat transfer

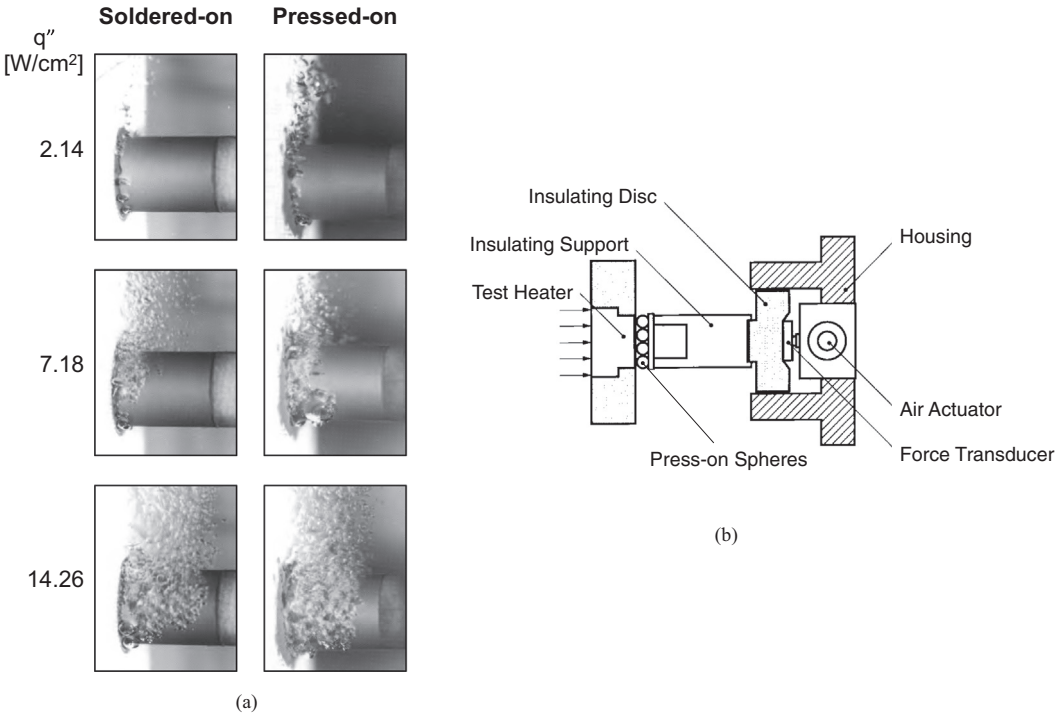

Fig. 8. (a) Boiling spread for soldered-on and pressed-on cylindrical fins (adapted from Reed and Mudawar [96]). (b) Using pressed-on spherical contact to achieve multiple zero-angle artificial nucleation sites (adapted from Reed and Mudawar [35]).

coefficient and CHF by 76.3% and 10%, respectively. Wen et al. [99], Zhou et al. [100], and Chen and Wang [101] reported nucleate boiling enhancement with a water pool packed with perforated copper or glass beads.

While prior studies provide ample evidence of the effectiveness of macro fins at enhancing both nucleate boiling heat transfer coefficient and CHF, further study is needed to provide systematic design guidelines concerning optimum fin size, geometry, and configurations for different coolant types, pressures and surface orientations. These issues are further complicated when using enhanced surfaces that are bonded to an electronic device, where increased junction temperature resulting from interface resistance may lead to undesirable overheating and/or thermal stress [102].

Recently, there has been a precipitous decline in pool boiling enhancement using macroscale surface modification, which may be rooted in rapid development of micro/nanofabrication techniques and interest in nanoparticle use in fluids to enhance nucleate boiling heat transfer. One obvious advantage that is lost in this transition is the ability of macroscale enhancement methods to greatly resist aging as well as both surface oxidation and clogging effects compared to micro/nano enhancement methods.

4. Porous mesh and foam attachments

4.1. Porous mesh

Prior studies pertaining to application of porous mesh atop the heat dissipating surface point to several nucleate boiling heat transfer benefits, including simplicity, increased number of active nucleation sites, and breakup of large vapor bubbles, as well as separation of paths of vapor and liquid in order to promote better liquid replenishment of the surface.

Shimada et al. [103] employed an ‘interferential plate’ having many holes to enhance nucleate boiling performance for water. The plate maintained a narrow fluid gap with a horizontal heating surface that was hermetically sealed along the perimeter, allowing vapor and liquid to be exchanged only through the holes. Optimum performance was achieved with a 0.12-mm gap and interferential plates containing 1-mm and 4-mm holes. Zhao et al. [104] reported that optimum nucleate performance for a horizontal heating surface in water when using wire mesh was achieved with 0.356-mm wire diameter with 1.23-mm wire spacing and a 3-mm fluid gap between the wire mesh and surface. Liu et al. [105] pointed out that, while covering the surface with a fine wire mesh did enhance nucleate boiling heat transfer for methanol and HFE-7100 at low superheats, it had an adverse effect on CHF, as well as on heat transfer in the film boiling regime. Hasegawa et al. [106] achieved boiling enhancement for water with a woven screen mesh.

Tsay et al. [107] investigated the effects of covering a horizontal heating surface with metal mesh, surface roughness, and height of liquid pool on nucleate boiling for water. The metal mesh augmented heat transfer substantially, especially for shallow water layers, when mesh size was comparable to vapor bubble departure diameter. However, the mesh compromised heat transfer effectiveness when applied over a rough surface. Franco et al. [108] found that use of wire mesh not only increased nucleation site density for R-141b, but also assisted vapor escape, thereby improving thermal stability of the cooling system. Penley and Wirtz [109] reported an increase in number of bubble nucleation sites and therefore better heat transfer for water when the heating surface was laminated with a fine-filament screen; boiling performance was sensitive to geometrical details of the screen lamination. Melendez and Reyes [110] found that covering the surface with a porous metal layer increased boiling heat transfer coefficient for binary ethanol-water mixtures. Tehver et al. [111] showed that boiling heat transfer of R-113 from a surface coated with a porous metal layer could be improved by a coating having high thermal conductivity. Using a honeycomb porous oxide layer that was placed on the heating surface, Mori and Okuyama [112] achieved 2.5-fold CHF enhancement for water, which they attributed to two effects: improved liquid

supply to the surface by capillary wicking, and reduced resistance to vapor release because of this technique's ability to promote separation of liquid and vapor flow paths.

4.2. Porous foam

Recently, metallic foam with high porosity (over 90%) has attracted significant attention because of its combined benefits of lightweight and heat transfer enhancement. Xu et al. [113] explored the pool boiling benefits of copper foam with tetrakaidecahedral unit cells for acetone. A key parameter influencing cooling performance was number of pores per inch (PPI), three examples of which are shown in Fig. 9. Low PPI foams showed better heat transfer performance at small superheats, while high PPI foams were better for moderate to large superheats. Cooling performance was also influenced by foam layer thickness; larger thickness increased nucleation density, but also increased resistance to vapor release. In a related study, Yang et al. [114], showed that welding copper foam to the heating surface reduced incipience superheat for water. They achieved maximum enhancement with a PPI of 60, and also pointed out that boiling performance was influenced by both PPI and foam layer thickness. Yang et al. [115] found that changing surface orientation from horizontal upward-facing to vertical had only minor impact on boiling performance with copper foam. A foam layer similar to that of Yang et al. was also employed by Zhu et al. [116] to enhance boiling performance.

Qu et al. [117] and Xu et al. [118–121] investigated pool boiling heat transfer of water, both with and without addition of sodium dodecyl sulfate (SDS) surfactant, on copper foam with crossing and one-directional V-shaped grooves. They showed that boiling performance was dictated by combined effects of resistance to vapor escape, heat transfer area, and capillary force. Presence of grooves in the porous foam provided added enhancement to the nucleate boiling heat transfer coefficient. Additionally, they showed existence of an optimal groove volume ratio for maximum enhancement, the effects of which was strongly dependent on foam layer thickness. Xu and Zhao [122,123] recommended use of non-uniform metal foam structure, having high pore density in vicinity of the heating surface and low pore density away from the surface, to enhance nucleate boiling performance for water. Pranoto et al. [124] and Jin et al. [125] demonstrated nucleate pool boiling enhancement with structured graphite foam for both FC-72 and HFE-7000, and concluded that block foam was more effective than foam with fin structures [124].

5. Microscale surface modification

5.1. Surface roughening

Surface roughness can have profound influences on heat transfer performance, including not only single-phase and two-phase convection, but radiation as well [126]. Increasing roughness of the heat-dissipating surface, achieved by sandblasting, chemical etching, mechanical roughing, or by forming numerous small artificial cavities, is a popular means for improving nucleate boiling performance. A key reason behind such enhancement is increased number of active nucleation sites on the surface [127–129], which has been shown in early boiling studies to enhance the nucleate boiling heat transfer coefficient by up to 600% [130].

Marto and Rohsenow [131] found that surface roughness affected both boiling incipience and nucleate boiling heat transfer coefficient for sodium. Rainey and You [87] showed, for FC-72, that increasing surface roughness provided all intended benefits of boiling enhancement: decreased incipience superheat and incipience excursion, and increases in both nucleate boiling heat transfer

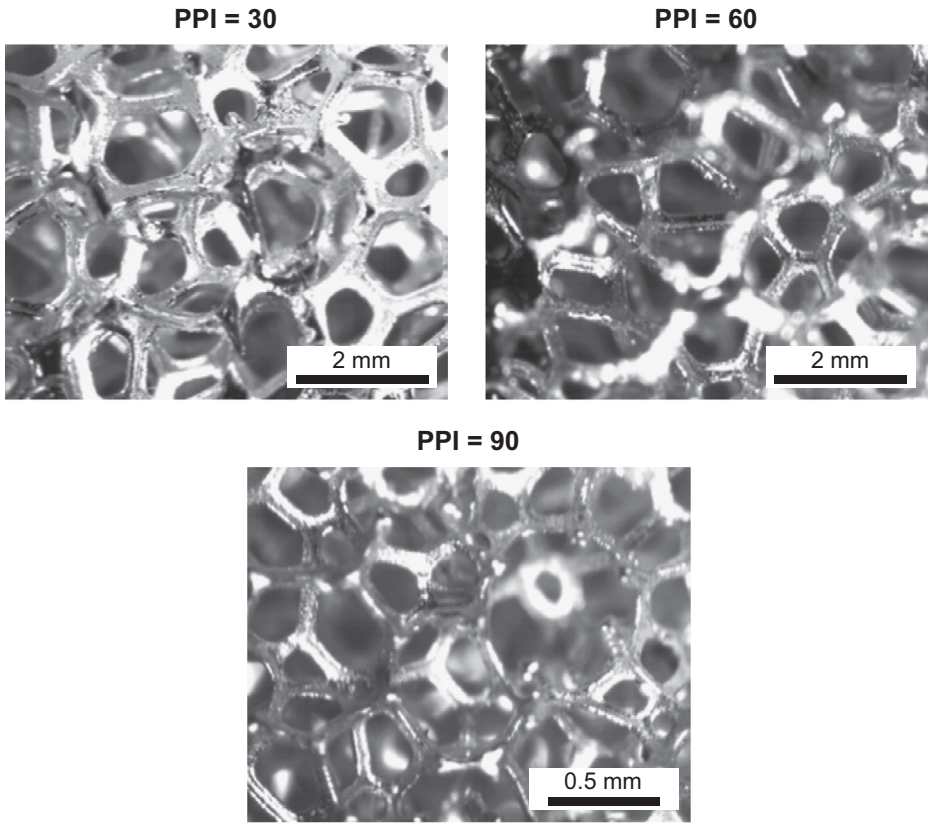

Fig. 9. Images of copper foam with 0.88 porosity and three different values of pores per inch (PPI). Adapted from Yang et al. [114].

coefficient and CHF. Jones et al. [132] pointed out that enhancement effects of surface roughness were highly fluid dependent. Jung and Kwak [133] pointed out substantial differences in effective heat transfer area even for surfaces with comparable values of average surface roughness R_a; they also showed that CHF for FC-72 increased with increases in effective area. Golobič and Ferjančič [134] noted significant impact of surface topography on CHF.

Vachon et al. [135] and Ferjančič and Golobič [136] emphasized dependence of nucleate boiling performance on technique used to achieve the surface roughening. Ferjančič and Golobič reported that CHF on an etched heating surface in water was 51% higher than that for a sanded surface with the same average surface roughness, meaning using a single surface statistical parameter, such as R_a, was insufficient for characterizing pool boiling CHF. Passos and Reinaldo [137] showed that the nucleate boiling heat transfer coefficient for R-113 could be improved with use of a surface having 33-μm wide and 310-μm deep microgrooves. Alangar [138] examined pool boiling of water on surfaces with V-shaped grooves featuring depths, widths, and groove angles of 1–3 mm, 0.5–2.5 mm, and 30–60°, respectively, and reported improved nucleate boiling heat transfer with increases in groove depth, and/or decreases in groove width and angle. Anderson and Mudawar [8] reported significant enhancement in the nucleate boiling heat transfer coefficient for FC-72 with both a sanded surface with parallel 0.6–1.0 μm gouges and a vapor blasted surface with pore sizes near 15 μm, and attributed this enhancement to substantial increases in number of active nucleation sites.

In a recent study, Raghupathi and Kandlikar [139] achieved CHF enhancement for water on a surface with 10–20 μm deep microgrooves, which they attributed to widening of contact line region at the base of nucleating bubbles caused by creation of a liquid meniscus adjacent to the microgrooves. Dong et al. [140] used thermodynamic analysis to assess the influence of microstructures on bubble nucleation in water. By looking into changes in Gibbs free energy, they showed that appreciable enhancement was possible only when curvature radius of the microstructures was 5–100 times smaller than bubble radius, and exceeding the upper limit of this radius range might greatly compromise the enhancement benefits of microstructures. In recent work, Ho et al. [141] employed a Selective Laser Melting technique to create surface microgrooves and microcavities, and demonstrated the effectiveness of this technique at enhancing both the nucleate boiling heat transfer coefficient and CHF for FC-72.

Guan et al. [142] achieved CHF enhancement for pentane, hexane, and FC-72 by increasing surface roughness over a range of 0.15–5 μm, or by decreasing feature size for reentrant, interconnected, microstructured hoodoo surfaces, Fig. 10(a), from 80 to 10 μm; the latter surface enhancement was introduced earlier by Bon et al. [143] for pool boiling enhancement. Guan et al. also proposed a model for CHF from enhanced surfaces, q''_{CHF}, based on their earlier formulation for smooth surfaces, $q''_{CHF,smooth}$, in order to address the effects of capillary wicking.

$$\frac{q''_{CHF}}{q''_{CHF,smooth}} = \sqrt{\frac{B^2+\sqrt{B^4+4}}{2}}, \tag{5}$$

where B is a dimensionless parameter that accounts for both fluid properties and wicking velocity, u_c,

$$B = 4.08\ u_c \left[\frac{\rho_g^2}{\sigma g\left(\rho_f-\rho_g\right)}\right]^{1/4}\left(\frac{\rho_f}{\rho_f+\rho_g}\right)^{1/4}\left(\frac{\rho_f}{\rho_g}\right)^{3/5} \tag{6}$$

In Eq. (5), $q''_{CHF,smooth}$ formulation was based on the 'Interfacial Lift-off' CHF mechanism proposed earlier by Galloway and Mudawar [144], which Guan et al. calculated according to [145]

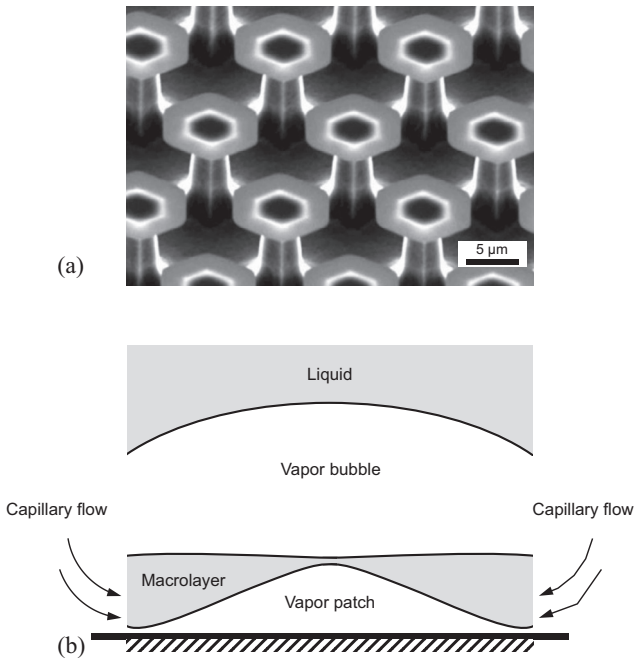

Fig. 10. (a) SEM image of silicon hoodoo surface, and (b) schematic of capillary induced flow into liquid macrolayer. Adapted from Guan et al. [142].

$$q''_{CHF,smooth} = 0.2445\ \left(1+\frac{\rho_g}{\rho_f}\right)^{1/4}\left(\frac{\rho_g}{\rho_f}\right)^{1/10}\rho_g h_{fg}\left[\frac{\sigma g\left(\rho_f-\rho_g\right)}{\rho_g^2}\right]^{1/4}. \tag{7}$$

Shown in Fig. 10(b) is a schematic of capillary induced flow into the liquid macrolayer beneath bubbles.

Kim et al. [146] reported strong dependence of water CHF on surface roughness for moderate contact angles in the range of 60–70°. CHF increased from 77.5 W/cm^2 for a smooth surface with R_a = 0.041 μm to 162.5 W/cm^2 for a rough surface with R_a = 2.36 - μm, an enhancement they ascribed to better capillary wicking on the rougher surface. Kim et al. proposed the following correlation to account for the wicking effects,

$$q''_{CHF} = 0.811\ \left(\frac{1+\cos\alpha}{16}\right)\left[\frac{2}{\pi}+\frac{\pi}{4}(1+\cos\alpha)+\frac{351.2\ \cos\alpha}{1+\cos\alpha}\left(\frac{R_a}{S_m}\right)\right]^{1/2} \times \rho_g h_{fg}\left[\frac{\sigma g\left(\rho_f-\rho_g\right)}{\rho_g^2}\right]^{1/4} \tag{8}$$

where α is contact angle and S_m mean spacing between surface peaks.

Despite many published studies confirming the benefits of surface roughening, this form of enhancement is not widely adopted in industry. A key reason behind lack of commercial implementation of roughened surfaces is rapid 'aging' of surface features, often lasting only a few hours, during which pool boiling performance gradually abates back to that of a plain surface [147]. Chaudhri and McDougall [148] measured long-term boiling performance for surfaces modified with parallel scratches 0.025 mm or less in width. They too showed that enhancement for perchloroethylene and isopropyl acetate was only temporary, and transfer performance after boiling for hundreds of hours degraded back to that of an untreated surface.

It is therefore imperative that future enhancement studies involving all forms of surface roughening achieved via mechanical

working or chemical etching (*e.g.,* reentrant grooves, 3-D discrete cavities, and open grooves with rectangular or triangular cross sections), involve thorough and systematic assessment of aging effect.

5.2. Micro-fin surfaces

5.2.1. Heat transfer trends

Patterning micro-fins on the heating surface not only increases heat transfer area (as with macro-fins), but also takes advantage of induced capillary flow and might aid in separating the paths of escaping vapor and replenishment liquid. These added benefits require proper configuring of micro-fin layout as well as optimization of the fin's width, height, and spacing. Micro-fin surfaces come in a variety of shapes, such as parallel vertical fins with rectangular cross-section (also called open micro-channels), parallel inclined fins (intended to trap vapor embryos), square fins, and cylindrical (pin) fins, as shown in Fig. 11.

Anderson and Mudawar [8] investigated the enhancement benefits of a broad variety of surfaces, including smooth, sanded, and vapor blasted, as well as surfaces modified with normal or inclined (vapor capturing) holes, and with normal and inclined (vapor capturing) rectangular sub-millimeter fins, and sub-millimeter square studs. Results for FC-72 showed that artificial cavities with diameters on the order of 0.3 mm were ineffective at lowering the incipience temperature. However, microstructures greatly enhanced nucleate boiling, shifting the nucleate boiling portion of the boiling curve toward lower superheats, albeit at the expense of increased incipience temperature drop and excursion. Anderson and Mudawar also reported that CHF for FC-72 was influenced by both surface microstructure and orientation, but independent of surface roughness or presence of large cavities. Most notably, a micro-stud surface yielded CHF values in excess of 50 W/cm^2, about three times that from a smooth surface. Follow-up work by Mudawar and Anderson [7] addressed effects of coolant type, system pressure, and liquid subcooling on boiling performance. While microstructured surfaces did improve both the nucleation boiling heat transfer coefficient and CHF, surface temperatures at higher heat fluxes exceeded 85 °C (maximum allowable electronic chip junction temperature around the mid-1980s). Mudawar and Anderson showed how using FC-87, whose saturation temperature at atmospheric pressure is 26 °C lower than that of FC-72, helped maintain surface temperature below 85 °C. Pressure effects were more complicated. Despite slightly improved nucleate boiling and CHF with increasing pressure, high pressure operation posed several practical challenges, including increased cost and weight of cooling chamber, and added complexity of electronic interconnect to devices contained in a pressurized chamber. On the other hand, they suggested that subcooling may be more beneficial than increased pressure, as much smaller bubbles and reduced bubble coalescence in the bubble layer adjacent to the surface, Fig. 12, might both provide better surface temperature uniformity for multi-device modules and delay CHF.

Honda et al. [149] investigated the effects of 50 × 50 × 60-μm^3 micro-fins and 25–32-nm roughness on boiling heat transfer from a silicon chip immersed in FC-72. The micro-fins were fabricated on a silicon chip using dry etching, while the submicron roughness was realized by sputtering a thin layer of SiO_2 on a silicon chip followed by wet etching the surface. Both the micro-pin-fins and submicron roughness were effective at enhancing both the nucleate boiling heat transfer coefficient and CHF. However, benefits of each enhancement technique were heat flux dependent: submicron roughness provided better nucleate boiling performance in the low flux region, while the micro-fins provided superior performance in the high flux region. Honda et al. also examined the influence of dissolved inert gas in FC-72. Presence of dissolved gas caused appreciable reduction in incipience temperature, which was caused by partial filling of cavities with gas embryos. However, because of eventual removal of the dissolved gas from cavities, nucleate boiling heat transfer performance in the high flux region was close to that for degassed FC-72. Somewhat similar findings were reported by O'Connor et al. [27] and You et al. [150], who also pointed out that boiling incipience in FC-72

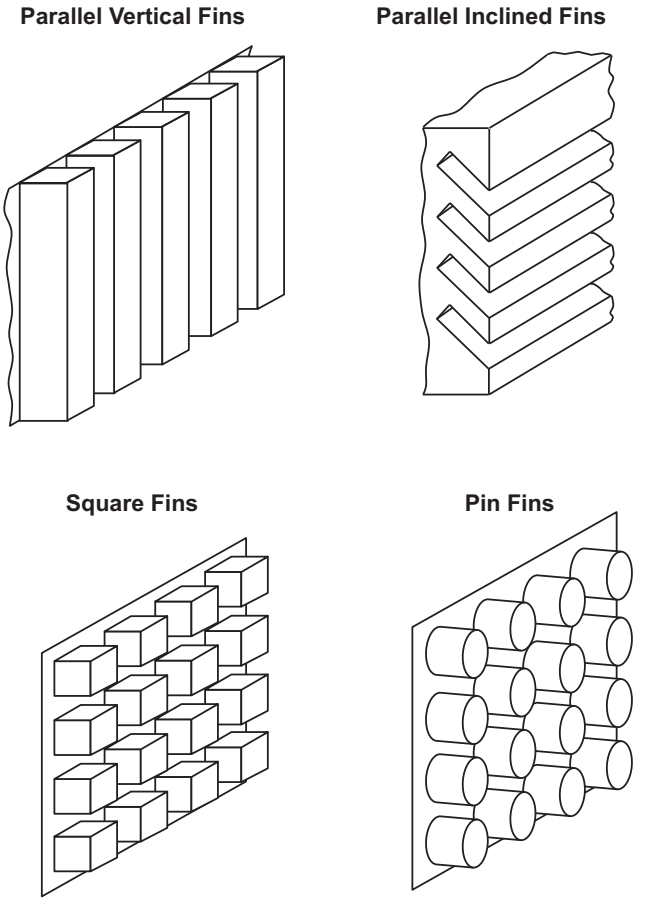

Fig. 11. Examples of micro-fin shapes used for boiling enhancement. Adapted from Anderson and Mudawar [7,8].

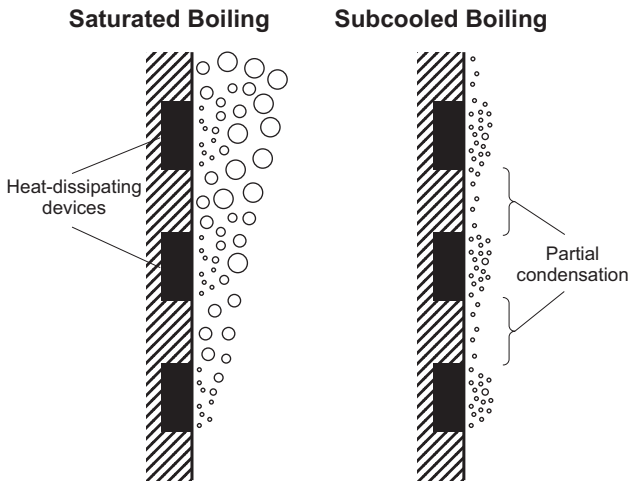

Fig. 12. Development of bubble layer along a multi-device module in saturated and subcooled pool boiling. Adapted from Mudawar and Anderson [7].

showed sensitivity to dissolved gas for concentrations exceeding 0.005 mol/mole. In follow-up to [149], Honda et al. [151] extended their findings to micro-fins with different widths but fixed height.

Kim et al. [152] used 'non-dimensional roughness,' defined as ratio of actual surface area with micro-fins to base area, to quantify effects of microstructure on boiling performance. By varying pin diameter, height, and inter-gap, they showed that the heat transfer coefficient for water increased with increasing non-dimensional roughness, by as much as 300% compared to that for a bare surface. CHF was also enhanced by up to 350%, limited by a critical inter-gap of 10–20 μm, exceeding which reduced the CHF enhancement. Based on experimental results, Kim et al. [153] suggested that CHF for microstructured surfaces was influenced by departure frequency of large bubbles formed by coalescence of smaller bubbles, and by ability of bulk liquid to continue feeding the surface macrolayer. Wei et al. [154,155] showed, for FC-72, that CHF for surfaces with square micro-fins increased with increasing fin height for a fixed fin width, while, for fixed non-dimensional roughness, CHF increased with increasing fin width [155]. They attributed the nucleate boiling enhancement to micro-convection effects and evaporation of superheated liquid in the gaps between fins. They also addressed the effects of surface orientation on boiling performance. For a smooth surface, vertical surface orientation yielded better performance in the nucleate boiling region but a slightly lower CHF than the horizontal orientation. On the other hand, the nucleate boiling heat transfer coefficient for the micro-finned surface was independent of orientation, and CHF for the vertical orientation was 20% lower than the horizontal.

One noteworthy observation from a study by Honda et al. [149] is that neither surface temperature nor bulk liquid temperature are uniform, and temperature uniformities might explain some of the discrepancies regarding extent of pool boiling enhancement among studies employing single point temperature measurements. As to improving ability to tackle high surface heat fluxes, Anderson and Mudawar [8], Honda et al. [149], and Wei et al. [154] all recommended using micro-fin surfaces in conjunction with subcooling.

Chu et al. [156] found that, for water, CHF for micro-fin surfaces increased with increasing non-dimensional roughness over a range of 1.79–5.94 for the latter. They modified an earlier model by Kandlikar [157] to better account of surface tension effects on the bottom of bubbles, and recommended the following relation for CHF for micro-fin surfaces,

$$q''_{CHF} = \frac{1+\cos\alpha}{16}\left[\frac{2}{\pi}\left(\frac{1+\alpha_m}{1+\cos\alpha}\right)+\frac{\pi}{4}(1+\cos\alpha)\cos\theta\right]^{1/2} \times \rho_g h_{fg}\left[\sigma g\left(\rho_f-\rho_g\right)/\rho_g^2\right]^{1/4}, \quad (9)$$

where r^+ is non-dimensional roughness, α liquid's contact angle on a smooth surface, α_{rec} liquid's receding angle on a smooth surface, and α_m modified contact angle on a micro-fin surface; the latter was related to non-dimensional roughness according to

$$\alpha_m = r^+\cos\alpha_{rec}. \quad (10)$$

By accounting for capillary wicking force and modifying the critical wavelength for interfacial instability, Quan et al. [158] recommended the following analytical CHF relation for micro/nanostructures,

$$q''_{CHF} = \frac{1+\cos\alpha}{16}\left[\frac{2}{\pi}(1-\sqrt{\varphi_s})^{-1/2}\left(\frac{r^+ +\cos\alpha}{1+\cos\alpha}\right) +\frac{\pi}{4}(1-\sqrt{\varphi_s})^{1/2}(1+\cos\alpha)\cos\theta\right]^{1/2} \times \rho_g h_{fg}\left[\sigma g\left(\rho_f-\rho_g\right)/\rho_g^2\right]^{1/4}, \quad (11)$$

where φ_s is the solid fraction, defined as ratio of cross-sectional area of enhancement structure to base area of heating surface.

Mitrovic and Hartmann [159] developed a novel micro-fin structure consisting of cylindrical fins with spherical tips using an electro-coating process. Using R-141b, they showed that wall superheat remained fairly constant with increasing heat flux. Zhang and Lian [160] explored performance variations in water for in-line square fin configurations with fixed 200-μm width and 35-μm height resulting from changes in fin spacing over a range of 200–1000 μm, and showed that the 200-μm spacing yielded the best boiling performance. Kim et al. [161] achieved superior boiling performance for PF-5060 on surfaces treated by sanding, micro-finning, and micro-particle coating when the surface was tilted at 45° compared to both horizontal and vertical orientations.

It should be noted that the rectangular micro-fin surface employed by Anderson and Mudawar [8] is commonly referred to as 'open micro-channel' surface since it is formed by cutting micro-channels into a conducting substrate. This surface offers several important advantages, especially increased surface area and routing of liquid through the channels to surface regions vacated by escaping bubbles. This concept has received increased attention in recent years. Cooke and Kandlikar [162] confirmed the effectiveness of etched open micro-channel surfaces at enhancing nucleate boiling for water. Follow-up study by Cooke and Kandlikar [163] employed a variety of micro-channel widths and depths, and fin thicknesses, and found that optimum heat transfer enhancement was achieved by increasing channel width and depth and decreasing fin thickness, a combination of which, in addition to the liquid channeling, facilitated bubble nucleation at lower wall superheats, and increased both bubble departure diameter and vapor generation rate. While their experiments did not reach CHF, the best performing surface was capable of dissipating 244 W/cm^2, with a corresponding nucleate boiling heat transfer coefficient of 269 kW/m^2 K, for water at atmospheric pressure. In a separate study, Kalani and Kandlikar [164] safely achieved over 90 W/cm^2 with ethanol while maintaining surface temperatures well below 85 °C at 33 kPa pressure.

Gheitaghy et al. [165] reported that open micro-channels (formed by wire cutting) inclined at 45° relative to the surface provided better performance in water than normal micro-channels, and the enhancement improved with increasing channel depth and decreasing channel pitch. Das et al. [166] employed open micro-channels with different reentrant pocket geometries at the channel's embedded end: curved, rectangular, and circular, of which the circular geometry provided the highest nucleate boiling heat transfer coefficient for water. Additionally, they achieved better enhancement with inclined than normal channels. Fig. 13(a) shows schematics of inclined channels with and without circular end pockets. Follow-up study by Das et al. [167] showed optimum performance is achieved with a 45° channel angle, as shown in Fig. 13(b).

5.2.2. Using micro-fin surfaces to separate vapor and liquid paths

As discussed earlier, a major factor to CHF development is blockage of the path of replenishment liquid by the escaping vapor. Mukherjee and Mudawar [77] provided arguably the most effective means for separating the two paths using the concept of two parallel-tube 'pumpless loop' depicted in Fig. 6(a). While path separation with this method is more global (loop-based), other investigators have attempted to achieve path separation on a more localized basis by using micro-finned surfaces.

One such example is a micro-fin surface developed by Kandlikar [168] in which the fin base was modified with sharp corners to promote localized nucleation, and as bubbles moved along the base, they induced bulk liquid to flow over the fins toward the

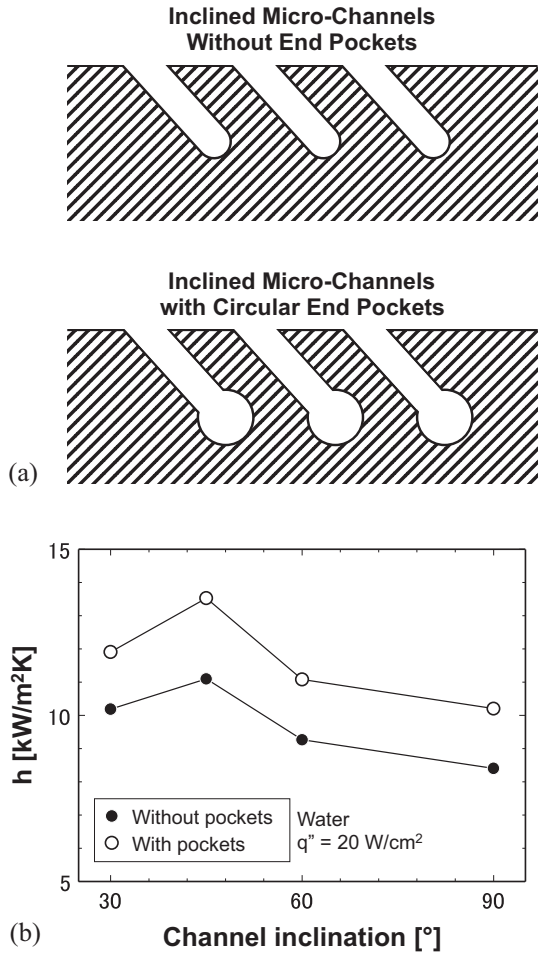

Fig. 13. (a) Schematics of inclined open micro-channels with and without circular end pockets. (b) Effects of channel inclination on heat transfer coefficient for water at 20 W/cm^2. Adapted from Das et al. [167].

nucleation corners. They demonstrated 8-fold enhancement in the nucleate boiling heat transfer coefficient and 2.5-fold in CHF compared to a smooth copper surface, using water as coolant. Using a somewhat similar concept, Rahman et al. [169] achieved enhancements in nucleate boiling heat transfer coefficient and CHF for water by creating alternating rows of low-conductivity epoxy separating rows of bare high conductivity copper substrate. This technique produced spatial variations in surface temperature during boiling. By adjusting wavelength of these variations to coincide with capillary length, the nucleate boiling heat transfer coefficient and CHF for water were increased by more than 5-fold and 2-fold, respectively. Fig. 14 illustrates the role of wavelength at achieving ordered separation between the paths of escaping vapor and replenishment bulk liquid. More recently, Jaikumar and Kandlikar [170] also adopted the concept of alternating nucleating and non-nucleating surface regions. The non-nucleating regions were modified to channel liquid to the nucleating regions, which also induced strong convective mixing over the non-nucleating regions. Optimum performance for water was achieved with 0.5-mm wide nucleating regions separated by 2.125-mm wide non-nucleating regions, the latter being closely related to both bubble departure diameter and critical capillary length.

5.3. Permanent microporous coatings

Unlike the use of porous layer attachments, porous microstructures could also be formed by permanently coating the surface.

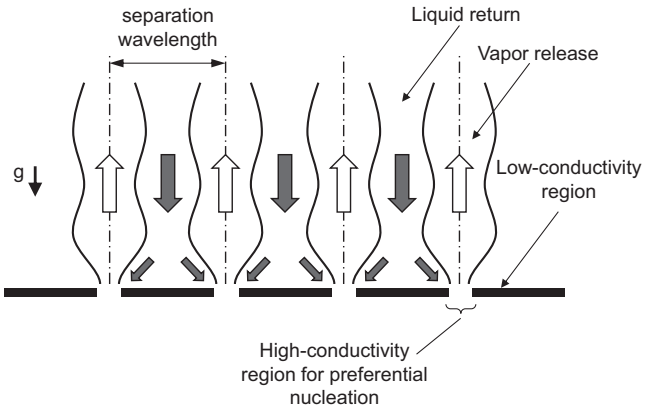

Fig. 14. Use of preferential nucleation and ordered bubble release to enhance nucleate pool boiling heat transfer by separating vapor and liquid paths.

Microporous coatings can be fabricated in a variety of ways, including welding, sintering or brazing of particles, electrolytic deposition, flame spraying, bond-plating of particles, galvanizing, polymer plasma spraying, and metallic coating of foam substrate [171]. The primary purpose of all these coatings is to produce a matrix of potential nucleation cavities. Borzenko and Malyshenko [172] also reported porous structures provide added thermal stability to the cooling system. As reported by Liter and Kaviany [173], the enhancement achieved with microporous coating is the combined outcome of increased surface area, capillary-assist liquid supply, increased nucleation site density, and preferential routing of released vapor.

You et al. [174] employed a particle layering method to enhance pool boiling heat transfer, which consisted of sputtering a flat heating surface with 0.3–3 μm Al_2O_3 particles, capitalizing upon the adhesion provided by molecular van der Waals forces. O'Connor and You [175] later developed a boiling enhancement paint containing 3–10 μm silver flakes in epoxy binder, which produced a thin porous microstructure with ~1 μm surface cavities. O'Connor et al. [176] combined the spray method of You et al. and painting method of Connor and You to produce an electrically non-conducting surface microstructure containing 0.3–5 μm Al_2O_3 and 1–3 μm or 8–12 μm diamond particles. This combined technique yielded CHF values for 45 °C subcooled FC-72 as high as 159 W/cm^2. Chang and You [177] assessed the nucleate boiling heat transfer performance of microporous surfaces coated with 1–50 μm copper particles and 1–20 μm aluminum particles. They achieved 80% reduction in incipient superheat in FC-72, and increased the nucleate boiling heat transfer coefficient and CHF by 330% and 100%, respectively. Furthermore, the heat transfer coefficient for the microporous surface was independent of surface orientation, a conclusion also shared by Rainey and You [178] in regards to 8–12 μm diamond particle coating. Follow-up study by Chang and You [179] optimized coating composition by varying both components and mixing ratio; they also examined physical strength of the coating through durability and adhesion tests. Rainey et al. [180] pointed out that effects of dissolved gas on nucleate boiling heat transfer are generally small. Kim et al. [181] investigated the boiling enhancement mechanisms of microporous coatings in FC-72. They reported that, at low heat fluxes below 12 W/cm^2, activation of normally dormant nucleation sites amounted to greater contribution of latent heat to the overall heat transfer process. On the other hand, heat fluxes exceeding 12 W/cm^2 reduced the amount of superheated liquid on the surface, which also reduced the latent heat contribution. In a more recent study, Kim et al. [182] improved the painting method

developed earlier by O'Connor and You, using metal solder to replace epoxy. This coating method broadened the operating nucleate boiling heat flux range significantly, especially when using water as coolant.

Jun et al. [183] investigated pool boiling for a copper surface that was coated with sintered copper particles, and achieved optimum microporous coating thicknesses of 78, 94, and 296 μm for 10, 25, and 67 μm particle sizes, respectively. Better enhancements in both the nucleate boiling heat transfer coefficient and CHF were achieved by increasing particle size from 10 to 25 μm, while benefits of increasing particle size from 25 to 67 μm were relatively minor. For water, the highest heat transfer coefficient of 400 kW/m^2 K and CHF of 210 W/cm^2 were achieved with 67-μm particles; these values were, respectively, eight fold and two fold of those for a plain surface. Additionally, changing orientation of the microporous surface from horizontal upward-facing to vertical had only minor effects on CHF, however, CHF decreased significantly for the horizontal downward-facing orientation [184]. Follow-up study by Jun et al. [185] addressed boiling performance for microporous surfaces achieved by brazing ~25-μm copper particles to coating with thicknesses of 49–283 μm. Shown in Fig. 15(a) is a comparison of microporous structures using soldered versus brazed copper particles. As shown in Fig. 15(b) for the brazed coatings in water, Jun et al. employed coating thickness to distinguish three different heat transfer regimes: (1) microporous regime, wherein both heat transfer coefficient and CHF increased with increasing coating thickness, (2) microporous-to-porous transition regime, in which CHF continued to increase with increasing coating thickness, while the heat transfer coefficient increased only at lower heat fluxes but decreased at higher heat fluxes, and (3) porous regime, in which both the heat transfer coefficient and CHF decreased with increasing coating thickness.

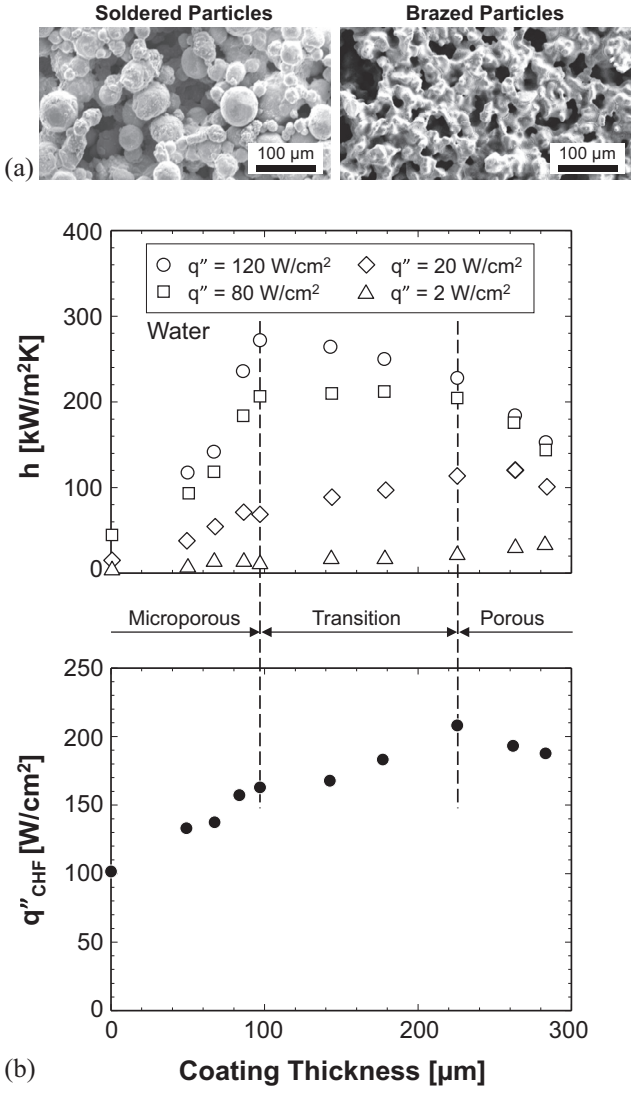

Fig. 15. (a) Comparison of microporous structures using soldered versus brazed copper particles. (b) Variations of heat transfer coefficient and CHF for water with brazed microporous coating thickness. Adapted from Jun et al. [185].

Bergles and Chyu [171] investigated porous structures formed by brazing copper powder onto a copper substrate, which resulted in a 0.38-mm coating with 50–65% porosity. They observed boiling incipience excursion in the highly wetting R-113, the extent of which was strongly dependent on surface aging, subcooling, and the manner in which heat flux was changed (continuously or stepwise). Hwang and Kaviany [186] examined thin, uniform porous coatings containing 40–80 μm copper particles with coating thicknesses of 3–5 particle diameters. They demonstrated significant improvement in the nucleate boiling heat transfer coefficient for pentane, along with 80% enhancement in CHF.

Chang and You [187] investigated the effects of diamond particle size and coating thickness on boiling enhancement in FC-72. For coatings thinner than the liquid layer along the surface, the latter estimated using one-dimensional transient thermal conduction premises, active nucleation site density increased with increasing particle size. However, for coatings thicker than the liquid layer, larger particles exhibited better enhancement at relatively low heat fluxes, and smaller particles at high fluxes. In an earlier study, Webb [188] reported that nucleate boiling performance of copper microporous surfaces in R-11 was weakly dependent on particle size for coating thicknesses in the range of three to four particle diameters. Sarangi et al. [189] explored the effects of copper particle size over a range of 45–1000 μm on pool boiling of FC-72. They employed coatings comprised of both loose and sintered particles, with coating thickness about four times the particle diameter. For both loose and sintered coatings, 100-μm particles yielded highest values of the nucleate boiling heat transfer coefficient, though this same size compromised CHF compared to that for a bare surface. Follow-up study by Sarangi et al. [190] showed that use of irregular particles yielded higher nucleate boiling heat transfer coefficients for FC-72 than spherical particles with uniform coating porosity. They also suggested that the heat transfer coefficient and CHF were strongly influenced by coating porosity, pore diameter, unit necking area, unit interfacial area, effective thermal conductivity, and effective permeability.

Scurlock [191] suggested existence of optimum thickness for aluminum and aluminum/silicon porous layers when aiming for maximum heat transfer coefficient in nitrogen, argon, oxygen, and R-12. Using copper coating with thickness of 100–700 μm, Thiagarajan et al. [192] reported that increasing coating thickness improved heat transfer performance at low heat fluxes, while decreasing the coating thickness enhanced CHF. Moreno et al. [193] reported enhancements of heat transfer coefficient of over 300% and CHF up to 120% for HFO-1234yf using copper microporous coating. They also found that increasing pressure compromised the heat transfer coefficient but increased CHF. Byon et al. [194] studied copper bi-porous sintered coatings, defined as having two distinct pore sizes. They showed that CHF for FC-72 was influenced by ratio of particle to cluster size, achieving maximum CHF for a ratio of 0.15, independent of coating thickness.

Nishikawa and Ito [195] developed an empirical correlation for the nucleate boiling region for R-113, R-11, and benzene from surfaces coated with copper and bronze particles.

$$\frac{q''\delta}{\Delta T_{sat}k_m} = 0.001\left(\frac{\sigma^2 h_{fg}}{q''^2\delta^2}\right)^{0.0284}\left(\frac{\delta}{q_p}\right)^{0.56}\left(\frac{q''d_p}{\varepsilon h_{fg}\mu_g}\right)^{0.593}\left(\frac{k_f}{k_m}\right)^{0.708} \times \left(\frac{\rho_f}{\rho_g}\right)^{1.67}, \quad (12)$$

where δ, d_p, and ε signify matrix (coating) thickness, particle diameter, and matrix porosity, respectively. The thermal conductivity of matrix, k_m, is a function of liquid conductivity, k_f, particle conductivity, k_p, and porosity,

$$k_m = k_f + (1-\varepsilon)k_p, \quad (13)$$

Equation (12) is applicable to $0.1 < d_p < 1$ mm, $1.6 < \delta/d_p < 20$, and $0.38 < \varepsilon < 0.71$.

By assuming that each pore in a porous surface contains a vapor bubble surrounded by spherical particles and acts as an active nucleation site, O'Neil et al. [196] proposed a simple heat transfer model for porous enhanced surfaces in a variety of fluids,

$$\Delta T_{sat} = \frac{\beta q'' r^2}{k_f} - \frac{2\sigma}{(dP/dT)r}, \quad (14)$$

where β is a geometrical factor that accounts for type of packing and density of active nucleation sites, and r pore radius. Follow up work by Czikk and O'Neill [197] classified porous surface pores into four different categories: (a) active or reentrant pores that always contain vapor bubbles, (b) intermittent pores that contain vapor supplied from surrounding interconnected active pores, (c) liquid-filled pores, and (d) nonfunctional pores. However, Webb [188] argued that the 'static' model represented by Eq. (14) did not satisfy requirements for a stable cavity, and suggested the model be modified to account for dynamic considerations as well as differences in interfacial phenomena associated with different pore categories.

Liter and Kaviany [173] devised a novel type of sintered copper 'modulated' porous-layer coating with periodically non-uniform thickness, which separated the liquid and vapor phases, thus reducing liquid-vapor counterflow resistance adjacent to the surface. Construction of this coating is depicted in SEM images in Fig. 16. This surface enhanced CHF for pentane by nearly three times over that of a plain one, better than previously reported enhancement values [179,198,199]. Liter and Kaviany proposed two different limits for CHF when using this coating: (a) hydrodynamic limit, based on Zuber's hydrodynamic theory [41–43], by accounting for coating modulation wavelength, and (b) viscous-drag limit, in which viscous drag surpassed capillary pumping capability, and suggested pool boiling CHF would correspond to the lower of the two limits. Min et al. [200] and Cora et al. [201] employed a hot-powder compaction technique to produce 2-D and 3-D modulated coatings similar in structure to those developed by Liter and Kaviany. Stacked porous structures were also investigated by Ji et al. [202].

Li et al. [203,204] employed a sintered modulated porous structure consisting of copper particles formed into four 3-mm diameter and 3.6-mm tall porous pillars atop a 0.55-mm thick porous base. They achieved nucleate boiling heat transfer coefficient and CHF values for water as high as 200 kW/m^2 K and 450 W/cm^2, respectively, several times better than from a bare surface. They explained the enhancement by ability of the surface structures to delay onset of hydrodynamic instability and promote efficient capillary pumping of liquid in both the horizontal and vertical directions. Furthermore, using smaller particles in the porous base yielded higher CHF independent of structure of the pillars. Follow-up study by Li [205] extended heat transfer enhancement findings concerning modulated porous cones atop a porous base.

Cieśliński [206] reported that, for a given porous coating material, provided the coating maintained good metal contact with the substrate, the main parameters contributing to boiling heat transfer enhancement were coating thickness and porosity, regardless of the coating technique used. For certain porous coatings, they observed a drop in wall superheat with increasing heat flux when approaching CHF. This phenomenon, which they termed 'inversed boiling crisis,' was attributed to liquid suction in the coating that extended the period of macrolayer evaporation and therefore delayed CHF.

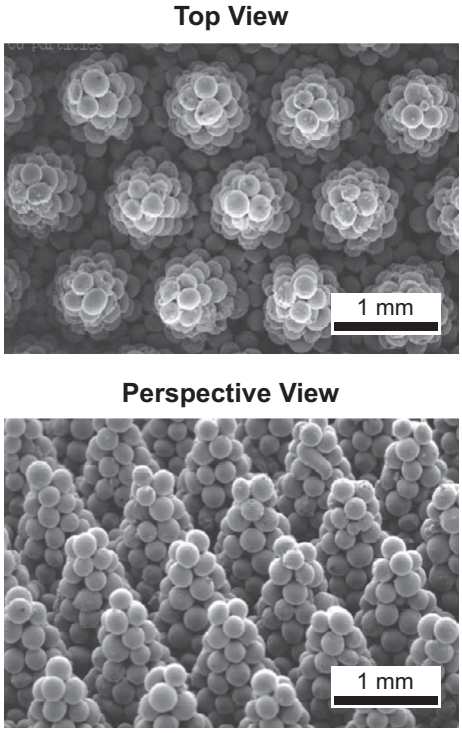

Fig. 16. SEM images of single height sintered modulated porous coating consisting of copper particles arranged into porous cones atop polished base. Adapted from Liter and Kaviany [173].

Jaikumar et al. [207] and Protich et al. [208] investigated heat transfer enhancement with surface microstructures containing a combination of graphene oxide and 15-μm copper particles. Three different techniques, screen-printing, chronoamperometry electrodeposition, and galvanostatic electrodeposition, were employed to produce these microstructures. Nucleate boiling heat transfer coefficient for water was improved by a combination of increased number of active nucleation sites and formation of wicking dendritic structures. CHF was also enhanced because of improved wettability resulting from increased surface roughness and formation of the dendritic structures.

It should be noted that the boiling curves for water presented in Jaikumar et al. [207] displayed a 'boiling inversion' behavior similar to that captured by Cieśliński [206] for water, wherein an increase in heat flux ultimately precipitated a decrease in wall superheat. Illustrated in Fig. 17, this phenomenon was also observed in studies of open micro-channel surfaces [170,209]. Jaikumar et al. attributed this abnormal phenomenon to vapor streams emanating from discrete regions of the surface inducing counterflow of liquid impinging upon non-boiling regions [210]. Using a femtosecond laser, Kruse et al. [211,212] produced self-organized mound-like microstructures on metallic surfaces. They also observed the boiling inversion phenomenon in water, which they referred to as 'secondary boiling effects' and attributed to temperature drop along the microstructures. While the boiling inversion phenomenon is closely associated with certain surface

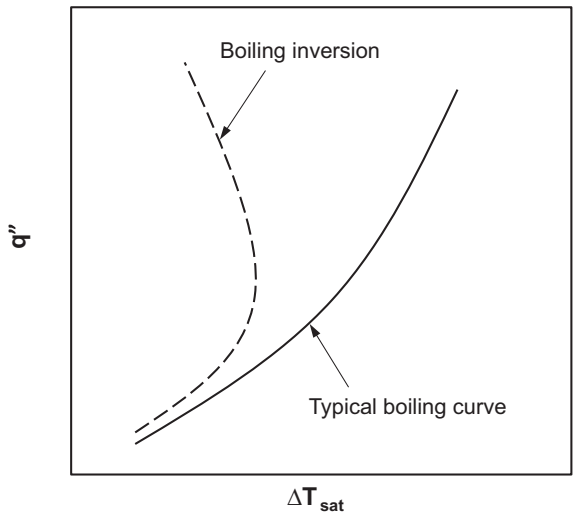

Fig. 17. Schematic of boiling inversion achieved with water boiling on microporous surface [210].

microstructures, further research is needed to uncover its underlying mechanisms in a more comprehensive manner.

Li and Peterson [213,214] reported that overall heat transfer performance and boiling patterns were strongly dependent on geometrical parameters of a porous coating, including coating thickness, volumetric porosity, and mesh size. They postulated that heat from the substrate was first conducted through the skeleton of the porous structure, then transferred to liquid within the structure through convection, and finally dissipated on the porous surface by boiling or evaporation. This sequence implies that a porous coating with higher thermal conductivity could enhance boiling performance, especially at the low heat fluxes. Li and Peterson proposed a list of mechanisms responsible for the heat transfer enhancement, including increased wetted area, increased nucleation site density, and intensified interaction among bubbles, as well as film evaporation and capillary action induced within the porous structure. Li et al. [215,216] developed a sintering process involving multiple uniform layers of isotropic copper mesh, which helped minimize thermal contact resistance between the heating surface and porous structure. They demonstrated the effectiveness of this process by achieving values for nucleate boiling heat transfer coefficient and CHF for water as high as 245.5 kW/m^2 K and 367.9 W/cm^2, respectively. The heat transfer coefficient showed strong dependence on mesh size, but much weaker dependence on porous layer thickness or porosity. On the other hand, CHF increased with increasing thickness and was also strongly influenced by both porosity and mesh size.

Chen et al. [217] reported significant enhanced wetting with microporous wicking structures with the shape of waffle and half-ladder, but did not test boiling performance. Jung et al. [218] showed experimentally that, when using highly-wetting fluids, large pores and channels in the microporous coating could easily be flooded with liquid at low heat fluxes, causing difficulties initiating bubble nucleation. But, once the superheat became high enough to activate the surface pores, rapid transition to vigorous boiling ensued, especially for surfaces with high porosity. Kubo et al. [219] reported that incipience superheat for FC-72 was strongly dependent on dissolved gas content, but independent of cavity size.

5.4. Surfaces with tunnels and reentrant cavities

Nakayama et al. [220] devised a boiling enhancement scheme, Fig. 18, that consisted of first gouging the heat dissipating surface

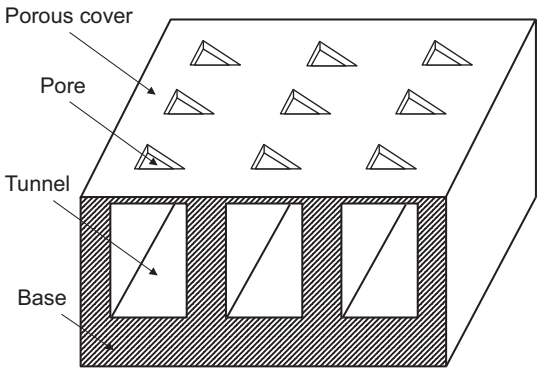

Fig. 18. Schematic of tunneled surface with microporous cover.

with 0.25-mm wide and 0.4-mm deep parallel rectangular tunnels, and then covering the tunnels with a thin copper plate having rows of 50 to 150-μm pores. Using this technique, boiling curves for R-11 exhibited trends that were determined mostly by diameter and population density of the pores. Nakayama et al. proposed three modes for boiling behavior with this surface. The first was 'dried-up mode', where tunnels were filled with vapor, and boiling took place outside the tunnels in a manner similar to that from a plain surface having regularly spaced artificial nucleation sites. The second 'suction-evaporation mode' referred to conditions where bubble release from active pores caused liquid to be sucked through inactive pores into the tunnels, from which it spread and evaporated, providing the best heat transfer performance of all three modes. The third 'flooded mode' corresponded to conditions were most of the tunnels were occupied by liquid, and an active pore acted as an isolated nucleation site. It should be noted that the suction-evaporation mode was also reported in earlier studies by Nakayama et al. [221,222], and provided a foundation for detailed models by Chien and Webb [223] and Das et al. [224] for boiling heat flux and bubble frequency for the same enhancement technique. Jiang et al. [225] developed a different heat transfer model for the Nakayama et al. enhancement technique based micro film evaporation and two-phase flow inside the microstructure, which they used to optimize microstructure dimensions. Murthy et al. [226] provided analysis for the flooded mode, which was based on interaction of fluid dynamic forces, to predict bubble departure diameter.

Chien and Webb [227,228] examined the boiling process for R-123 and methanol on the tunneled surface with surface pores, and proposed that bubble frequency and nucleation site density were controlled by vaporization occurring at menisci in tunnel corners, an observation also shared by Arshad and Thome [229]. Chien and Webb [230] also reported that tunnels with larger height, smaller pitch, and sharper corners provided better boiling enhancement. In another study, they provided further details concerning effects of pore size and pitch [231]. Ramaswamy et al. [232] examined the boiling process for FC-72 on a microporous surface with a design somewhat similar to that of Nakayama et al. [220]. However, the surface developed by Ramaswamy et al. used wafer dicing and wet etching, resulting in a network of interconnecting micro-channels. Experimental observations aided development of a semi-analytical model, which they used to predict bubble departure diameter and frequency, and nucleation site density for this structure [233]. Ghiu and Joshi [234] showed that heat transfer performance for PF-5060 was improved by increasing channel width and pore size from 65 to 105 μm and decreasing channel pitch and pore pitch from 0.2 to 0.7 mm. They also suggested that contribution of internal evaporation to total heat dissipation was significant, especially at low heat fluxes

[235]. Ramaswamy et al. [236] studied the effects of using multiple tunneled layers instead of a single layer. Nucleate boiling heat transfer for water improved with increasing number of layers only in the low superheat (4–6 °C) and high superheat (25–30 °C) regions, but there was little difference in performance between a three-layer stack and a single-layer around 10 °C superheat, corresponding to the beginning of fully developed boiling. Wang et al. [237] and Hao et al. [238] employed shape memory titanium-nickel alloy to fabricate a deformable interconnected microchannel structure, the shape of which could change during the boiling process; this technique yielded better nucleate boiling performance in ethanol than both closed and open microstructures.

Phadke et al. [239] showed that a surface with an array of pyramidal reentrant cavities was capable of reducing incipient superheat and incipience temperature drop for R-113 substantially. Nimkar et al. [240] identified an optimum inter-cavity spacing for pyramidal reentrant cavities for best nucleate pool boiling heat transfer performance in FC-72. Zhang and Shoji [241] and Calka and Judd [242] recommended using ratio of cavity spacing to average bubble departure diameter to demarcate different bubble interaction regions. Chatpun et al. [243] showed that an in-line cavity pattern provided better boiling performance than a triangular pattern with the same cavity spacing. Moita et al. [244] emphasized the importance of bubble dynamics and bubble interaction for pool boiling enhancement, noting that improper control of these parameters might result in large bubbles with strong vertical and/or horizontal coalescence and eventual vapor blanket formation. Teodori et al. [245] used PIV measurements to prove the existence of an optimal cavity pattern that balanced the positive effects of promoting activation of nucleation sites and negative effect of horizontal coalescence of bubbles. Yu et al. [246] showed that a larger number of cavities per unit area were beneficial to nucleate boiling of FC-72.

Messina and Park [247] examined the effects of shallow pits with depth-to-diameter ratios of 0.03–0.145 formed into a copper surface, and showed that even the shallowest pits could serve as effective nucleation sites. Furthermore, boiling heat transfer improved with increasing pit density up to maximum limit, above which performance became independent of pit density. Das et al. [248] tested copper surfaces having 600-μm diameter holes, and showed improvement in boiling performance for water when increasing hole pitch over a range of 5 to 10 mm. Hutter et al. [249] used chemical etching to create artificial cavities with 10-μm diameter and depths of 40 to 100 μm to enhance pool boiling in FC-72. Fukada et al. [250] attributed the CHF enhancement achieved with porous structure produced by fouling to enhanced wettability and nucleation site density.

5.5. Dendritic porous structures

Li et al. [251] and Furberg and Palm [252] used a rather simple electrodeposition technique with in-situ grown dynamic gas bubble templates to produce dendritic, microporous structures on copper surfaces. They reported up to 17 times enhancement in nucleate boiling heat transfer coefficient for R-134a and FC-72 compared to a plain surface [251]. Later, Patil et al. [253] used electrodeposition with hydrogen bubbles as templates but incorporated a two-step surface preparation technique involving application of high current density for a short duration, followed by lower current density for a longer duration, which improved control of pore size and porous layer thickness, resulting in appreciable enhancement in nucleate boiling performance for water. Gheitaghy et al. [254] used electrodeposition to produce surfaces with open and interconnected pores, covered with different-sized micro-grains. By increasing electrolyte temperature, they showed how grain shape could be changed from rounded to angular, with increased mechanical stability. Xu et al. [255] devised a composite porous surface using an electrochemical technique, which was strengthened further by sintering. This method resulted in a surface with 200 and 2-μm diameter pores, and 400-nm diameter internal dendritic structures. Xu et al. demonstrated effectiveness of this surface at enhancing CHF for water.

El-Genk and Ali [256–258] investigated pool boiling enhancement of PF-5060 on microporous copper surfaces prepared using the two-stage electrodeposition, and measured an increase in CHF as the porous layer thickness was increased from 80 to 230 μm [44]. Fig. 19 shows SEM images of the microporous copper surface layer at different magnifications. The basic dendrite structures and layer thickness were achieved during the first stage of deposition, which involved supplying current at a density of 3 A/cm^2 for a short duration, typically from 15 to 44 s, depending on desired thickness. This first stage resulted in a surface with high porosity (over 90%) and ordered arrangement of open macro-pores surrounded by dense, but fine and branching dendrites. The microstructure was structurally strengthened in the second stage by further electrochemical deposition but using much lower current density over a longer duration of 100 s. During the second stage, the layer thickness remained virtually unchanged, but the dendrite microstructure became masked with clusters of microparticles, and some of the pores were also filled with particles. These changes were reflected in reduced porosity (65–80%) and increased wetted surface area. A summary of pool boiling enhancement findings by El-Genk and co-workers for dielectric fluids (FC-72, HFE-7100, and PF-5060) on porous graphite, microporous, and macro-finned copper surfaces can be found in [259].

5.6. Other types of microstructured surfaces

5.6.1. Surfaces with dimples

Using surfaces with microstructures consisting of hexagonal dimples and rectangular trenches, Wright and Gebhart [261,262] achieved heat fluxes for water 4.2 and 3.1 times, respectively, those for a plain surface. Miller et al. [263] studied the effects of pre-boiling history on incipience excursion for FC-72 from a surface featuring an array of 9.4-μm diameter and 3.3-μm tall hexagonal dimples. They concluded that incipience excursion was independent of immersion time provided the surface was carefully degassed, and might be even avoided if a large number of stable vapor filled cavities were retained on the surface. The ability of the surface to provide effective vapor retention depended on both feature size and geometry of the enhanced surface. El-Genk and Suszko [264] experimented with surfaces modified with circular dimples that were 200-μm deep and with diameters of 300, 400, and 500 μm, arranged in a triangular pattern with pitch-to-diameter ratio of 2. For PF-5060, the 400-μm diameter dimples yielded the highest nucleate boiling heat transfer coefficient of 10.6 kW/m^2 K and CHF of 19.3 W/cm^2.

Holguin et al. [265] devised a binary surface consisting of numerous micro/nano cavities filled with a non-boiling liquid (*e.g.*, water), which created puddles around solid islands, to assist nucleate boiling of the primary working fluid (*e.g.*, dielectric fluid PF-5060). Presence of immiscible non-boiling liquid in the puddles was found to provide the combined benefits of aiding bubble departure from the solid island, resisting bubble coalescence, and assisting surface re-wetting. A binary copper surface with water puddles provided 7.5 times enhancement in average heat transfer coefficient for PF-5060, and 2.2 times CHF improvement. However, performance of this binary surface was limited by saturation temperature of the non-boiling liquid, exceeding which the non-boiling liquid would begin to boil and be depleted from the heating surface.

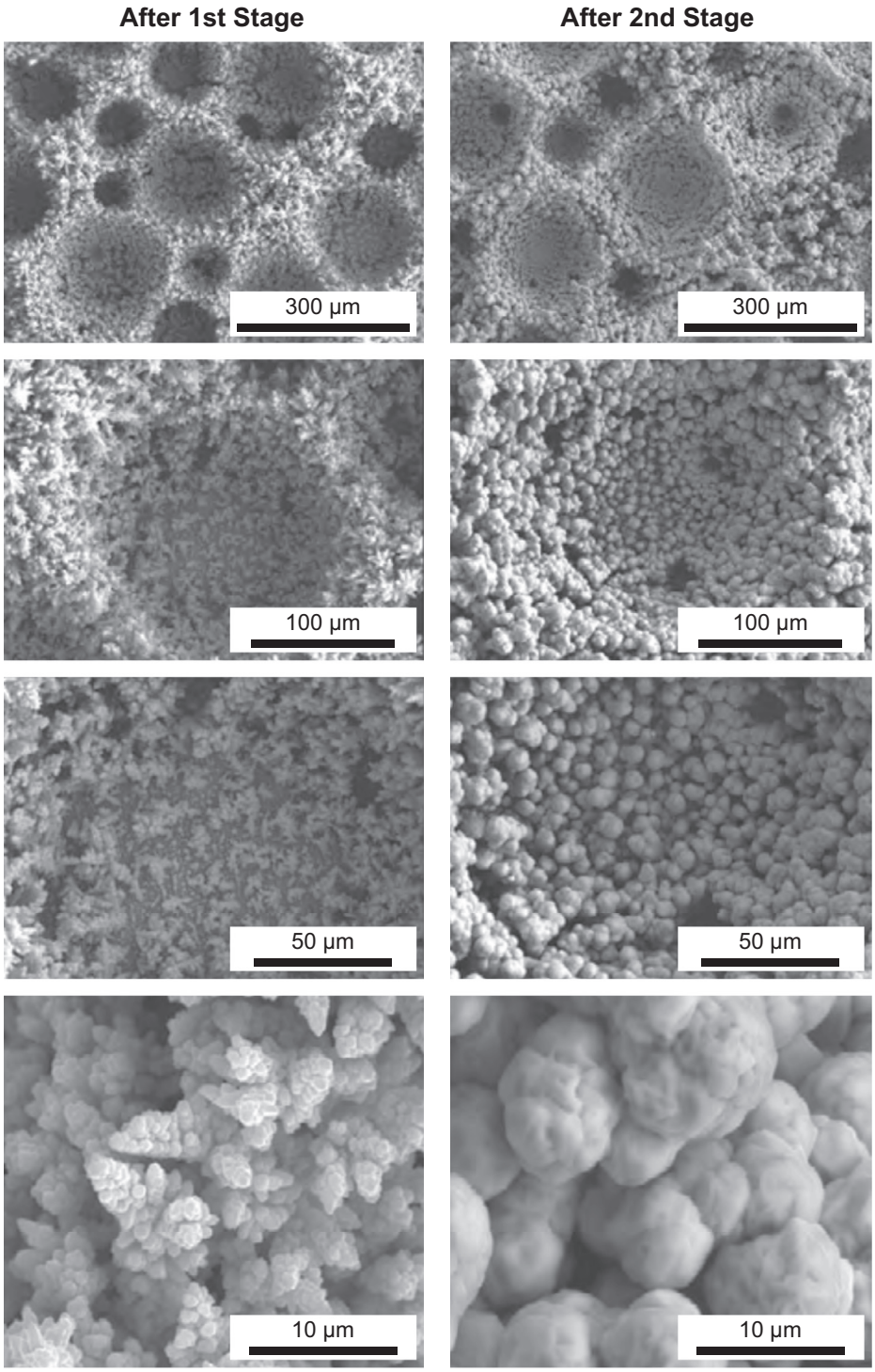

Fig. 19. SEM images at different magnifications for a 197.4-μm thick copper microporous surface layer fabricated using two-stage electrodeposition. Shown are dendrite structures masked with clusters of micro-particles. Adapted from El-Genk and Ali [260].

5.6.2. Surfaces with graphite coating

El-Genk and Parker [266] investigated boiling enhancement in HFE-7100 using commercial porous graphite surfaces. Compared to incipience excursion of over 30 °C on a smooth surface, the porous graphite surface eliminated the excursion by trapping large amounts of air in surface pores and reentrant cavities. At 10 °C surface superheat, the nucleate boiling heat flux for this surface was 16 times higher than for a smooth surface, however, performance deteriorated rapidly with increasing wall superheat. And, CHF was 60% higher, and was reached at 25% lower wall superheat compared to a smooth surface. Parker and El-Genk [267,268] also did not encounter any incipience excursion when testing the same surface in FC-72 at different orientations. Follow-up study by El-Genk and Parker [269] compared boiling performances of FC-72 and HFE-7100 on the porous graphite surface. CHF increased linearly with increasing liquid subcooling but at a rate ~10% higher for HFE-7100 than for FC-72. However, maximum nucleate boiling heat transfer coefficient, which occurred at or near the upper limit

of the fully developed nucleate boiling region, was 57% higher for FC-72 than that for HFE-7100, and increased linearly with increasing subcooling for both fluids.

Seo et al. [270] compared CHF for FC-72 from four different highly hydrophilic surfaces: a nonporous graphene layer-deposited surface, a nonporous SiC layer-deposited surface, a porous graphene layer-deposited surface, and a SiC layer-deposited surfaces, using indium tin oxide (ITO) surface as substrate. Compared to a plain ITO surface, CHF values for these surfaces were, respectively, 9%, 15.7%, 90%, and 58% higher. These differences were attributed to heat dissipation limits, dictated by thermal properties of graphene and SiC, and both hydrodynamic and capillary pumping limits associated with surface morphology and porous structure. Jaikumar et al. [271] reported boiling enhancement of water using copper surfaces that were first dip coated in a carbon tetrachloride and water solution containing graphene oxide and graphene to produce inner microstructures, followed by chemical vapor deposition (CVD) to create nanoscale coating [272]. They identified important mechanisms associated with these nano/microscale graphene oxide/graphene coatings, including contact angle hysteresis, and microlayer evaporation partitioned by protruding ridges.

Overall, aside from increasing liquid-solid contact area, a major purpose of microscale surface modification is to enhance nucleate boiling heat transfer coefficient by increasing active nucleation site density. A major drawback to certain surface fabrication techniques, including sintering, flame spraying, and mechanical milling and/or drilling, is potential damage to the substrate, which may not be permissible for temperature and vibration sensitive devices. Another drawback associated with enhancement schemes involving dissolved gas inclusion in liquid is difficulty in maintaining fluid stability and desired concentrations at the system level. Despite these shortcomings, techniques that separate vapor and liquid paths in pursuit of higher CHF, including modulated microporous structures and use of pumpless loops, warrant further attention.

6. Nanoscale enhancement

6.1. Nanotube, nanowire, and nanofiber

6.1.1. Nanotubes

Carbon nanotubes (CNTs), defined as extremely thin tubes of graphitic carbon with outer diameters ranging from 1 to 100 nm and lengths from 1 to 50 μm, have been adopted in the past decade as coating material for boiling enhancement, taking advantage of their extraordinarily high thermal conductivity and mechanical properties. Besides CNTs, there have also been attempts to generate TiO_2 nanotubes on substrate to improve boiling performance.

Ujereh et al. [273] investigated nucleate pool boiling performance for heating surfaces coated with CNTs. Shown in Fig. 20(a) are SEM images of a silicon substrate coated with dense and light CNT arrays. Fig. 20(b) shows that silicon substrate coated with a light CNT array was far more superior to bare silicon surface in terms of reducing incipience superheat and increasing both nucleate boiling heat transfer coefficient and CHF for FC-72. The enhanced performance was attributed to CNT mesh's ability to provide an abundance of zero cone angle and 'reservoir-type' cavities that were ripe for nucleation with minimal superheat. Ujereh et al. found that increasing CNT mesh density on the silicon substrate reduced the incipience superheat slightly, but very dense CNT arrays also decreased CHF by reducing effective heat transfer surface area compared to light arrays. Additionally, greater enhancement was achieved with CNTs on silicon substrate than on copper because the uncoated copper surface was rougher than the uncoated silicon surface to start with and therefore provided an abundance of active nucleation sites before the coating. It is important to note that the nearly vertical slope of boiling curve in Fig. 20(b) for the CNT-coated surface is highly desirable in electronic cooling because it allows a chip to maintain fairly constant temperature in response to relatively large fluctuations in heat dissipation during operation.

Dharmendra et al. [274] tested a copper surface coated with CNTs, but incorporated an intermediate diamond layer between the CNTs and copper surface to improve adhesion. They too achieved earlier initiation of boiling compared to a bare copper surface, which they attributed to both high hydrophobicity and increased roughness.

Ahn et al. [275,276] and Sathyamurthi et al. [277] assessed pool boiling heat transfer for PF-5060 from a silicon surface coated with normally aligned CNTs in both the nucleate and film boiling regimes. They showed that nucleate boiling enhancement was only weakly dependent on coating height. However, in the film boiling regime, enhancement was observed with 25-μm thick CNT coating, while no enhancement was realized with 9-μm coating. They suggested that pool boiling heat transfer enhancement with the CNTs during film boiling was related to several factors, including high thermal conductivity of CNTs, larger sized cold spots, improved ability to collapse the vapor film, enhanced liquid-solid contact, and increased surface areas. Bertossi et al. [278] found that CNT coating a stainless steel surface organized micro-bubbles into vapor mist that detached from the surface at high frequency, enhancing the nucleate boiling heat transfer coefficient for water. They also observed an increase in heat transfer coefficient as CNT length was increased from 3 to 10 μm. Ho et al. [279] addressed surface orientation effects on nucleate boiling performance of FC-72 using both a fully CNT-coated surface and an interlaced CNT-patterned surface with 215-μm coating. They observed that heat transfer enhancement was primarily the result of large number of submicron cavities created by intertwining CNT structures.

It should be noted that Ujereh et al. [273], Dharmendra et al. [274], Ahn et al. [275,276], Sathyamurthi et al. [277], Bertossi et al. [278], and Ho et al. [279] all used chemical vapor deposition (CVD) or modified CVD to coat the substrate with CNTs. On the other hand, Seo et al. [280] used a vacuum filtration process to form randomly-oriented CNT coatings with 296, 613, 845, and 1432-nm thicknesses on stainless steel substrates. They measured deterioration in nucleate boiling heat transfer coefficient for water, which was attributed to decreased surface roughness on the CNT-coated surface. However, CHF did increase with the CNT coatings. Follow-up study by Seo and his co-workers [281,282] involved use of multiple bilayers of polyethylenimine and CNTs on a stainless steel substrate. Both surface roughness and wettability were observed to increase in water with increasing number of bilayers, and CHF enhancement was attributed to capillary wicking characteristics of the coating. They suggested that this technique provided better boiling enhancement than vacuum filtration.

Zhang et al. [283] formed TiO_2 nanotube surface arrays by anodic oxidation of a plain titanium surface. They demonstrated that wettability of this surface could be controlled by irradiation with ultraviolet (UV) light, with better wettability achieved by increasing irradiation time. This technique resulted in deterioration in nucleate boiling heat transfer coefficient, but increased CHF for water. However, Chen et al. [284] achieved appreciable enhancement in the nucleate boiling heat transfer coefficient for water on a titanium surface with TiO_2 nanotube arrays compared to a bare titanium surface.

6.1.2. Nanowires

Nanowire is defined as a nanoscale rod having a diameter of tens of nanometers and large length to diameter ratio. Chen et al.

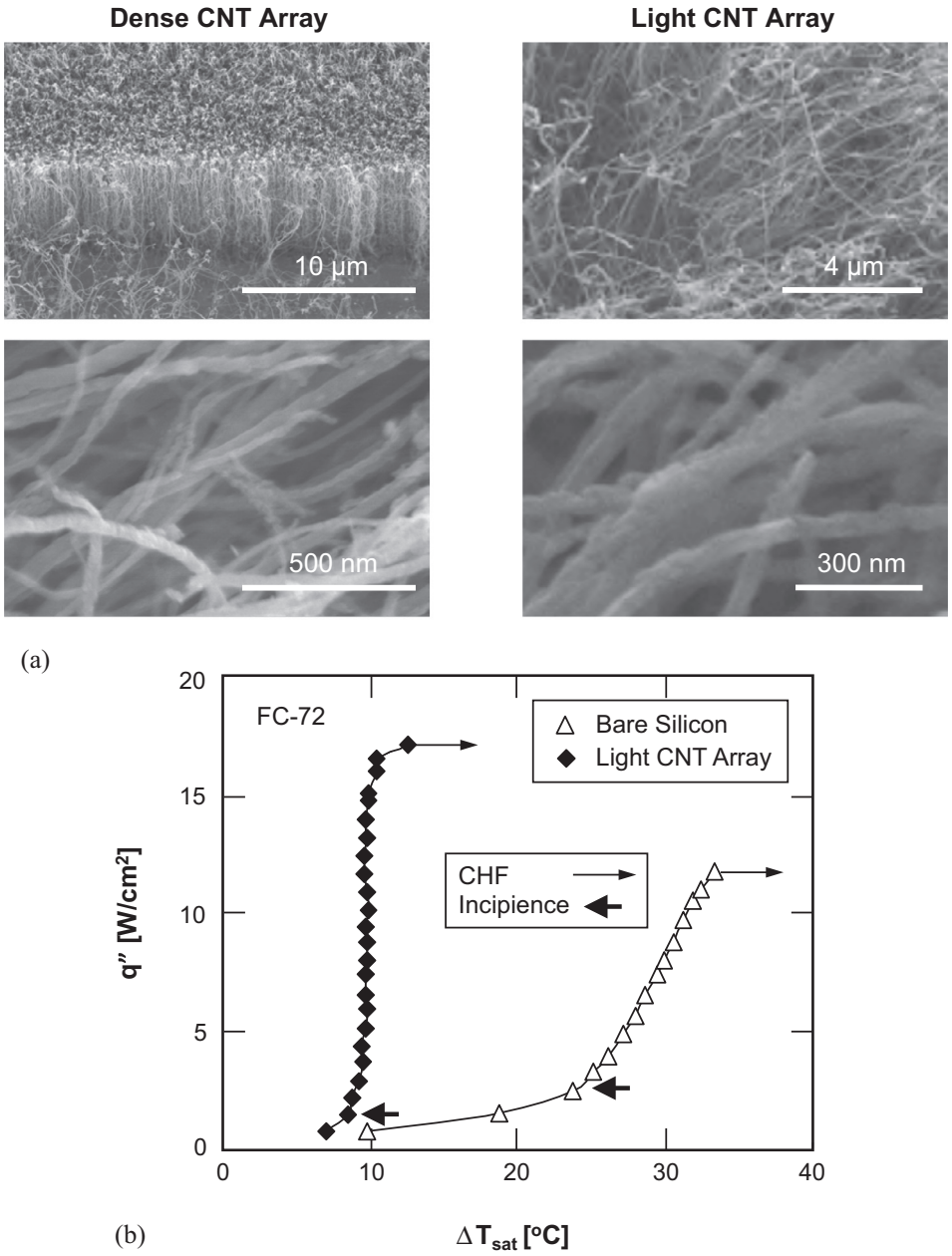

Fig. 20. (a) SEM images of silicon substrate coated with CNT arrays, and (b) comparison of boiling curves of FC-72 for bare and fully CNT-coated silicon surfaces. Adapted from Ujereh et al. [273].

[285] reported over 100% enhancements in both nucleate boiling heat transfer coefficient and CHF for water on silicon surfaces coated with arrays of silicon nanowire, Fig. 21(a), and copper nanowire, Fig. 21(b), which were synthesized by electroless etching and electroplating, respectively. The improved performances were attributed to high nucleate site density, superhydrophilicity, and enhanced capillary pumping.

Lu et al. [287] investigated pool boiling of saturated water on plain silicon surfaces and silicon surfaces covered with dense arrays of silicon nanowire, prepared by wafer-scale electroless etching. They were able to increase CHF, which was attributed to improved liquid spreadability on the nanowire surface. By assuming critical Helmholtz wavelength of vapor jets emanating normal to the surface remained unchanged from that for a bare surface, but varying ratio of surface area occupied by jets to total surface area, they showed good agreement of their CHF data with Zuber's hydrodynamic instability model [41–43].

Using a custom temperature-array sensor, Kim et al. [288] showed that rough morphology and high wettability of silicon nanowires in water provided the merits of efficient, reliable, and stable pool boiling. By controlling wicking quantitatively, Kim et al. [289] were able to construct a CHF model for silicon nanopillar surfaces that accounted for the wicking effects,

$$q''_{CHF} = \frac{C\rho_f h_{fg} W^2 (1-\varphi)}{\lambda_c^2} + q''_{CHF,Kandlikar}, \tag{15}$$

where C is a factor that compensates for wicking capacity, W a wicking coefficient, and φ solid fraction of the solid-liquid interface.

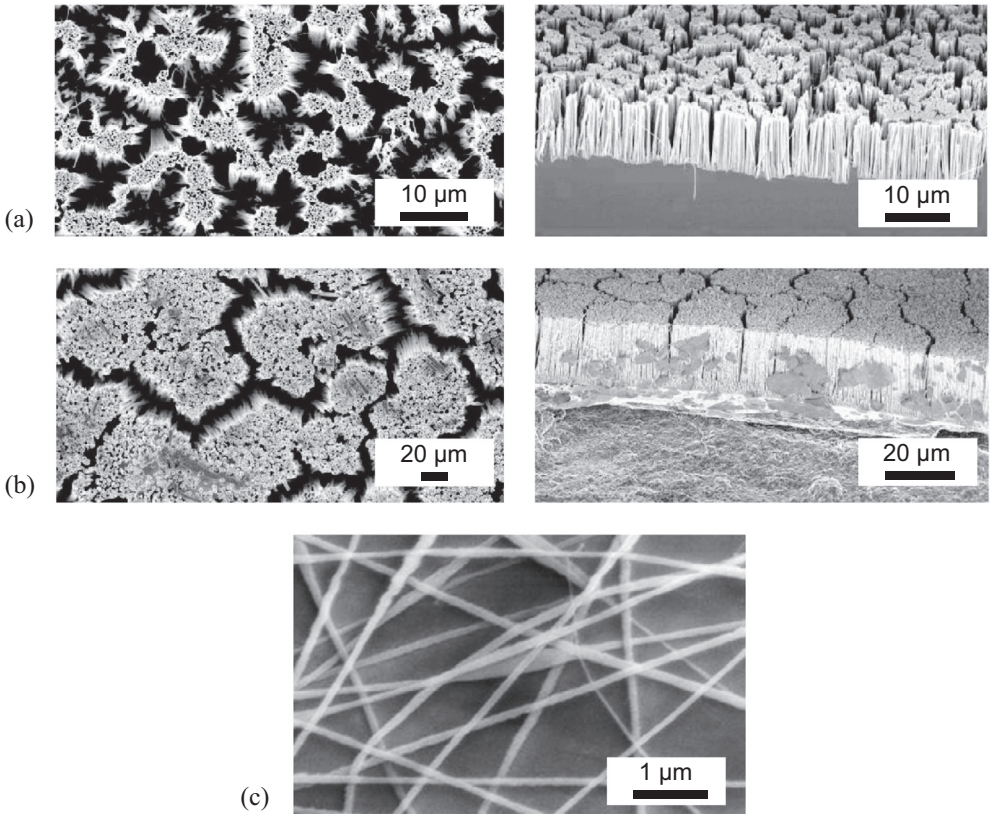

Fig. 21. (a) Silicon nanowire arrays and (b) copper nanowire arrays (adapted from Chen et al. [285]). (c) Electrically-assisted supersonic solution-blown nanofibers (adapted from Sahu et al. [286]).

The model also relied on a prior CHF model by Kandlikar [157], which was used to compute $q''_{CHF,\ Kandlikar}$ in Eq. (15),

$$q''_{CHF,Kandlikar} = \frac{1+\cos\alpha}{16}\left[\frac{2}{\pi}+\frac{\pi}{4}(1+\cos\alpha)\cos\theta\right]^{1/2} \times \rho_g h_{fg}\left[\sigma g\left(\rho_f-\rho_g\right)/\rho_g^2\right]^{1/4}. \quad (16)$$

Shim et al. [290] prepared a silicon surface with normally aligned silicon nanowires prepared by metal-assisted chemical etching and nanospherical-lens lithography. They reported significant CHF enhancement for water, as high as 245.6 W/cm^2, far better than a surface with random silicon nanowires, and attributed the enhancement to increased volumetric wicking. Demir et al. [291] examined the effects of nanorod length, over a range of 0.9–3.2 μm, on boiling performance, and, while these surfaces did enhance nucleate boiling heat transfer coefficient for water, the enhancement abated with increasing nanorod length. A noteworthy observation from the same study was slight rounding of nanorod tops following boiling tests, which pointed to potential aging effects and changes in boiling performance over time. Jo et al. [292] reported that $BiVO_4$ nanopillars fabricated by electrospraying increased both the nucleate boiling heat transfer coefficient and CHF for water.

Yao et al. [293,294] developed a technique to grow copper nanowires on silicon substrate without an interfacial bonding layer, and used different synthesis parameters to control nanowire height. They reported that this technique improved durability and interfacial strength of the copper nanowire structure, and, in the absence of an epoxy layer between the nanowire arrays and substrate, also reduced interfacial thermal resistance. By increasing nanowire height from 2 to 35 μm, they achieved gradual improvement in heat transfer coefficient for water, which they attributed to increased density and size of surface cavities, independent of nanowire material. Shi et al. [295] controlled copper nanowire height, over a range of 3–30 μm, by electroplating using a commercially available porous alumina membrane template. Like Yao et al., they achieved improvement in nucleate boiling performance for water, which they attributed to increased wettability and number of nucleation sites. Im et al. [296] formed copper nanowires as high as 8 μm on silicon substrate using electrochemical deposition. Experiments showed an increase in incipience excursion with increasing nanowire height, with 2-μm height yielding the best CHF enhancement. Kumar et al. [297] examined effects of copper nanowire diameter over a range of 35 to 200 nm on boiling performance of FC-72, and showed that both nucleate boiling heat transfer coefficient and CHF increased with increasing nanowire diameter. They explained this by increases in microscale cavity size and density, which were achieved by coagulation and grouping of nanowires during the drying phase of the template-based electrodeposition technique used.

Li et al. [298] demonstrated boiling enhancement of water using a technique comprised of depositing copper nanorods obliquely (with an incident angle of ~85°) on copper substrate inside an electron-beam evaporator. Wen et al. [299] developed a two-level hierarchical surface, patterned by long copper nanowire arrays surrounded by short copper nanowires, which promoted formation of microscale cavities between short nanowire clusters. They reported enhancement in pool boiling performance for water, which was attributed to abundance of high-density nucleation sites, capillary-induced liquid rewetting, and separation of liquid and vapor paths. Compared to a plain copper surface, the two-level hierarchical surface achieved 37% lower incipience superheat, 185% higher nucleate boiling heat transfer coefficient, and 71%

higher CHF. Shin et al. [300] used double-templated electrodeposition to form a micro/nano hybrid structure, consisting of individual micro-cavities surrounded by copper nanowires, to enhance pool boiling for water.

Ray et al. [301] synthesized normal TiO_2 nanowire arrays on copper substrate in thicknesses of 150, 300 and 450 nm by glancing angle deposition (GLAD) using an electron beam evaporator. They measured improvement in boiling performance for R-134a with the nanowire arrays compared to a plain substrate. Optimum performance was achieved with the 450-nm coating, which yielded 44.86% reduction in incipience superheat and 81.34% increase in nucleate boiling heat transfer coefficient. Lee et al. [302] achieved improvements in both nucleate boiling heat transfer coefficient and CHF with ZnO 'nanowire forests' comprised of lengthwise grown backbone and branched nanowires, and attributed the enhancement to superhydrophilic nature of this technique greatly increasing nucleation site density.

6.1.3. Nanofibers

Nanofiber is a type of fiber generated from polymers with diameters of less than 100 nm. Jun et al. [303] investigated boiling performance of copper-plated electrospun copper nanofibers. They measured nucleate boiling heat transfer coefficients for water and ethanol three to eight times those from the bare surface, but observed no enhancement in CHF. They suggested that the heat transfer enhancement during nucleate boiling was the result of this technique's ability to increase average temperature of liquid surrounding bubbles, thereby promoting more effective bubble growth. In follow-up study, Sahu et al. [286] described a novel process to fabricate copper-plated polymer nanofibers on copper substrate, employing electrically-assisted supersonic solution-blowing. The nanofibers produced, Fig. 21(c), showed strong adhesion to the substrate, allowing them to withstand repeated pool boiling cycles in ethanol, water, and ethanol-water mixture without delamination or degradation in heat transfer enhancement. In another study, Sahu et al. [304] reported that copper-plated polymer nanofibers grown on copper substrate using the same technique provided important benefits for electronic cooling, evidenced by enhancements in both nucleate boiling heat transfer coefficient and CHF for Novec 7300. By eliminating the rather complicated process of copper-plating the nanofibers, Sinha-Ray et al. [305] noted slight reduction in the heat transfer coefficient enhancement. They also pointed out that supersonically-blown polymer nanofibers provided better enhancement than electrospun nanofibers because of their ability to increase nucleation site density and maintain both good adhesion to substrate and retention of surface structure even after 7.5 h of boiling.

6.2. Nano coating

6.2.1. Nanoporous coating

Zhang and Kim [306] employed anodic oxidation to develop a 3-D, interconnected Al_2O_3 nanoporous surface on aluminum 6061 alloy substrate, which showed significant enhancements in both nucleate boiling heat transfer coefficient and CHF for water. Using electrochemical impedance spectroscopy, they showed that CHF enhancement was dominated by liquid spread and absorption induced by capillary pressure developed in the porous wicks. Follow-up study by Zhang et al. [307–309] employed the same surface along with hydrophobic self-assembly monolayer coating (to reduce wettability) and sodium dodecyl sulfate (SDS) surfactant, and achieved 7.3-fold enhancement in nucleate boiling heat transfer coefficient for water. However, they reported problematic aging effects caused by further oxidation with prolonged boiling in water, which changed surface morphology with formation of aluminum hydroxide surface deposits [310], decreasing both number of active cavities and nucleate boiling heat transfer coefficient [308]. Similar Al_2O_3 nanoporous structures, also formed by anodic oxidation, were reported by Hu et al. [311], Arya et al. [312], and Nazari and Saedodin [313].

Vemuri and Kim [314] showed 30% reduction in incipience superheat for FC-72 with nanoporous alumina coating having a thickness of ~70 μm and pore diameters of 50–250 nm that was attached to an aluminum surface. Using self-assembly of Tobacco Mosaic Virus (TMV) to prepare nickel nanostructures on gold, copper, aluminum, and stainless steel substrates, Rahman et al. [315] reported up to 200% improvements in both nucleate boiling heat transfer coefficient and CHF for water, with no observable physical degradation following 24 h of boiling. Using the facile hot-dip galvanizing/dealloying process, Tang et al. [316,317] and Lu et al. [318] formed nanoporous cooper surfaces having 50–200 nm pores on copper substrate, with which they achieved 63.3% reduction in incipience superheat and 172.7% increase in nucleate boiling heat transfer coefficient for water. However, the 3-D nanostructure and porosity were observed to change slightly after 100 h of boiling [318], with the nanostructure getting continuously coarsened with time [319].

Gao et al. [320] fabricated copper nanoporous dendritic structures on copper substrate using electrodeposition and annealing to enhance nucleate boiling in water. With this technique, binding force between nanostructures and substrate was strengthened by controlling both annealing temperature and time. Hendricks et al. [321] produced flower-like ZnO nanostructures on aluminum and copper substrates using a relatively low-temperature microreactor-assisted nanomaterial deposition process. They demonstrated significant reductions (25–38 °C) in wall superheat during nucleate boiling, and up to 4-fold enhancement in CHF in water. Jo et al. [322] used an electroplating technique to fabricate fractal-like Cu_2O nanostructures on NiCr substrate, whose wettability was controlled by electroplating time, and demonstrated enhancement in boiling performance for water.

Kalaiselvam et al. [323] reported ~130% enhancement in nucleate boiling heat transfer coefficient for water using nanoporous structures prepared by electrochemical anodization and spray pyrolysis on brass, copper, and aluminum substrates. Using cold spraying, Pialago et al. [324] fabricated CNT-Cu composite powder coating on copper substrate, which yielded up to 74% enhancement in nucleate boiling heat transfer coefficient for R-134a. Follow-up study by Pialago et al. [325] explored enhancement of nucleate boiling using Cu-CNT-Al composite coating. Zheng and Park [326] reported boiling enhancement with CNT-Cu composite powder coating on copper substrate, which was fabricated using electrostatic spraying followed by sintering. Park et al. [327] examined boiling benefits of spraying CNT and graphene onto zirconium substrate. While they showed an increase in CHF for water (mainly because of reduced contact angle), they also reported deterioration in nucleate boiling heat transfer coefficient, which they attributed to surface fouling. Using CVD, Sadaghiani et al. [328] applied pHEMA coatings with thicknesses of 50, 100, and 200 nm on silicon substrate, and achieved better enhancement in nucleate boiling heat transfer coefficient for water from inclined surfaces than a horizontal surface, and attributed this trend to better venting along inclined surfaces. Jones et al. [329] employed molecular dynamics simulations to propose a mechanism for sustaining superheated liquid within hydrophilic pores for water by offering an additional pathway for wetting via vapor condensation within surface textures. This concept was shown to be valid for small spacings between surface texture features, especially in the nanoscale.

Lee et al. [330] employed an anodizing technique to produce well-ordered Al_2O_3 nanoporous structures on aluminum alloy substrate. Their study was focused on long-term changes in

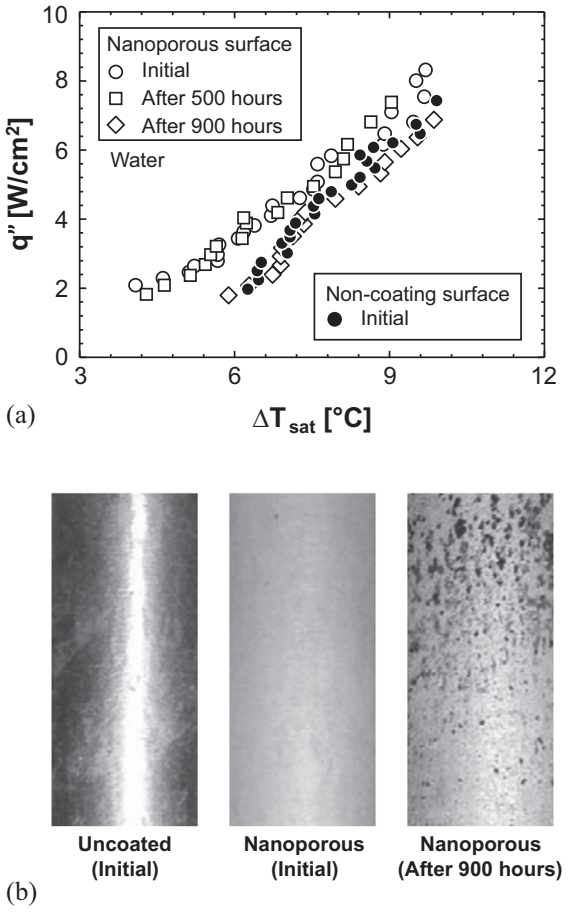

Fig. 22. (a) Long-term boiling performance with saturated water on Al_2O_3 nanoporous surface at atmospheric pressure, and (b) surface images of test sections. Adapted from Lee et al. [330].

performance of this surface in water. Fig. 22(a) shows only minor differences in boiling performance between an initial test and one lasting 500 h. However, there was obvious deterioration in boiling performance after 900 h. Lee et al. attributed this degradation to profound physical changes to the nanoporous structures. These changes are clearly manifest in Fig. 22(b), which shows the nanoporous coating almost completely worn off.

Overall, nanoporous structures pose major challenges for implementation in cooling applications involving pool boiling. Given the observed changes in boiling performance in long-term tests, it is crucial that such surfaces should be carefully assessed for any changes in surface nanostructure over time.

6.2.2. Nano film coating

Several studies have been published which involved coating heat transfer surfaces with nanoscale-thickness films in an effort to enhance boiling performance by improving surface wettability. Forrest et al. [331] fabricated a polymer/silica nanoparticle film coating on nickel substrate using a layer-by-layer technique, and achieved good surface adhesion and adsorption of subsequent layers onto the surface. Their tests showed over 100% enhancements in both nucleate boiling heat transfer coefficient and CHF for water, which were attributed to improved nucleation as well as improved wettability. An et al. [332] employed a method involving supersonic spraying of graphene oxide flakes on copper substrate, forming a nanoporous film. They too achieved enhancements in both nucleate boiling heat transfer coefficient and CHF for FC-72, both outcomes of increased surface roughness and better wettability. Feng et al. [333] fabricated a microporous alumina coating on platinum substrate using atomic layer deposition. CHF for water increased with increasing coating thickness up to 20 nm because of improved wettability, but no further enhancement was realized above 20 nm. Seo et al. [334] improved boiling performance for FC-72 with the aid of a hybrid film composed of graphene and CNTs deposited on an ITO surface, and attributed the enhancement to interconnected network of carbon structures in the film.

Yeom et al. [335] employed 4–6 μm nanoparticle coatings formed by electrophoretic deposition of 60–80 nm Ti and TiO_2 particles. The coatings were observed to increase bubble departure frequency, but average bubble departure volume and nucleation site density were reduced. Though the coatings increased CHF for water, they also delayed boiling incipience. Overall, the TiO_2-nanoparticle coating provided better CHF enhancement than the Ti coating, but the latter was deemed more mechanically durable [336]. Son et al. [337] used DC magnetron sputtering to form 1-μm chromium nanostructures on stainless steel substrate. This surface exhibited outstanding superhydrophilicity and enhanced CHF for water because of improved wicking. However, Kam et al. [338] showed that electroplating chromium on stainless steel decreased CHF regardless of coating thickness. On the other hand, SiC-coated surfaces enhanced CHF. Seo et al. [339] also used DC sputtering to form a coating of FeCrAl, and showed enhancement in CHF because of increased roughness.

Using electron beam physical vapor deposition, Das et al. [340–342] produced SiO_2 nanoparticle coatings featuring well-ordered micro/nanostructures in thicknesses up to 1000 nm on copper substrate, which achieved 80% enhancement in nucleate boiling heat transfer coefficient for water. Follow-up study by Das et al. [343] involved fabrication of TiO_2 coatings, also comprised of micro/-nanostructures, on copper substrate, using which increased the nucleate boiling heat transfer coefficient for water as coating thickness was increased over a range of 250 to 1000 nm. However, topographies of the micro/nanostructures were significantly altered after boiling because of changes in mechanical properties, such as hardness, ductility, and tensile strength, resulting in more densely populated and smoother structures, and blocking pores in the nanostructures. These changes caused appreciable degradation from the initial enhancement with repeated tests.

6.2.3. Other coating types

Maroo and co-workers [344–346] fabricated surfaces with silicon and silica ridge formations, which were shown to enhance CHF for water provided ridge height was greater than thickness of the metastable superheated liquid layer beneath the bubbles, measuring 450 and 900 nm for Si and SiO_2, respectively, materials commonly used in chip making. Fig. 23(a) and (b) show an SEM image of SiO_2 surface ridges, and schematic of microlayer evaporation over the ridges, respectively. Fig. 23(c) shows 120% enhancement in CHF for water compared to a pain surface, which was obtained with the ridges increasing surface area by only 18%.

Li et al. [347] experimented with three kinds of plain nickel-based chemically treated surfaces, and four kinds of nickel-based electrochemically treated surfaces, the latter having nanocone array structures, and achieved boiling heat transfer enhancement with the nanostructures. Ahn et al. [348,349] reported that the CHF enhancement for water with micro/nanostructures achieved by anodization was not the outcome of improved surface wettability alone, but improved liquid spreadability as well. In other studies, Ahn et al. [350,351] suggested another important contributor to the CHF enhancement, capillary wicking. They recommended the following relation for CHF prediction,

$$q''_{CHF} = Sq''_{CHF,Kandlikar} + q''_{wicking}, \quad (17)$$

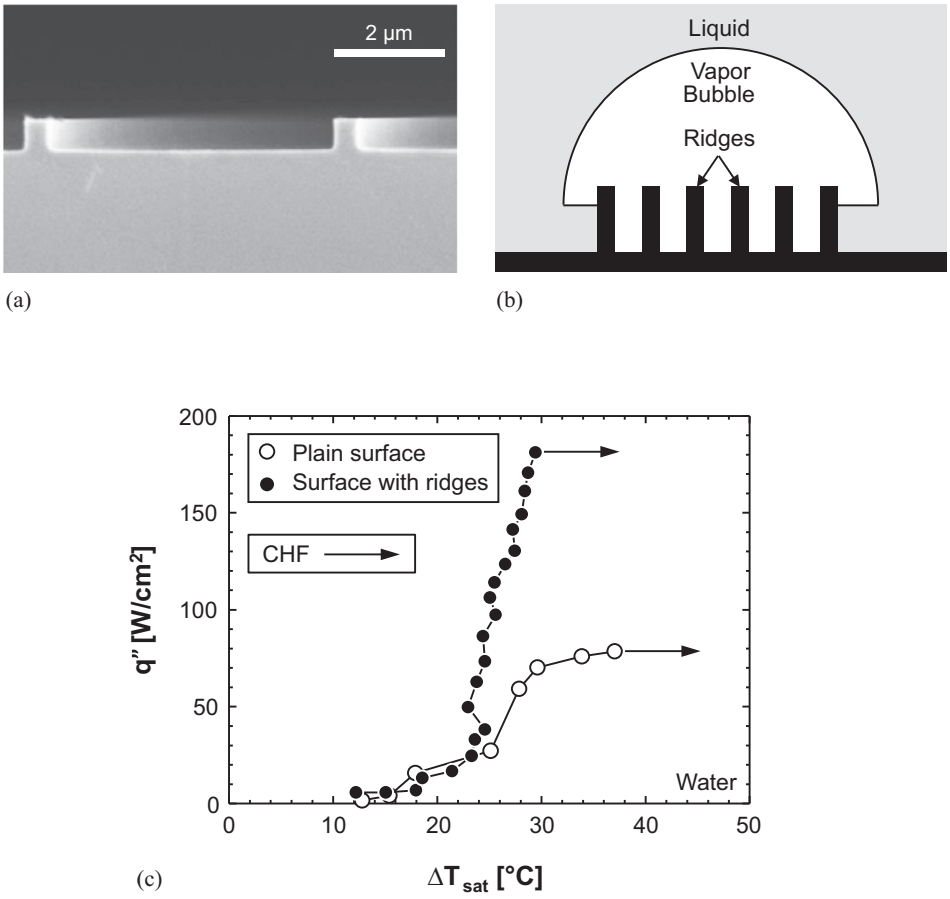

Fig. 23. (a) SEM image of SiO_2 ridges, (b) schematic of microlayer evaporation, and (c) boiling curves for both enhanced and plain surfaces in water. Adapted from Zou et al. [345].

where $q''_{CHF,Kandlikar}$ is CHF predicted according to Kandlikar's model [157], Eq. (16), S an area factor equal to 0.823, used to modify the original model, and $q''_{wicking}$ the heat flux gained by capillary wicking,

$$q''_{wicking} = \frac{\varepsilon \ \delta \ \rho_f \ h_{fg} K}{A_{heating}} \ \frac{d\bar{A}_{wetted}}{dt}, \tag{18}$$

where ε, δ, $A_{heating}$, and A_{wetted} signify porosity of structured surface, thickness of structures, area of heating surface, and wetted area resulting from capillary wicking, respectively, and K is a fitting factor equal to 0.55. Saeidi and Alemrajabi [352] also showed CHF enhancement with nanostructures formed by anodization. Follow-up study by Saeidi et al. [353] examined a method involving aluminization on a copper surface, which achieved up to 37% enhancement in CHF for water, but had insignificant influence on the nucleate boiling heat transfer coefficient.

6.3. Boiling-induced nanoparticle deposition

Nanoparticle deposition on a substrate is achieved by nanofluid boiling and controlled by varying boiling time, nanoparticle concentration, and heat flux [354,355]. Kwark et al. [355] and Amaya et al. [356] showed that water-based Al_2O_3 nanofluid coating enhanced CHF but degraded the heat transfer coefficient compared to an uncoated surface, as shown in Fig. 24(a). When the base fluid was changed to ethanol, the coating became more uniform because of smaller bubble diameter resulting from lower surface tension of ethanol compared that for water. Subsequently, boiling water on the coating created in ethanol-based nanofluid outperformed that in water-based nanofluid, by significantly enhancing CHF, albeit without affecting the nucleate boiling heat transfer coefficient, as shown in Fig. 24(b). Follow-up study by Kwark et al. [357] showed that the enhancement was independent of average nanoparticle size, but determined by other parameters, such as pressure, surface size, and surface orientation. Similar trends regarding impact of the coating on CHF and heat transfer coefficient were observed by Huang et al. [358] and Hegde et al. [359] for water with surfaces coated with TiO_2 and CuO nanoparticle deposits, respectively. And coverage of the surface by the coating was observed to become more complete with increasing nanoparticle concentration and heat flux during initial preparation of the surface [358]. Kim et al. [360] also achieved CHF enhancement in water with a surface having thin nanoparticle-deposited wires, and suggested that the enhancement was related to both surface wettability and liquid spreadability (capillary wicking).

Kiyomura et al. [361] investigated water boiling performance for copper surfaces having roughnesses of 0.05 and 0.23 μm, achieved by depositing Fe_2O_3 nanoparticles in concentrations of 0.029 and 0.29 g/l. The highest nucleate boiling heat transfer coefficient was obtained with the smoothest surface having nanoparticles deposited at low mass concentration, and all other surfaces degraded heat transfer performance because of increased thermal resistance and decreased nucleation site density associated with thicker layers. Increasing the Fe_2O_3 nanoparticle concentration in water during the surface preparation increased both surface roughness and wettability. Souza et al. [362] reported that deposition of 10-nm Fe_2O_3 nanoparticles enhanced nucleate boiling heat

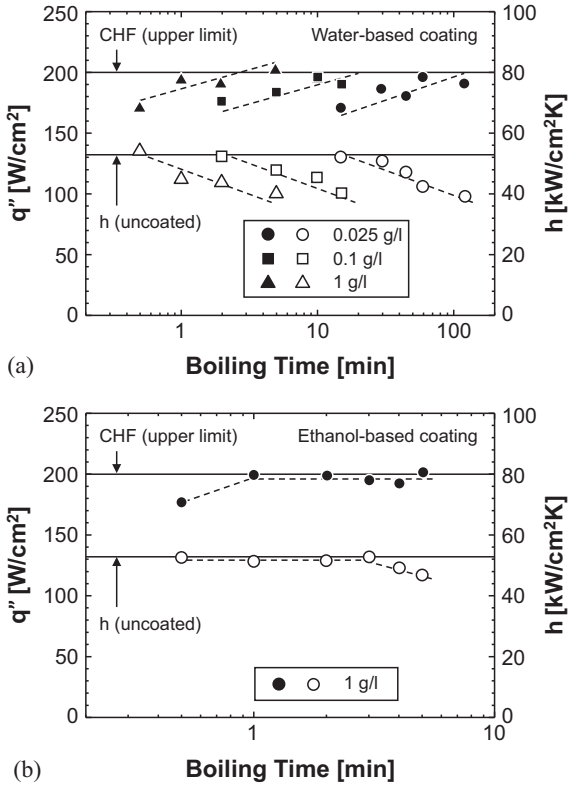

Fig. 24. Pure water CHF (solid symbol) and heat transfer coefficient (hollow symbol, at $q'' = 100\ W/cm^2$) on (a) water-based Al_2O_3 nanofluid coating, and (b) ethanol-based Al_2O_3 nanofluid coating. Adapted from Kwark et al. [355].

transfer coefficient for HFE-7100, while 80-nm nanoparticles degraded performance, compared to a surface without nanoparticle deposition.

Heitich et al. [363] showed that nanostructures on constantan substrate generated by both nanofluid boiling and sputtering increased surface wettability for water, leading to an increase in CHF, while increasing the nucleate boiling heat transfer coefficient only at high heat fluxes. Additionally, they found that sputtering produced more homogeneous structures than nanofluid boiling, and that an initially rough substrate with hydrophobic features provided better nucleate boiling performance. Stutz et al. [364] showed that Fe_2O_3 nanoparticle deposition on platinum substrate created by both nanofluid boiling and electrophoresis increased CHF for water and pentane, due to enhanced wettability, but decreased the nucleate boiling heat transfer coefficient because of added thermal resistance of the deposition layer. Their tests pointed to weak reproducibility of the nanoparticle layer formed initially by vigorous nanofluid boiling, evidenced by formation of random and multi-scale nucleation sites. Experiments by Sakashita [365] showed little difference in liquid-vapor interfacial behavior during nucleate boiling in water between TiO_2-coated and uncoated copper surfaces, but the former did enhance CHF by virtue of increased thickness of macrolayer beneath large hovering bubbles.

Overall, many studies have been published in recent years that focused on pool boiling enhancement using nanofluids instead of pure liquids. Despite certain heat transfer merits, nanofluids pose several practical challenges, including sedimentation, clustering and precipitation of nanoparticles, surface erosion, all of which contribute to variations in boiling performance over time. It does appear that nanoparticle deposition might alleviate some of these concerns. Nonetheless, more research is needed to assess deposition strength and surface homogeneity when using nanoparticle deposition.

7. Hybrid enhancement

7.1. Macro/micro hybrid techniques

7.1.1. Fins with microstuds

As discussed earlier, the most crucial goals for pool boiling enhancement are to promote incipient boiling at lower surface superheat, reduce incipience excursion, increase nucleate boiling heat transfer coefficient, and ameliorate CHF. Enhancement techniques discussed thus far have been shown to achieve one or more of these goals, but fail with others. The main premise of 'hybrid enhancement,' which was pioneered by Mudawar and Anderson [7,8], is to combine the benefits achieved with different surface enhancement scales in pursuit of superior performance.

Mudawar and Anderson [7] explored the merits of combining macro extended surfaces (studs) having different shapes, microfins, and cavity-promoting surface finish, to improve boiling performance for vertically-mounted heating surfaces in both FC-72 and FC-87. The macro extended surfaces included single square studs with uniform and tapered (pyramidal) cross-sections, and an array of four cylindrical pins, all protruding horizontally from the heating surface. Rectangular microfins were formed around the entire perimeter of the square studs. After fabricating the microfin-enhanced studs, the entire surface was vapor blasted, producing an abundance of cavities having an effective pore size near 15 μm. Both microfin enhanced studs promoted nucleation in grooves separating the microfins, but the tapered stud produced expected behavior, where, because of buoyancy effects, bubbles forming in the groove closest to the base quickly propagated towards the tip, resulting in a temperature drop shortly following boiling incipience. However, there were no incipience excursions with surfaces with pin arrays or uniform square stud. Overall, those latter two surfaces produced two important benefits sought with hybrid enhancement: elimination of incipience excursion and appreciable enhancement in CHF. Most notably, the four-pin surface yielded CHF in excess of $100\ W/cm^2$ for saturated FC-72, a 7-fold increase compared to a plain surface. Follow-up study by Mudawar and Anderson [47] provided a systematic methodology for designing and fabricating surfaces for hybrid enhancement. Optimum enhancement was achieved with a surface combining three enhancement scales: (1) a single extended cylindrical stud, (2) square microfins machined into the stud's perimeter, and (3) final surface finish produced by blasting with air/water/silica slurry, as shown in Fig. 25(a). Performance in FC-72 was especially improved with 30 °C subcooling. Fig. 25(b) compares development of boiling pattern for this surface with increasing heat flux for saturated and subcooled FC-72. Most notable is the greatly reduced bubble size and overall bubble volume with subcooling. This is especially useful when cooling an array of vertically oriented surfaces, where any detrimental impact of vapor production from a surface on surfaces mounted above would be greatly minimized. Fig. 25(c) compares boiling curves for saturated and subcooled FC-72 for the microfin-enhanced stud. Aside from absence of incipience excursion, this figure shows very high CHF values achieved with the surface, $105.4\ W/cm^2$ (7.5-fold enhancement compared to plain surface) for saturated boiling, and $159.3\ W/cm^2$ (11.3-fold enhancement compared to plain surface) for subcooled.

Honda et al. [149] showed that a silicon surface modified with $50 \times 50 \times 60\ \mu m^3$ square microfins with 25–32 nm surface roughness provided better nucleate boiling performance at high heat fluxes in FC-72 than surfaces employing the same enhancement scales separately. They achieved CHF values 1.8–2.3 times that

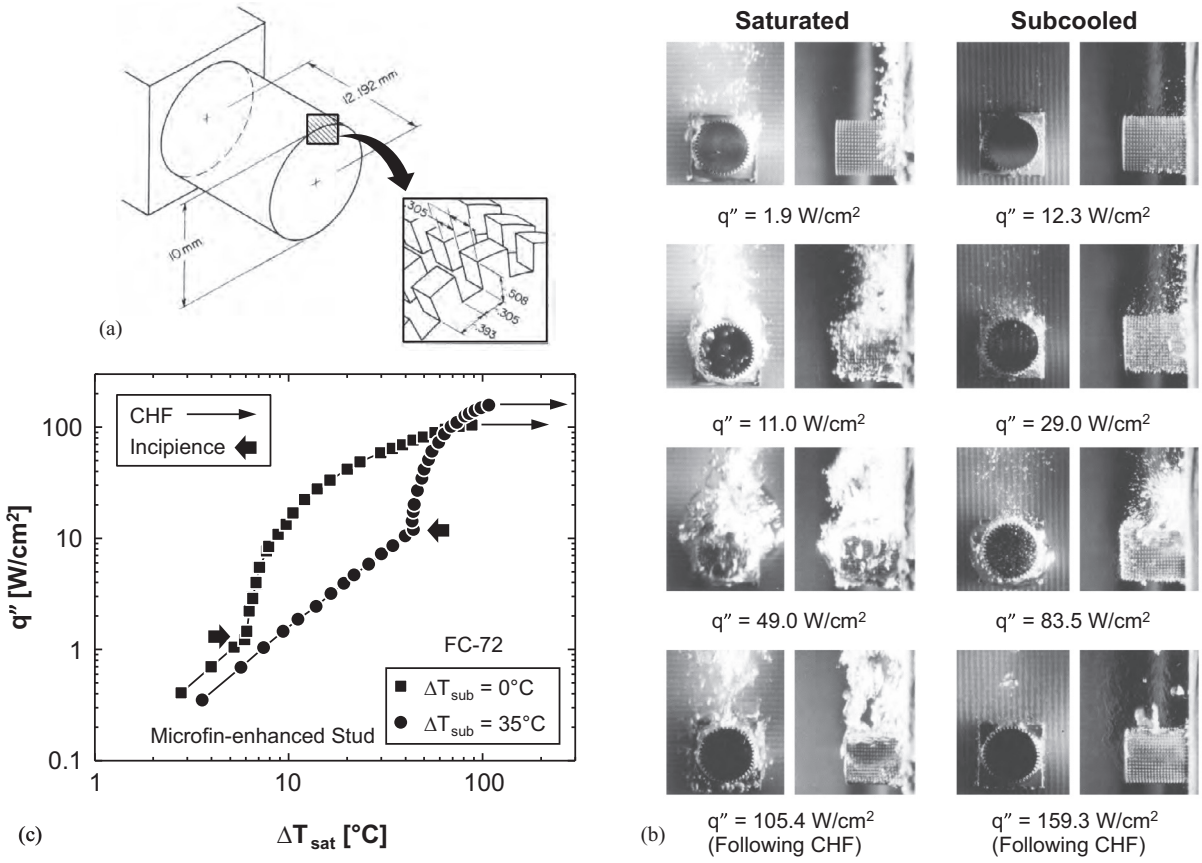

Fig. 25. (a) Microfin-enhanced-stud configuration and dimensions. (b) Evolution of boiling pattern with increasing heat in saturated and 30 °C subcooled FC-72. (c) Boiling curves for saturated and subcooled FC-72. Adapted from Mudawar and Anderson [47].

for a smooth silicon chip, and reported more significant enhancement with subcooled than saturated boiling.

7.1.2. Fins with microporous structures

Rainey and You [87] experimented with a hybrid enhancement surface modified with square 1 × 1-mm^2 microfins with heights up to 8 mm and microporous coating. Compared to a plain surface, they achieved significant enhancement in both nucleate boiling heat transfer coefficient and CHF for FC-72, but CHF was insensitive to fin height for heights below 4 mm. They pointed out that nucleate boiling heat transfer coefficient and CHF were influenced by a number of conflicting factors, including increased area, fin efficiency, surface microstructure, vapor bubble departure resistance, and resistance to liquid re-wetting. They also reported slightly better performance in the horizontal surface orientation with vertical fins than in vertical orientation with horizontal fins [366]. Chang and You [367] investigated boiling performances of FC-87 and R-123 from a 15.6-mm diameter cylindrical surface with prism-shaped 0.88-mm tall microfins with a pitch of 1.39 mm, which was finished with a microporous coating of aluminum brushable ceramic-M.E.K (ABM). For relatively low heat fluxes below 5 W/cm^2, the nucleate boiling heat transfer coefficient was 50–60% higher than for an uncoated surface. However, this trend reversed above 10 W/cm^2, where both the nucleate boiling heat transfer coefficient and CHF were lower than for the uncoated surface. This latter trend was explained by a significant increase in bubble generation on the coated surface resulting in vapor trapping between fins.

Pastuszko et al. [368] experimented with a surface having rectangular fins, that was covered with sintered copper foil with numerous micropores, and showed better enhancement in heat transfer coefficient than the finned surface without the foil for water over the entire nucleate boiling region, and for FC-72 below 2.5 W/cm^2. Pastuszko and co-workers also investigated use of joined horizontal and vertical channels formed in copper, overlaid by porous foil [369–371], and finned surface covered by wire mesh [372]; they also constructed models to predict corresponding nucleate boiling heat transfer performances. Shown in Fig. 26(a) are schematics of two types of surfaces having joined horizontal and vertical channels before being overlaid with the porous foil. A recent study by Halon et al. [373] examined boiling performance for this hybrid surface in water at sub-atmospheric pressures, and showed boiling curves shifting to higher superheats in comparison to those obtained at atmospheric pressure. Rioux et al. [374] and Li et al. [375] proposed a hierarchical multi-scale surface, including copper macrostuds composed by sintered particles that formed microporous structures. The multi-scale enhancement yielded the most significant improvements in heat transfer coefficient and CHF for water compared to individual enhancement schemes.

Overall, it can be concluded that combining multiple enhancement techniques does not necessarily achieve boiling enhancement equivalent to the sum of enhancements derived from individual techniques. For example, combining confinement with copper finned structures yielded nucleate boiling heat transfer coefficients in FC-72 smaller than those for the finned surface alone [377].

7.1.3. Channels with microporous structures

Deng et al. [376,378] reported porous coating generated by sintering copper powder on copper surface having 12 parallel inverted

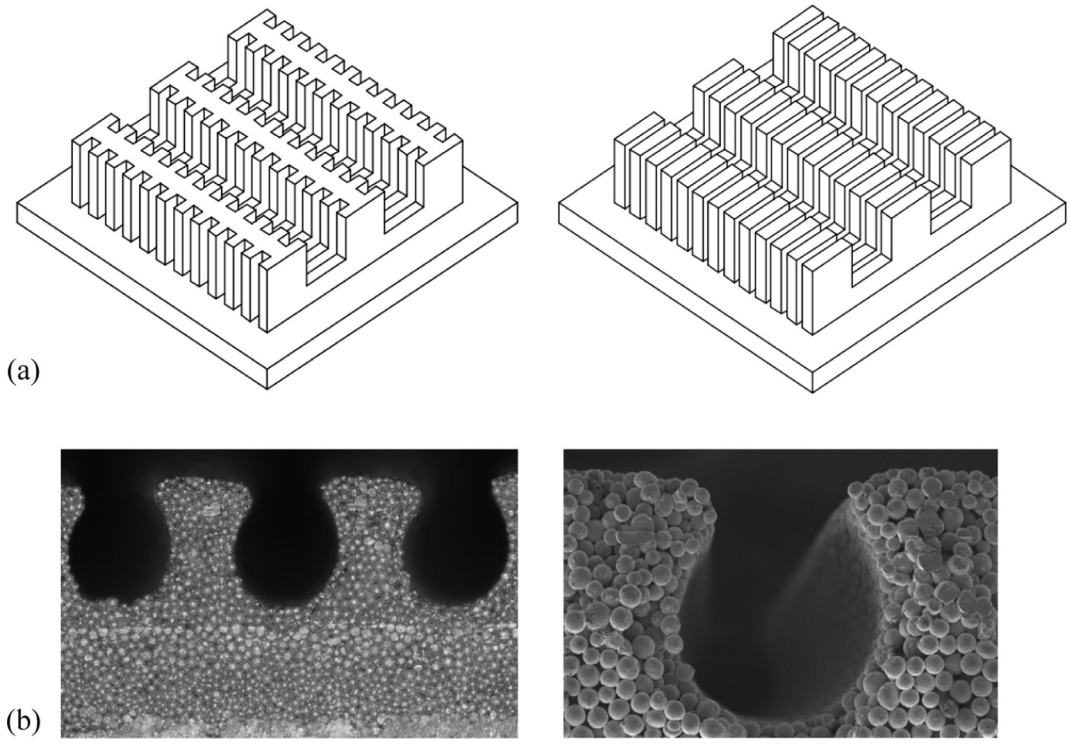

Fig. 26. (a) Schematics of joined horizontal and vertical channels before being overlaid with porous foil (adapted from Pastuszko [369]). (b) Cross-sectional view of microporous structures with reentrant channels (adapted from Deng et al. [376]).

Ω-shaped reentrant channels, Fig. 26(b), and provided the combined merits of significantly reducing incipient superheat and enhancing nucleate heat transfer coefficient for water and ethanol at low to moderate heat fluxes, compared to the same surface without the coating. Despite reduced enhancement for moderate to high heat fluxes, the porous coating was observed to sustain separated vapor/liquid counterflow and liquid replenishment through the horizontal channels, as well as maintain efficient surface rewetting by capillary wicking, which served to resist vapor blanket formation and premature occurrence of CHF. Stubos and Buchlin [379] and Wu et al. [380] developed a surface with vapor channels formed by bronze porous modules on copper substrate; the channels provided pathways for vapor release in R-11. They also proposed an equivalent dual porous model employing one-dimensional formulation to predict two-phase flow within the enhanced structure.

Tang and co-workers [381,382] fabricated porous interconnected micro-channel nets using loose copper powder sintering and wire electrical discharge machining. The powder morphology had negligible influence on the nucleate boiling heat transfer coefficient for water, which increased with decreasing channel width at low heat fluxes, but decreased at high heat fluxes. And powder with 50–75 μm particles yielded the highest heat transfer coefficients by providing trade-off between increases in nucleation site density and capillary wicking. Using an orthogonal ploughing/extrusion technique, Sun et al. [383] fabricated micro-grooved surfaces with reentrant cavities, and achieved reduction in incipience superheat as well as enhancement in the nucleate boiling heat transfer coefficient for water. They observed two types of bubbles depending on nucleation source, groove bubbles and cavity bubbles. The size of cavity bubbles was smaller than that on a smooth surface and did not change with increasing heat flux, while the size of groove bubbles first increased then decreased appreciably with increasing heat flux.

7.2. Micro/nano hybrid techniques

7.2.1. Microfins and particles with nanostructures

Dong et al. [384] argued that microstructures acted to enhance bubble nucleation by significantly increasing active nucleation site density at low heat fluxes, while nanostructures served to increase bubble departure frequency by decreasing departure diameter. They therefore proposed combining the two enhancement scales to improve pool boiling performance.

Chu et al. [385] examined boiling enhancement in water for two types of hybrid enhancement surfaces on silicon substrate: (a) 5–10-μm diameter and 10-μm tall silicon micropillars, with 14-nm SiO_2 nanoparticles overlaid on the micropillars by electrophoretic deposition, and (b) 30–35-μm diameter and 35–68-μm tall electroplated copper micropillars covered with CuO nanostructures having non-dimensional roughness values between 3.6 and 13.3 by oxidation. Highest CHF enhancement of ~200% was achieved with the latter surface and largest non-dimensional roughness of 13.3. Wang et al. [386] introduced a simple electrochemical method to fabricate vertical copper micro-dendritic fin arrays with controllable shape, number density, and height on copper substrate, which yielded ~200% enhancement in nucleate boiling heat transfer coefficient for water compared to a plain copper surface. Jo et al. [387] employed supersonic spray-coating of copper nanoparticles to create micro-fins with triangular cross section, and showed improvement in nucleate boiling heat transfer for HFE-7100, which they attributed to more efficient bubble release caused by the surface's tendency to reduce bubble interference.

Rahman et al. [388] fabricated four types of micro-fins on silicon wafers using deep reactive ion etching (DRIE), which they coated with nickel nanostructures using a biotemplated nanofabrication technique based on self-assembly and metallization of Tobacco Mosaic Virus (TMV) structure, as shown in Fig. 27(a). By measuring the volume flux of liquid wicked into the surface

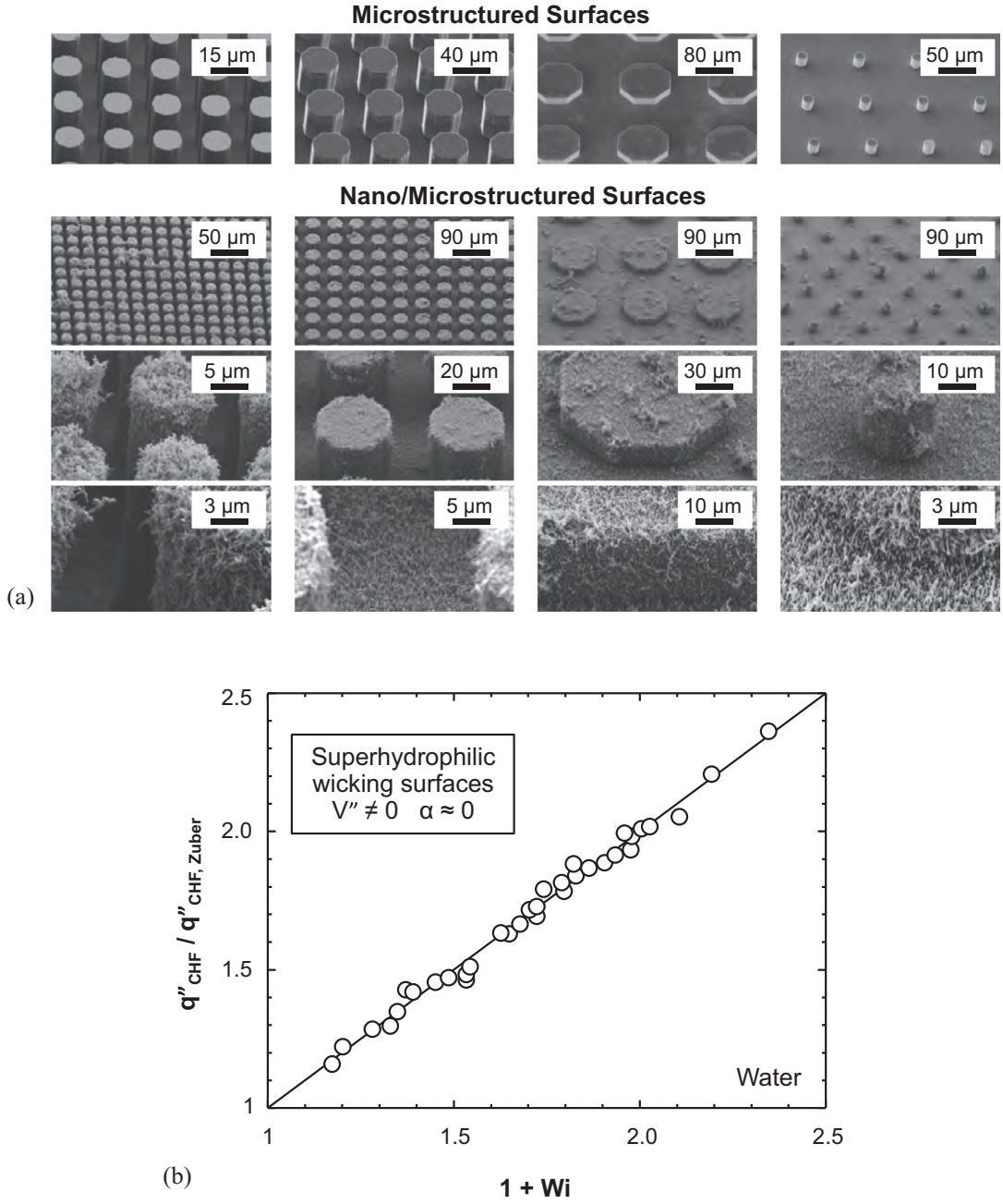

Fig. 27. (a) SEM images of four types microstructures consisting of micro-fin arrays formed on silicon wafers with and without nanostructures. (b) Comparison of measured and predicted CHF for water. Adapted from Rahman et al. [388].

structures, they showed that wickability was the key factor influencing CHF for water on structured superhydrophilic surfaces with negligible contact angle. They also proposed the following correlation for CHF as a function of dimensionless wicking number, *Wi*,

$$\frac{q''_{CHF}}{q''_{CHF,Zuber}} = 1 + Wi, \tag{19}$$

where $q''_{CHF,Zuber}$ is CHF predicted according to the Zuber model [41–43],

$$q''_{CHF,Zuber} = 0.131\rho_g h_{fg}\left[\sigma g\left(\rho_f - \rho_g\right)/\rho_g^2\right]^{1/4}, \tag{20}$$

Wi is defined as the ratio of liquid mass flux wicked into the surface structures to critical mass flux of vapor leaving the surface, calculated according to Zuber's hydrodynamic instability analysis,

$$Wi = \frac{V''\rho_f}{\rho_g\left[\sigma g\left(\rho_f - \rho_g\right)/\rho_g^2\right]^{1/4}}, \tag{21}$$

and V'' is the measured wicked volume flux. Fig. 26(b) compares measured and predicted CHF results. Follow-up study by Rahman and McCarthy [389] examined pool boiling for copper substrates fabricated with multi-scale structures, including channel arrays with characteristic lengths from 300 μm to 3 mm, nano-coatings with characteristic lengths from 50 nm to 50 μm, and combined micro-channels and nano-coatings. The micro-channels and nanostructures were fabricated using electric discharge machining and hydrothermal oxidation, respectively. The nano-coatings increased CHF for water because of improved surface wicking, but decreased the nucleate boiling heat transfer coefficient due to suppression of

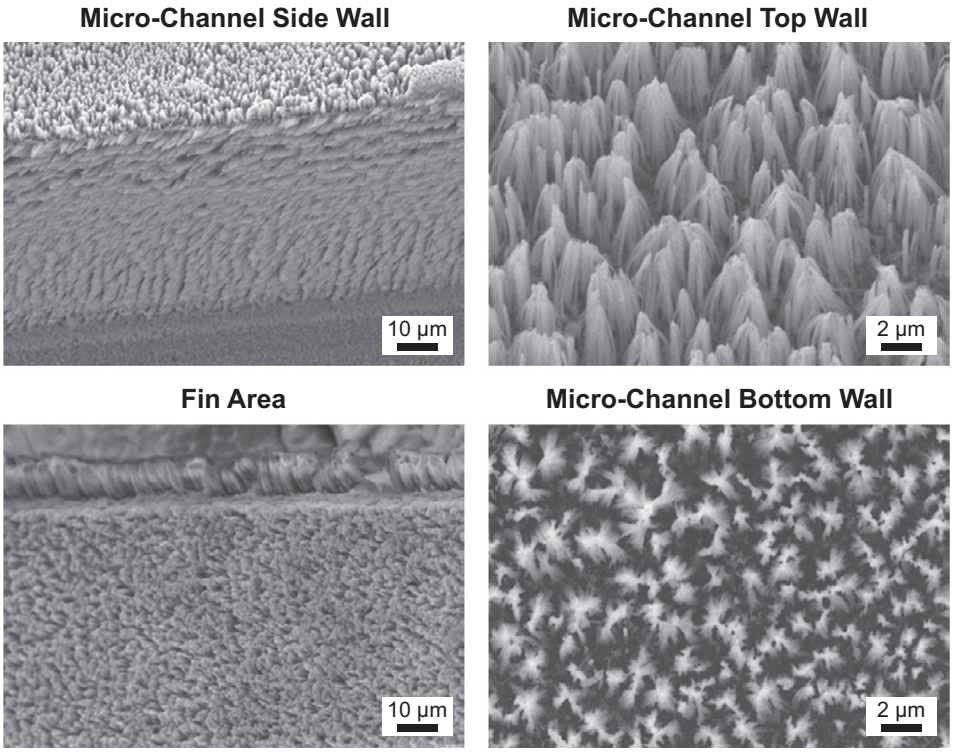

Fig. 28. SEM images of silicon nanowires on different micro-channel walls. Adapted from Yao et al. [397].

the nucleation process. On the other hand, the micro-channels increased both CHF and the heat transfer coefficient. The hybrid surface achieved by combining both enhancement scales showed the most superior performance, reaching values of heat transfer coefficient and CHF as high as 461 kW/m^2 K and 313 W/cm^2, respectively. Rahman and McCarthy [390] reported that the nano-coating tendency to suppress nucleation and therefore decrease the heat transfer coefficient could be overcome with addition of patterned low-surface-energy films, which created mixed wettability on the enhanced surface. By combining nano-coating with mixed wettability, and in-plane variations of thermal conductivity, Rahman and McCarthy [169] achieved values for heat transfer coefficient and CHF that were, respectively, 10 and 2.5 times higher than those for a plain surface.

McHale et al. [391] coated CNTs on sintered copper micro–particles using wave plasma enhanced CVD, and tested this hybrid technique in both water and HFE-7300. For water, no enhancement resulted from the CNT coating. However, the hybrid (sintered with CNT) surface produced the lowest wall superheat for HFE-7300 at high heat fluxes, and increased CHF by more than 45% compared to a smooth copper surface because of increased surface area and improved capillarity. Dhillon et al. [392] reported an upper CHF limit for water when increasing micropillar spacing on nanotextured micropillar surfaces. Moon et al. [393] investigated boiling enhancement in water for hierarchically structured surfaces with nanowires on well-ordered micropillars and micro-holes, and concluded that nanowires were quite effective at enhancing liquid imbibition for the hierarchically structured surfaces. Mori et al. [394,395] used nanoparticle deposition on a honeycomb porous plate to enhance both nucleate boiling heat transfer coefficient and CHF for water.

7.2.2. Channels with nanostructures

Yao et al. [396] developed a two-step metal-assist etching technique to fabricate silicon nanowires, which covered all exposed walls of a silicon micro-channel surface as shown in Fig. 28. They achieved significant improvements in both nucleate boiling heat transfer coefficient and CHF for water compared to the micro-channel surface without the nanowires. Follow-up study by Yao et al. [397] addressed the effects of micro-channel dimensions on pool boiling performance of water with a hybrid enhancement technique combining the use of micro-channels and silicon nanowires, and achieved enhancements in maximum heat flux of 120% and over 400% compared to the micro-channel surface without the nanowires and to a plain silicon surface, respectively. Im et al. [398] used an alkali-assisted surface oxidation technique to create flower-like CuO nanostructures on microgrooves, composed by 3-μm diameter buds and 20-nm thick petals. This technique's high surface area to volume ratio greatly improved capillary wicking, which was manifest in measureable improvement in nucleate boiling heat transfer coefficient for PF-5060. In follow-up study, Sathyanarayana et al. [399] also achieved enhancement in nucleate boiling heat transfer coefficient for a mixture of HFE-7200 and $C_4H_4F_6O$ on a micro-grooved surface coated with CuO nanostructures.

Patil and Kandlikar [400] combined the use of open micro-channels, with microporous coating electrodeposited on fin tops of micro-channels. This hybrid enhancement technique yielded values for nucleate boiling heat transfer coefficient and CHF for water as high as 995 kW/m^2 K and 325 W/cm^2, respectively. They suggested that the channels served as water supply conduits, and the microporous structures as effective nucleation sites. Additionally, bubbles departing from the fin tops induced strong localized liquid circulation within the micro-channels, which enhanced micro-convective heat transfer. Jaikumar and Kandlikar [401] reported that micro-channel width to depth ratio of unity provided the best enhancement for this hybrid enhancement surface in both water and FC-87. Jaikumar and Kandlikar [402] also tested three different hybrid enhancement surfaces with open micro-channels and sintered porous coatings applied to all micro-channel walls, fin tops alone, and channel walls alone. The surface with full coverage by the sintered coating provided the best enhancement in

nucleate boiling heat transfer coefficient for water. Follow-up study by Jaikumar and Kandlikar [209] investigated effects of channel width (300, 500 and 762 μm) for the three hybrid surface configurations. For the surface with coated channel walls, 300-μm channels yielded values of nucleate boiling heat transfer coefficient and CHF for water as high as 2.9 MW/m^2 K and 420 W/cm^2, respectively [403]. Similar studies were carried out by Gheitaghy et al. [404], who combined the use of 400-μm wide and 500-μm deep micro-channels, with a porous coating applied by two-stage electrodeposition, and by Akbari et al. [405], who deposited silver nanoparticles on inner walls of reentrant inclined mini-channels; both studies achieved measurable enhancements in both nucleate boiling heat transfer coefficient and CHF for water. Bai et al. [406,407] used a finned copper surface covered with a 2-mm thick microporous copper plate to achieve separation of liquid and vapor paths, and achieved a maximum heat flux for water of 610 W/cm^2.

Overall, rapid development of new micro/nano-fabrication techniques has significantly broadened implementation of hybrid surfaces, which have shown impressive enhancements in both nucleate boiling heat transfer coefficient and CHF. However, these surfaces pose two challenges, which warrant careful further study. First, while dominant heat transfer mechanisms and models for nucleate boiling heat transfer coefficient [408,409] and CHF [64,410] at the macroscale have been carefully assessed, those concerning mechanisms at micro/nanoscales (*e.g.,* microlayer evaporation and capillary wicking) are far less understood. Second, a vast majority of studies concerning micro/nanoscale surface modification lack thorough investigation of aging effects. In fact, some studies [147,148,291] involving long-duration boiling tests have shown that micro/nanoscale surface features may degrade or even lose their enhancing capabilities with time.

7.3. Hybrid wettability

7.3.1. Role of wettability in pool boiling

Bourdon et al. [411–413] showed that a hydrophobic surface lowered the incipience boiling superheat for water compared to a hydrophilic surface. Jo et al. [414] observed early bubble nucleation on a silicon surface modified with very few hydrophobic dots, regardless of milli or microscale, and achieved enhancement in nucleate boiling heat transfer coefficient for water at the expense of lower CHF compared to a surface without the dots. Follow-up study by Jo et al. [415] involved testing of identical nano/microstructures (micro-patterns surrounded by nanograss structures) but two distinct types of surface wettability: silicon-oxidized, with a contact angle of ~0°, and Teflon-coated, with 162° angle. Both wettability types were shown to enhance the nucleate boiling heat transfer coefficient and CHF appreciably. However, while the Teflon-coated yielded earlier boiling incipience and higher heat transfer coefficients, its CHF was lower than that of the oxidized silicon surface. Kim et al. [360,416] employed hybrid surfaces with microstructures similar to those used by Jo et al., but modified with nanorods. The nanorods improved surface wettability and liquid spreadability significantly, and the hybrid surface yielded CHF enhancement almost equal to the sum of enhancements achieved with the microstructures and nanorods separately.

Phan et al. [417,418] used metal-organic CVD, plasma enhanced CVD, and nanoparticle deposition by nanofluid boiling to produce surfaces with different wettability in an investigation into effects of contact angle on nucleate boiling heat transfer for water. Hydrophobic surfaces were found to lower incipience superheat, but rendered detachment of bubbles more difficult and caused the bubbles to spread and coalesce in the high heat flux region, culminating in vapor blanketing over a large portion of the surface. On the other hand, hydrophilic surfaces caused an increase in bubble departure radius, but bubble frequency decreased with the increased wettability. And surfaces with moderate contact angles of 45–90° showed deterioration in nucleate boiling heat transfer coefficient with decreasing contact angle. However, surfaces with small contact angles of less than 45° showed improvement in nucleate boiling performance with decreasing contact angle. Phan et al. suggested that highest heat transfer coefficients could be obtained with a surface having contact angles close to either 0° or 90°.

As revealed by Sun et al. [419], oxygen vacancies in crystal structure of TiO_2 improved wettability by virtue of their tendency to absorb water molecules; this effect was achieved by ultraviolet (UV) irradiation, heat treatment, and Ar^+ sputtering. Based on the same mechanism, Takata et al. [420,421] observed a two-fold increase in CHF for water and enhanced nucleate boiling heat transfer with a TiO_2 sputtered copper surface compared to an uncoated surface. Additionally, the Leidenfrost temperature was greatly increased with decreasing contact angle. Similar CHF enhancement was achieved in water by Liaw and Dhir [422] as a result of increased wettability for a copper surface whose contact angle was controlled by varying degrees of surface oxidation. However, Maeng et al. [423] found that improved wettability by plasma sputtering TiO_2 on a nickel surface that was not accompanied by porous nanostructure formation had no effect on CHF. Wang et al. [424] showed that vacuum coating a nanoscale TiO_2 film on a copper surface without UV irradiation might yield enhancement or deterioration in boiling heat transfer depending upon coating thickness since the coating did not change contact angle. However, Das and Bhaumik [425] showed that enhanced wettability with 100–300 nm TiO_2 coatings (also without UV irradiation) yielded 29.6–80.3% enhancement in nucleate boiling heat transfer coefficient for water. Using 1-μm TiO_2 coating, Wu et al. [426] arrived at similar conclusions for water and FC-72.

A recent study by Kim et al. [427] showed that transitions in wetting characteristics of the TiO_2 coating with temperature had profound influences on both nucleate boiling heat transfer coefficient and CHF. The coated surface was found to be hydrophobic at low wall temperatures, but became hydrophilic with increasing temperature. For example, increasing surface-temperature from 100 to 200 °C decreased contact angle for water from 83.1 to 32.7°. Aside from these temperature effects, Kim et al. [428] found wetting transitions to be time-dependent, causing boiling performance to improve further when increasing boiling time in the high heat flux region.

7.3.2. Non-uniform wettability surfaces

Patankar [429] reported that hydrophobicity provided the benefit of earlier boiling incipience but with the disadvantage of lower CHF, while hydrophilicity improved nucleate pool boiling heat transfer at the expense of delayed boiling incipience. He proposed development of a 'super-nucleating surface' having hydrophobic pores atop a hydrophilic surface.

Jo et al. [430,431] used hydrophilic silica coating and hydrophobic Teflon coating on silicon substrates to investigated the effects of surface wettability on pool boiling performance. Hydrophobic surfaces were found to improve nucleate boiling performance for water at low heat fluxes, compared to better performance with hydrophilic surfaces at high fluxes. And a heterogeneous surface composed of hydrophobic dots on a hydrophilic surface provided better nucleate boiling performance than either homogeneous hydrophilic or homogeneous hydrophobic surfaces. But CHF for the heterogeneous surface was almost identical to that for the homogeneous hydrophilic surface. Follow-up study by Jo et al. [432] found that increasing area ratio of hydrophobic dots to heating surface decreased CHF for water without influencing the nucleate boiling heat transfer coefficient. Based on this finding, they proposed a variety of surfaces having micro-sized hydrophobic

dots with small area ratio. Jo et al. [433] used photoresist lithography and dry etching to form a hydrophilic self-assembled monolayer pattern atop surface micro-pins, in which contact angle on the patterns was larger than on the plain surface, and demonstrated effectiveness of this technique at separating vapor and liquid paths during vigorous boiling, thereby improving nucleate boiling performance in water, but without affecting CHF.

Betz et al. [434] produced hydrophobic and hydrophilic patterns with maximum height of 100 nm on oxidized silicon wafers, with surface roughness maintained below 5 nm. They showed that combining hydrophilic and hydrophobic patterns improved nucleate boiling and CHF for water by 100% and 65%, respectively, better than a homogeneous hydrophilic surface with 7° contact angle. Furthermore, a hydrophilic surface with hydrophobic dots yielded higher CHF than a hydrophobic surface with hydrophilic dots. Follow-up study by Betz et al. [435] extended these findings to hybrid-wettability surfaces having superhydrophilic (~0° contact angle) and superhydrophobic (with contact angles >150°) patterns, achieving further heat transfer enhancement, with nucleate boiling heat transfer coefficients and CHF for water as high as 100 kW/m^2 K and in excess of 100 W/cm^2, respectively.

Hsu et al. [436,437] formed superhydrophilic stripes on a hydrophobic copper surface to enhance nucleate boiling for water. They achieved reduction in wall superheat when the heating surface had more 'interlaced lines' - interfaces between different wettability regions. Interestingly, the bubbles were generated mostly along the interlaced lines, rather than in the superhydrophilic or hydrophobic regions. Hsu et al. also achieved higher CHF with decreasing contact angle difference between opposite sides of the interlaced line [438].

Gong and Cheng [439] simulated pool boiling from a smooth surface having mixed wettability using the lattice Boltzmann method, and confirmed improvement in boiling heat transfer coefficient along with substantial reduction in nucleation time. They also showed that hydrophobic spots beneath growing bubbles possessed higher local heat flux than hydrophilic regions lacking bubble nucleation, with the highest local heat flux and lowest temperature presenting along the triple-phase contact line. Using the volume of fluid method, Zhao et al. [440] simulated pool boiling of water on hydrophilic micro-finned aluminum surfaces with hydrophobic aluminum fin tops, and confirmed effectiveness of the hybrid wettability technique for boiling enhancement.

Choi et al. [441] reported a novel method for fabricating a hybrid-wettability surface depicted in Fig. 29(a), by first printing hydrophobic polymer dot arrays with 110° contact angle on stainless steel substrate, followed by hydrophilic ZnO nanostructure with 20° contact angle, which was formed using a microreactor-assisted nanomaterial deposition process. This surface achieved three-fold improvement in nucleate boiling heat transfer coefficient for water. Fig. 29(b) shows boiling curves for water on the different surfaces tested in their study. Suroto et al. [442] produced a hybrid-wettability surface by patterning a hydrophilic TiO_2-coated copper surface using PTFE hydrophobic dots with different diameters while maintaining equal total PTFE area. They achieved improvement in nucleate boiling heat transfer coefficient for water with increases in total peripheral length of the

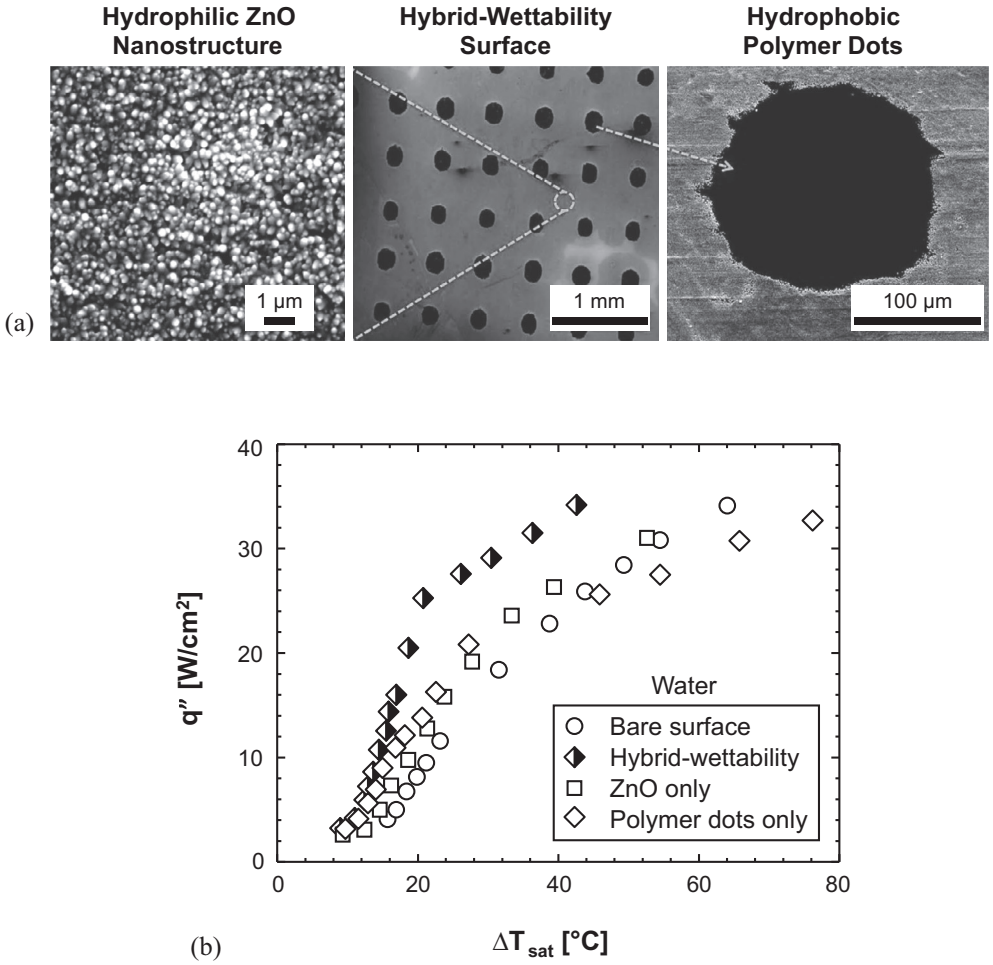

Fig. 29. (a) SEM images of hybrid-wettability surface, and (b) boiling curves for water on different surfaces. Adapted from Choi et al. [441].

dots, but performance was compromised under subcooled conditions. Noh et al. [443] devised a hydrophilic silicate glass surface with hydrophobic micropillars using inorganic polymer-based soft lithography. Zupančič et al. [444] fabricated a hydrophobic polydimethylsiloxane-silica coating, which was then treated by a nanosecond pulsed laser to generate hybrid-wettability patterns. Follow-up study by Zupančič et al. [445] used the nanosecond pulsed laser to create a variety of microtextures on stainless steel foil having both uniform and non-uniform wettability, and demonstrated their effectiveness at enhancing nucleate boiling performance for water.

Dai et al. [446] synthesized a composite-wettability interface from functionalized multiwall CNTs, by introducing hydrophilic functional groups on defect sites of pristine CNTs, to enhance nucleate pool boiling for water. Lee and Lee [447] devised a technique for adaptive control of patterned wettability, consisting of a surface having low area fraction of hydrophobic dots at the surface center. This method both delayed CHF in the central region, and intensified bubble nucleation in the outer region. They also optimized the number density of hydrophobic dots using lattice Boltzmann simulations.

Bertossi et al. [448] designed a 'switchable' surface, with thermo-responsive polymers coated on a stainless steel heating surface. As surface temperature reached the polymer switching temperature (usually slightly higher than saturation temperature of the working fluid), the polymer wettability changed from hydrophilic to hydrophobic, thereby aiding bubble nucleation. But during bubble growth, heat conducted near the triple-phase contact line caused a local decrease in polymer temperature, which switched wettability back from hydrophobic to hydrophilic, and wall temperature increased, launching a new cycle. However, the enhancement in boiling heat transfer coefficient for water with this technique was limited, averaging about only 20%.

Overall, studies performed during the past decade have provided ample evidence of the effectiveness of hydrophilic surfaces with hydrophobic patterns or dots at enhancing nucleate boiling performance. Key areas of improvement include ability to fabricate hydrophobic patterns over a large surface area, and better guidance concerning optimization of these patterns.

A major conclusion regarding all the surface modification techniques presented in this review article is scarcity of sufficiently sized databases for the enhancement methods presented in terms of fluid type, surface material, size, and orientation, enhancement shape, pattern, and scale, and operating pressure. As indicated in [449–451], such databases are becoming essential tools for both design and performance prediction for a variety of phase change parameters important to development of modern thermal management systems.

8. Concluding remarks

This paper provided a comprehensive review of published articles addressing passive enhancement of pool boiling by surface modification techniques. They include macroscale, microscale, and nanoscale surfaces, as well as multiscale (hybrid-scale) and hybrid-wettability techniques. This article also discussed potential problems and challenges associated with implementing individual enhancement methods in temperature sensitive applications, such as cooling of electronic and power devices. Key observations from the review can be summarized as follows:

(1) Applications requiring cooling of temperature sensitive electronic and power devices by pool boiling necessitate the use of dielectric coolants. These fluids possess relatively poor thermophysical properties, often resulting in unacceptably low values for both nucleate boiling heat transfer coefficient and CHF for bare surfaces. They are also highly wetting, causing flooding of potential nucleation sites, which is reflected in high incipience superheat followed by sharp temperature drop. These drawbacks necessitate the use of highly effective surface enhancement techniques when using these fluids.

(2) Macroscale enhancement techniques include use of extended surfaces, porous mesh, and porous foam. They provide various degrees of enhancement of both nucleate boiling heat transfer coefficient and CHF, along with elimination of the incipience superheat for some. And use of extended surfaces along with fluid subcooling is especially effective at achieving the enhancement benefits. But, attaching an extended surface atop a temperature sensitive device creates a contact resistance that increases device temperature, and may induce thermal stresses. However, relatively large macroscale attachments are better able to resist aging effects than both microscale and nanoscale enhancement techniques.

(3) Microscale enhancement techniques include surface roughening and use of micro-fins, open micro-channels, sintered and brazed particle coatings, graphite coatings, tunnels with reentrant cavities, and dendritic microporous structures. The major benefit of these techniques is increased nucleation site density, which increases the nucleate boiling heat transfer coefficient, but their impact on CHF varies. Among the different microscale techniques, use of modulated microporous structures is especially noteworthy because of their potential to improve CHF by separating vapor and liquid paths using critical instability wavelength as guideline in the surface modulation. Other methods, such as sintering, flame spraying, milling, and drilling, may be detrimental to the heat dissipating device.

(4) Nanoscale enhancement techniques involve coating the surface with nanotubes, nanowires, and nanofibers, and nanoporous and nanofilm layers, as well as nanoparticle deposition by nanofluid boiling. The major benefit of surface enhancement at this scale is boiling enhancement by capillary wicking within nanostructures. However, topographies of nanostructures are highly susceptible to blockage, causing decay in any enhancement over time.

(5) Hybrid-scale enhancement techniques include extended surfaces with micro-studs, finned and grooved surfaces with microporous finish, and micro-fins and micro-channels with nanoscale coatings. While these surfaces show very promising heat transfer enhancement trends, like the nanoscale surfaces, hybrid enhancement surfaces involving use of nanocoatings are susceptible to blockage and decline in performance over time.

(6) High CHF enhancement has been achieved for water using a variety of techniques. These include modulated porous structure (CHF = 450 W/cm^2), combined micro-channels and microporous coating (CHF = 420 W/cm^2), and finned surface covered with microporous copper plate (CHF = 610 W/cm^2); by comparison, pool boiling CHF for a bare surface is about 120 W/cm^2. All these enhancement techniques are based on the concept of separating liquid and vapor paths to replenish liquid toward dry patches beneath vapor bubbles near CHF. Other strategies, including improved heat transfer area, wettability, and surface wicking, have also shown CHF enhancement benefits. It is expected that combining these methods might increase CHF even further, which warrants further study of the underlying mechanisms at play.

(7) From a design standpoint, despite the large body of published articles addressing pool boiling enhancement, there is a scarcity of sufficiently sized databases for these enhancement methods in terms of fluid type, surface material, size, and orientation, enhancement shape, pattern, and scale, and operating pressure. This renders available findings less-than-adequate for design of enhanced surfaces for practical cooling applications.

Conflict of interest

The authors declared that there is no conflict of interest.

Acknowledgement

Support of the National Natural Science Foundation of China under Grant Nos. 51876025 and 51506023 is gratefully acknowledged.

Appendix A. Supplementary material

Supplementary data to this article can be found online at https://doi.org/10.1016/j.ijheatmasstransfer.2018.09.026.

References

[1] I. Mudawar, Assessment of high-heat-flux thermal management schemes, IEEE Trans. Compon. Packag. Technol. 24 (2001) 122–141.
[2] I. Mudawar, Two-phase microchannel heat sinks: theory, applications, and limitations, J. Electron. Packag. 133 (2011) 041002.
[3] I. Mudawar, Recent advances in high-flux, two-phase thermal management, J. Therm. Sci. Eng. Appl. 5 (2013) 021012.
[4] G. Liang, I. Mudawar, Review of spray cooling–Part 1: Single-phase and nucleate boiling regimes, and critical heat flux, Int. J. Heat Mass Transfer 115 (2017) 1174–1205.
[5] G. Liang, I. Mudawar, Review of spray cooling–Part 2: High temperature boiling regimes and quenching applications, Int. J. Heat Mass Transfer 115 (2017) 1206–1222.
[6] J.D. Bernardin, I. Mudawar, A cavity activation and bubble growth model of the Leidenfrost point, J. Heat Transfer 124 (2002) 864–874.
[7] I. Mudawar, T.M. Anderson, Parametric investigation into the effects of pressure, subcooling, surface augmentation and choice of coolant on pool boiling in the design of cooling systems for high-power-density electronic chips, J. Electron. Packag. 112 (1990) 375–382.
[8] T.M. Anderson, I. Mudawar, Microelectronic cooling by enhanced pool boiling of a dielectric fluorocarbon liquid, J. Heat Transfer 111 (1989) 752–759.
[9] J.A. Shmerler, I. Mudawwar, Local heat transfer coefficient in wavy free-falling turbulent liquid films undergoing uniform sensible heating, Int. J. Heat Mass Transfer 31 (1988) 67–77.
[10] J.A. Shmerler, I. Mudawwar, Local evaporative heat transfer coefficient in turbulent free-falling liquid films, Int. J. Heat Mass Transfer 31 (1988) 731–742.
[11] T.H. Lyu, I. Mudawar, Statistical investigation of the relationship between interfacial waviness and sensible heat transfer to a falling liquid film, Int. J. Heat Mass Transfer 34 (1991) 1451–1464.
[12] T.C. Willingham, I. Mudawar, Forced-convection boiling and critical heat flux from a linear array of discrete heat sources, Int. J. Heat Mass Transfer 35 (1992) 2879–2890.
[13] C.O. Gersey, I. Mudawar, Effects of heater length and orientation on the trigger mechanism for near-saturated flow boiling critical heat flux—I. Photographic study and statistical characterization of the near-wall interfacial features, Int. J. Heat Mass Transfer 38 (1995) 629–641.
[14] J.C. Sturgis, I. Mudawar, Critical heat flux in a long, rectangular channel subjected to one-sided heating—II. Analysis of critical heat flux data, Int. J. Heat Mass Transfer 42 (1999) 1849–1862.
[15] J. Lee, I. Mudawar, Fluid flow and heat transfer characteristics of low temperature two-phase micro-channel heat sinks–Part 1: Experimental methods and flow visualization results, Int. J. Heat Mass Transfer 51 (2008) 4315–4326.
[16] J. Lee, I. Mudawar, Critical heat flux for subcooled flow boiling in micro-channel heat sinks, Int. J. Heat Mass Transfer 52 (2009) 3341–3352.
[17] I. Mudawar, D.C. Wadsworth, Critical heat flux from a simulated chip to a confined rectangular impinging jet of dielectric liquid, Int. J. Heat Mass Transfer 34 (1991) 1465–1479.
[18] M.E. Johns, I. Mudawar, An ultra-high power two-phase jet-impingement avionic clamshell module, J. Electron. Packag. 118 (1996) 264–270.
[19] W.P. Klinzing, J.C. Rozzi, I. Mudawar, Film and transition boiling correlations for quenching of hot surfaces with water sprays, J. Heat. Treat. 9 (1992) 91–103.
[20] D.D. Hall, I. Mudawar, Experimental and numerical study of quenching complex-shaped metallic alloys with multiple, overlapping sprays, Int. J. Heat Mass Transfer 38 (1995) 1201–1216.
[21] M. Visaria, I. Mudawar, Application of two-phase spray cooling for thermal management of electronic devices, IEEE Trans. Compon. Packag. Technol. 32 (2009) 784–793.
[22] M.K. Sung, I. Mudawar, Single-phase hybrid micro-channel/micro-jet impingement cooling, Int. J. Heat Mass Transfer 51 (2008) 4342–4352.
[23] M.K. Sung, I. Mudawar, Single-phase and two-phase heat transfer characteristics of low temperature hybrid micro-channel/micro-jet impingement cooling module, Int. J. Heat Mass Transfer 51 (2008) 3882–3895.
[24] R.D. Boyd, Subcooled flow boiling critical heat flux (CHF) and its application to fusion energy components. Part I. a review of fundamentals of CHF and related data base, Fusion Sci. Technol. 7 (1985) 7–30.
[25] I. Mudawar, M.B. Bowers, Ultra-high critical heat flux (CHF) for subcooled water flow boiling—I: CHF data and parametric effects for small diameter tubes, Int. J. Heat Mass Transfer 42 (1999) 1405–1428.
[26] C.S. Rogers, D.M. Mills, W.K. Lee, G.S. Knapp, J. Holmberg, A. Freund, M. Wulff, M. Rossat, M. Hanfland, H. Yamaoka, Performance of a liquid-nitrogen-cooled, thin silicon crystal monochromator on a high-power, focused wiggler synchrotron beam, Rev. Sci. Instrum. 66 (1995) 3494–3499.
[27] J.P. O'Connor, S.M. You, J.Y. Chang, Gas-saturated pool boiling heat transfer from smooth and microporous surfaces in FC-72, J. Heat Transfer 118 (1996) 662–667.
[28] R.W. Murphy, A.E. Bergles, Subcooled flow boiling of fluorocarbons, MIT Heat Transfer Laboratory, Cambridge, USA, 1971.
[29] A. Bar-Cohen, T.W. Simon, Wall superheat excursions in the boiling incipience of dielectric fluids, Heat Transfer Eng. 9 (1988) 19–31.
[30] Y.Y. Hsu, On the size range of active nucleation cavities on a heating surface, J. Heat Transfer 84 (1962) 207–213.
[31] C.Y. Han, P. Griffith, The mechanism of heat transfer in nucleate pool boiling—Part I: Bubble initiaton, growth and departure, Int. J. Heat Mass Transfer 8 (1965) 887–904.
[32] E.J. Davis, G.H. Anderson, The incipience of nucleate boiling in forced convection flow, AIChE J. 12 (1966) 774–780.
[33] M. Reeber, R. Frieser, Heat transfer of modified silicon surfaces, IEEE Trans. Compon. Hybrid Manuf. Technol. 3 (1980) 387–391.
[34] S.M. You, A. Bar-Cohen, T.W. Simon, Boiling incipience and nucleate boiling heat transfer of highly wetting dielectric fluids from electronic materials, IEEE Trans. Compon. Hybrid Manuf. Technol. 13 (1990) 1032–1039.
[35] S.J. Reed, I. Mudawar, Elimination of boiling incipience temperature drop in highly wetting fluids using spherical contact with a flat surface, Int. J. Heat Mass Transfer 42 (1999) 2439–2454.
[36] M. Blander, J.L. Katz, Bubble nucleation in liquids, AIChE J. 21 (1975) 833–848.
[37] S.G. Bankoff, A.J. Hajjar, B.B. McGlothin Jr., On the nature and location of bubble nuclei in boiling from surfaces, J. Appl. Phys. 29 (1958) 1739–1741.
[38] T.O. Hui, J.R. Thome, A study of binary mixture boiling: boiling site density and subcooled heat transfer, Int. J. Heat Mass Transfer 28 (1985) 919–928.
[39] P.J. Marto, V.J. Lepere, Pool boiling heat transfer from enhanced surfaces to dielectric fluids, J. Heat Transfer 104 (1982) 292–299.
[40] K.A. Park, A.E. Bergles, Boiling heat transfer characteristics of simulated microelectronic chips with detachable heat sinks, in: Proceedings of the 8th International Heat Transfer Conference, San Francisco, USA, 1986, pp. 2099–2104.
[41] N. Zuber, Hydrodynamic aspects of boiling heat transfer PhD Dissertation, University of California, Los Angeles, USA, 1959.
[42] N. Zuber, On the stability of boiling heat transfer, Trans. ASME 80 (1958) 711–720.
[43] N. Zuber, M. Tribus, J.W. Westwater, The hydrodynamic crisis in pool boiling of saturated and subcooled liquids, in: International Developments in Heat Transfer: Proceedings of the International Heat Transfer Conference, Boulder, USA, 1961, pp. 230–236.
[44] M.S. El-Genk, A.F. Ali, Saturation boiling critical heat flux of PF-5060 dielectric liquid on microporous copper surfaces, J. Heat Transfer 137 (2015) 041501.
[45] A.E. Bergles, R.L. Webb, G.H. Junkhan, M.K. Jensen, Bibliography on augmentation of convective heat and mass transfer Heat Transfer Laboratory Report HTL-19, Iowa State University, 1979.
[46] A.E. Bergles, Some perspectives on enhanced heat transfer-second-generation heat transfer technology, J. Heat Transfer 110 (1988) 1082–1096.
[47] I. Mudawar, T.M. Anderson, Optimization of enhanced surfaces for high flux chip cooling by pool boiling, J. Electron. Packag. 115 (1993) 89–100.
[48] H. Zhang, I. Mudawar, M.M. Hasan, Experimental and theoretical study of orientation effects on flow boiling CHF, Int. J. Heat Mass Transfer 45 (2002) 4463–4477.
[49] H. Zhang, I. Mudawar, M.M. Hasan, Flow boiling CHF in microgravity, Int. J. Heat Mass Transfer 48 (2005) 3107–3118.
[50] C. Konishi, I. Mudawar, Review of flow boiling and critical heat flux in microgravity, Int. J. Heat Mass Transfer 80 (2015) 469–493.
[51] I. Mudawar, Flow boiling and flow condensation in reduced gravity, Adv. Heat Transfer 49 (2017) 225–306.
[52] R.L. Webb, G.H. Junkhan, A.E. Bergles, Bibliography of US patents on augmentation of convective heat and mass transfer Heat Transfer Laboratory Report HTL-25, Iowa State University, 1980.

[53] S. Bhavnani, V. Narayanan, W. Qu, M. Jensen, S. Kandlikar, J. Kim, J. Thome, Boiling augmentation with micro/nanostructured surfaces: current status and research outlook, Nanoscale Microscale Thermophys. Eng. 18 (2014) 197–222.
[54] M. Shojaeian, A. Koşar, Pool boiling and flow boiling on micro-and nanostructured surfaces, Exp. Therm. Fluid Sci. 63 (2015) 45–73.
[55] M. McCarthy, K. Gerasopoulos, S.C. Maroo, A.J. Hart, Materials, fabrication, and manufacturing of micro/nanostructured surfaces for phase-change heat transfer enhancement, Nanoscale Microscale Thermophys. Eng. 18 (2014) 288–310.
[56] D.E. Kim, D.I. Yu, D.W. Jerng, M.H. Kim, H.S. Ahn, Review of boiling heat transfer enhancement on micro/nanostructured surfaces, Exp. Therm. Fluid Sci. 66 (2015) 173–196.
[57] D. Attinger, C. Frankiewicz, A.R. Betz, T.M. Schutzius, R. Ganguly, A. Das, C.-J. Kim, C.M. Megaridis, Surface engineering for phase change heat transfer: a review, MRS Energy Sustain. 1 (2014) E4.
[58] H. Honda, J.J. Wei, Enhanced boiling heat transfer from electronic components by use of surface microstructures, Exp. Therm. Fluid Sci. 28 (2004) 159–169.
[59] Y.-W. Lu, S.G. Kandlikar, Nanoscale surface modification techniques for pool boiling enhancement—a critical review and future directions, Heat Transfer Eng. 32 (2011) 827–842.
[60] C.M. Patil, S.G. Kandlikar, Review of the manufacturing techniques for porous surfaces used in enhanced pool boiling, Heat Transfer Eng. 35 (2014) 887–902.
[61] S. Mori, Y. Utaka, Critical heat flux enhancement by surface modification in a saturated pool boiling: A review, Int. J. Heat Mass Transfer 108 (2017) 2534–2557.
[62] G. Liang, I. Mudawar, Review of mass and momentum interactions during drop impact on a liquid film, Int. J. Heat Mass Transfer 101 (2016) 577–599.
[63] G. Liang, I. Mudawar, Review of drop impact on heated walls, Int. J. Heat Mass Transfer 106 (2017) 103–126.
[64] G. Liang, I. Mudawar, Pool boiling critical heat flux (CHF)–Part 1: Review of mechanisms, models, and correlations, Int. J. Heat Mass Transfer 117 (2018) 1352–1367.
[65] G. Liang, I. Mudawar, Review of pool boiling enhancement with additives and nanofluids, Int. J. Heat Mass Transfer 124 (2018) 423–453.
[66] K.J.L. Geisler, A. Bar-Cohen, Confinement effects on nucleate boiling and critical heat flux in buoyancy-driven microchannels, Int. J. Heat Mass Transfer 52 (2009) 2427–2436.
[67] T. Guo, T. Zhu, Experimental research on the enhancement of boiling heat transfer of liquid helium in narrow channel, Cryogenics 37 (1997) 67–70.
[68] E. Ishibashi, K. Nishikawa, Saturated boiling heat transfer in narrow spaces, Int. J. Heat Mass Transfer 12 (1969) 863–894.
[69] A. Bar-Cohen, H. Schweitzer, Thermosyphon boiling in vertical channels, J. Heat Transfer 107 (1985) 772–778.
[70] C. Xia, W. Hu, Z. Guo, Natural convective boiling in vertical rectangular narrow channels, Exp. Therm. Fluid Sci. 12 (1996) 313–324.
[71] J. Bonjour, M. Lallemand, Flow patterns during boiling in a narrow space between two vertical surfaces, Int. J. Multiphase Flow 24 (1998) 947–960.
[72] S.-C. Yao, Y. Chang, Pool boiling heat transfer in a confined space, Int. J. Heat Mass Transfer 26 (1983) 841–848.
[73] Y. Fujita, H. Ohta, S. Uchida, K. Nishikawa, Nucleate boiling heat transfer and critical heat flux in narrow space between rectangular surfaces, Int. J. Heat Mass Transfer 31 (1988) 229–239.
[74] C.M. Rops, R. Lindken, J.F.M. Velthuis, J. Westerweel, Enhanced heat transfer in confined pool boiling, Int. J. Heat Fluid Flow 30 (2009) 751–760.
[75] M. Monde, H. Kusuda, H. Uehara, Critical heat flux during natural convective boiling in vertical rectangular channels submerged in saturated liquid, J. Heat Transfer 104 (1982) 300–303.
[76] J. Bonjour, M. Lallemand, Effects of confinement and pressure on critical heat flux during natural convective boiling in vertical channels, Int. Commun. Heat Mass Transfer 24 (1997) 191–200.
[77] S. Mukherjee, I. Mudawar, Pumpless loop for narrow channel and micro-channel boiling, J. Electron. Packag. 125 (2003) 431–441.
[78] S. Mukherjee, I. Mudawar, Smart pumpless loop for micro-channel electronic cooling using flat and enhanced surfaces, IEEE Trans. Compon. Packag. Technol. 26 (2003) 99–109.
[79] M. Misale, G. Guglielmini, A. Priarone, Nucleate boiling and critical heat flux of HFE-7100 in horizontal narrow spaces, Exp. Therm. Fluid Sci. 35 (2011) 772–779.
[80] B. Stutz, M. Lallemand, F. Raimbault, J. Passos, Nucleate and transition boiling in narrow horizontal spaces, Heat Mass Transfer 45 (2009) 929–935.
[81] M. Misale, G. Guglielmini, A. Priarone, HFE-7100 pool boiling heat transfer and critical heat flux in inclined narrow spaces, Int. J. Refrig. 32 (2009) 235–245.
[82] J.C. Passos, F.R. Hirata, L.F.B. Possamai, M. Balsamo, M. Misale, Confined boiling of FC72 and FC87 on a downward facing heating copper disk, Int. J. Heat Fluid Flow 25 (2004) 313–319.
[83] J.C. Passos, L.F.B. Possamai, F.R. Hirata, Confined and unconfined FC72 and FC87 boiling on a downward-facing disc, Appl. Therm. Eng. 25 (2005) 2543–2554.
[84] J.C. Passos, E.L. da Silva, L.F.B. Possamai, Visualization of FC72 confined nucleate boiling, Exp. Therm. Fluid Sci. 30 (2005) 1–7.
[85] E.M. Cardoso, O. Kannengieser, B. Stutz, J.C. Passos, FC72 and FC87 nucleate boiling inside a narrow horizontal space, Exp. Therm. Fluid Sci. 35 (2011) 1038–1045.
[86] G.J. Klein, J.W. Westwater, Heat transfer from multiple spines to boiling liquids, AIChE J. 17 (1971) 1050–1056.
[87] K.N. Rainey, S.M. You, Pool boiling heat transfer from plain and microporous, square pin-finned surfaces in saturated FC-72, J. Heat Transfer 122 (2000) 509–516.
[88] J.L. Parker, M.S. El-Genk, Saturation boiling of HFE-7100 dielectric liquid on copper surfaces with corner pins at different inclinations, J. Enhanced Heat Transfer 16 (2009) 103–122.
[89] C.K. Yu, D.C. Lu, Pool boiling heat transfer on horizontal rectangular fin array in saturated FC-72, Int. J. Heat Mass Transfer 50 (2007) 3624–3637.
[90] G. Guglielmini, M. Misale, C. Schenone, Experiments on pool boiling of a dielectric fluid on extended surfaces, Int. Commun. Heat Mass Transfer 23 (1996) 451–462.
[91] G. Guglielmini, M. Misale, C. Schenone, Boiling of saturated FC-72 on square pin fin arrays, Int. J. Therm. Sci. 41 (2002) 599–608.
[92] N. Abuaf, S.H. Black, F.W. Staub, Pool boiling performance of finned surfaces in R-113, Int. J. Heat Fluid Flow 6 (1985) 23–30.
[93] Z.H. Ayub, A.E. Bergles, Pool boiling from GEWA surfaces in water and R-113, Heat Mass Transfer 21 (1987) 209–219.
[94] D. Zhong, J.a. Meng, Z. Li, Z. Guo, Critical heat flux for downward-facing saturated pool boiling on pin fin surfaces, Int. J. Heat Mass Transfer 87 (2015) 201–211.
[95] M.A. Chan, C.R. Yap, K.C. Ng, Pool boiling heat transfer of water on finned surfaces at near vacuum pressures, J. Heat Transfer 132 (2010) 031501.
[96] S.J. Reed, I. Mudawar, Enhancement of boiling heat transfer using highly wetting liquids with pressed-on fins at low contact forces, Int. J. Heat Mass Transfer 40 (1997) 2379–2392.
[97] T.Y. Kim, S.V. Garimella, Investigation of boiling heat transfer in water using a free-particles-based enhancement technique, Int. J. Heat Mass Transfer 71 (2014) 818–828.
[98] T.Y. Kim, J.A. Weibel, S.V. Garimella, A free-particles-based technique for boiling heat transfer enhancement in a wetting liquid, Int. J. Heat Mass Transfer 71 (2014) 808–817.
[99] M.-Y. Wen, K.-J. Jang, C.-Y. Ho, Pool boiling heat transfer of deionized and degassed water in packed-perforated copper beads, Heat Mass Transfer 52 (2016) 2447–2457.
[100] L. Zhou, Z. Wang, X. Du, Y. Yang, Boiling characteristics of water and self-rewetting fluids in packed bed of spherical glass beads, Exp. Therm. Fluid Sci. 68 (2015) 537–544.
[101] W. Chen, J. Wang, Experiment analysis of pool boiling heat transfer in bead packed porous layers, Heat Transfer Asian Res. 45 (2016) 758–772.
[102] R.D.M. Carvalho, A.E. Bergles, The influence of subcooling on the pool nucleate boiling and critical heat flux of simulated electronic chips, in: Proceedings of 9th International Heat Transfer Conference, Jerusalem, Israel, 1990, pp. 289–294.
[103] R. Shimada, J. Komai, Y. Hirono, S. Kumagai, T. Takeyama, Enhancement of boiling heat transfer in a narrow space restricted by an interference plate with holes, Exp. Therm. Fluid Sci. 4 (1991) 587–593.
[104] Y. Zhao, T. Tsuruta, C. Ji, Experimental study of nucleate boiling heat transfer enhancement in a confined space, Exp. Therm. Fluid Sci. 28 (2003) 9–16.
[105] J.W. Liu, D.J. Lee, A. Su, Boiling of methanol and HFE-7100 on heated surface covered with a layer of mesh, Int. J. Heat Mass Transfer 44 (2001) 241–246.
[106] S. Hasegawa, R. Echigo, S. Irie, Boiling characteristics and burnout phenomena on heating surface covered with woven screens, J. Nucl. Sci. Technol. 12 (1975) 722–724.
[107] J.Y. Tsay, Y.Y. Yan, T.F. Lin, Enhancement of pool boiling heat transfer in a horizontal water layer through surface roughness and screen coverage, Heat Mass Transfer 32 (1996) 17–26.
[108] A. Franco, E.M. Latrofa, V.V. Yagov, Heat transfer enhancement in pool boiling of a refrigerant fluid with wire nets structures, Exp. Therm. Fluid Sci. 30 (2006) 263–275.
[109] S.J. Penley, R.A. Wirtz, Correlation of subatmospheric pressure, saturated, pool boiling of water on a structured-porous surface, J. Heat Transfer 133 (2011) 041501.
[110] E. Melendez, R. Reyes, The pool boiling heat transfer enhancement from experiments with binary mixtures and porous heating covers, Exp. Therm. Fluid Sci. 30 (2006) 185–192.
[111] J. Tehver, H. Sui, V. Temkina, Heat transfer and hysteresis phenomena in boiling on porous plasma-sprayed surface, Exp. Therm. Fluid Sci. 5 (1992) 714–727.
[112] S. Mori, K. Okuyama, Enhancement of the critical heat flux in saturated pool boiling using honeycomb porous media, Int. J. Multiphase Flow 35 (2009) 946–951.
[113] J. Xu, X. Ji, W. Zhang, G. Liu, Pool boiling heat transfer of ultra-light copper foam with open cells, Int. J. Multiphase Flow 34 (2008) 1008–1022.
[114] Y. Yang, X. Ji, J. Xu, Pool boiling heat transfer on copper foam covers with water as working fluid, Int. J. Therm. Sci. 49 (2010) 1227–1237.
[115] Y. Yang, X. Ji, J. Xu, Effect of inclination angle on the pool boiling heat transfer of ultra-light copper foams, Heat Mass Transfer 46 (2010) 695–706.
[116] Y. Zhu, H. Hu, G. Ding, H. Peng, X. Huang, D. Zhuang, J. Yu, Influence of oil on nucleate pool boiling heat transfer of refrigerant on metal foam covers, Int. J. Refrig. 34 (2011) 509–517.

[117] Z.G. Qu, Z.G. Xu, C.Y. Zhao, W.Q. Tao, Experimental study of pool boiling heat transfer on horizontal metallic foam surface with crossing and single-directional V-shaped groove in saturated water, Int. J. Multiphase Flow 41 (2012) 44–55.
[118] Z.G. Xu, Z.G. Qu, C.Y. Zhao, W.Q. Tao, Pool boiling heat transfer on open-celled metallic foam sintered surface under saturation condition, Int. J. Heat Mass Transfer 54 (2011) 3856–3867.
[119] Z.G. Xu, Z.G. Qu, C.Y. Zhao, W.Q. Tao, Experimental correlation for pool boiling heat transfer on metallic foam surface and bubble cluster growth behavior on grooved array foam surface, Int. J. Heat Mass Transfer 77 (2014) 1169–1182.
[120] Z.G. Xu, C.Y. Zhao, Thickness effect on pool boiling heat transfer of trapezoid-shaped copper foam fins, Appl. Therm. Eng. 60 (2013) 359–370.
[121] Z.G. Xu, C.Y. Zhao, Pool boiling heat transfer of open-celled metal foams with V-shaped grooves for high pore densities, Exp. Therm. Fluid Sci. 52 (2014) 128–138.
[122] Z.G. Xu, C.Y. Zhao, Enhanced boiling heat transfer by gradient porous metals in saturated pure water and surfactant solutions, Appl. Therm. Eng. 100 (2016) 68–77.
[123] Z.G. Xu, C.Y. Zhao, Experimental study on pool boiling heat transfer in gradient metal foams, Int. J. Heat Mass Transfer 85 (2015) 824–829.
[124] I. Pranoto, K.C. Leong, L.W. Jin, The role of graphite foam pore structure on saturated pool boiling enhancement, Appl. Therm. Eng. 42 (2012) 163–172.
[125] L.W. Jin, K.C. Leong, I. Pranoto, Saturated pool boiling heat transfer from highly conductive graphite foams, Appl. Therm. Eng. 31 (2011) 2685–2693.
[126] C.-D. Wen, I. Mudawar, Emissivity characteristics of roughened aluminum alloy surfaces and assessment of multispectral radiation thermometry (MRT) emissivity models, Int. J. Heat Mass Transfer 47 (2004) 3591–3605.
[127] H.M. Kurihara, J.E. Myers, The effects of superheat and surface roughness on boiling coefficients, AIChE J. 6 (1960) 83–91.
[128] S.K.R. Chowdhury, R.H.S. Winterton, Surface effects in pool boiling, Int. J. Heat Mass Transfer 28 (1985) 1881–1889.
[129] S.T. Hsu, F.W. Schmidt, Measured variations in local surface temperatures in pool boiling of water, J. Heat Transfer 83 (1961) 254–260.
[130] P.J. Berenson, Experiments on pool-boiling heat transfer, Int. J. Heat Mass Transfer 5 (1962) 985–999.
[131] P.J. Marto, W.M. Rohsenow, Effects of surface conditions on nucleate pool boiling of sodium, J. Heat Transfer 88 (1966) 196–203.
[132] B.J. Jones, J.P. McHale, S.V. Garimella, The influence of surface roughness on nucleate pool boiling heat transfer, J. Heat Transfer 131 (2009) 121009.
[133] J.-Y. Jung, H.-Y. Kwak, Effect of surface condition on boiling heat transfer from silicon chip with submicron-scale roughness, Int. J. Heat Mass Transfer 49 (2006) 4543–4551.
[134] I. Golobič, K. Ferjančič, The role of enhanced coated surface in pool boiling CHF in FC-72, Heat Mass Transfer 36 (2000) 525–531.
[135] R.I. Vachon, G.E. Tanger, D.L. Davis, G.H. Nix, Pool boiling on polished and chemically etched stainless-steel surfaces, J. Heat Transfer 90 (1968) 231–238.
[136] K. Ferjančič, I. Golobič, Surface effects on pool boiling CHF, Exp. Therm. Fluid Sci. 25 (2002) 565–571.
[137] J.C. Passos, R.F. Reinaldo, Analysis of pool boiling within smooth and grooved tubes, Exp. Therm. Fluid Sci. 22 (2000) 35–44.
[138] S. Alangar, Nucleate pool boiling heat transfer from a flat-plate grooved surface, J. Enhanced Heat Transfer 22 (2015) 247–265.
[139] P.A. Raghupathi, S.G. Kandlikar, Pool boiling enhancement through contact line augmentation, Appl. Phys. Lett. 110 (2017) 204101.
[140] L. Dong, X. Quan, P. Cheng, An analysis of surface-microstructures effects on heterogeneous nucleation in pool boiling, Int. J. Heat Mass Transfer 55 (2012) 4376–4384.
[141] J.Y. Ho, K.K. Wong, K.C. Leong, Saturated pool boiling of FC-72 from enhanced surfaces produced by Selective Laser Melting, Int. J. Heat Mass Transfer 99 (2016) 107–121.
[142] C.-K. Guan, B. Bon, J. Klausner, R. Mei, Comparison of CHF enhancement on microstructured surfaces with a predictive model, Heat Transfer Eng. 35 (2014) 452–460.
[143] B. Bon, J.F. Klausner, E. Mckenna, The hoodoo: a new surface structure for enhanced boiling heat transfer, J. Therm. Sci. Eng. Appl. 5 (2013) 011003.
[144] J.E. Galloway, I. Mudawar, CHF mechanism in flow boiling from a short heated wall—II. Theoretical CHF model, Int. J. Heat Mass Transfer 36 (1993) 2527–2540.
[145] C.-K. Guan, J.F. Klausner, R. Mei, A new mechanistic model for pool boiling CHF on horizontal surfaces, Int. J. Heat Mass Transfer 54 (2011) 3960–3969.
[146] J. Kim, S. Jun, R. Laksnarain, S.M. You, Effect of surface roughness on pool boiling heat transfer at a heated surface having moderate wettability, Int. J. Heat Mass Transfer 101 (2016) 992–1002.
[147] R.L. Webb, The evolution of enhanced surface geometries for nucleate boiling, Heat Transfer Eng. 2 (1981) 46–69.
[148] I.H. Chaudhri, I.R. McDougall, Ageing studies in nucleate pool boiling of isopropyl acetate and perchloroethylene, Int. J. Heat Mass Transfer 12 (1969) 681–688.
[149] H. Honda, H. Takamastu, J.J. Wei, Enhanced boiling of FC-72 on silicon chips with micro-pin-fins and submicron-scale roughness, J. Heat Transfer 124 (2002) 383–390.
[150] S.M. You, T.W. Simon, A. Bar-Cohen, Y.S. Hong, Effects of dissolved gas content on pool boiling of a highly wetting fluid, J. Heat Transfer 117 (1995) 687–692.
[151] H. Honda, H. Takamatsu, J.J. Wei, Enhanced boiling heat transfer from silicon chips with micro-pin fins immersed in FC-72, J. Enhanced Heat Transfer 10 (2003) 211–223.
[152] S.H. Kim, G.C. Lee, J.Y. Kang, K. Moriyama, M.H. Kim, H.S. Park, Boiling heat transfer and critical heat flux evaluation of the pool boiling on micro structured surface, Int. J. Heat Mass Transfer 91 (2015) 1140–1147.
[153] D.E. Kim, D.I. Yu, S.C. Park, H.J. Kwak, H.S. Ahn, Critical heat flux triggering mechanism on micro-structured surfaces: coalesced bubble departure frequency and liquid furnishing capability, Int. J. Heat Mass Transfer 91 (2015) 1237–1247.
[154] J.J. Wei, L.J. Guo, H. Honda, Experimental study of boiling phenomena and heat transfer performances of FC-72 over micro-pin-finned silicon chips, Heat Mass Transfer 41 (2005) 744–755.
[155] J.J. Wei, H. Honda, Effects of fin geometry on boiling heat transfer from silicon chips with micro-pin-fins immersed in FC-72, Int. J. Heat Mass Transfer 46 (2003) 4059–4070.
[156] K.-H. Chu, R. Enright, E.N. Wang, Structured surfaces for enhanced pool boiling heat transfer, Appl. Phys. Lett. 100 (2012) 241603.
[157] S.G. Kandlikar, A theoretical model to predict pool boiling CHF incorporating effects of contact angle and orientation, J. Heat Transfer 123 (2001) 1071–1079.
[158] X. Quan, L. Dong, P. Cheng, A CHF model for saturated pool boiling on a heated surface with micro/nano-scale structures, Int. J. Heat Mass Transfer 76 (2014) 452–458.
[159] J. Mitrovic, F. Hartmann, A new microstructure for pool boiling, Superlatt. Microstruct. 35 (2004) 617–628.
[160] M. Zhang, K. Lian, Using bulk micromachined structures to enhance pool boiling heat transfer, Microsyst. Technol. 14 (2008) 1499–1505.
[161] Y.-H. Kim, K.-J. Lee, D. Han, Pool boiling enhancement with surface treatments, Heat Mass Transfer 45 (2008) 55–60.
[162] D. Cooke, S.G. Kandlikar, Pool boiling heat transfer and bubble dynamics over plain and enhanced microchannels, J. Heat Transfer 133 (2011) 052902.
[163] D. Cooke, S.G. Kandlikar, Effect of open microchannel geometry on pool boiling enhancement, Int. J. Heat Mass Transfer 55 (2012) 1004–1013.
[164] A. Kalani, S.G. Kandlikar, Enhanced pool boiling with ethanol at subatmospheric pressures for electronics cooling, J. Heat Transfer 135 (2013) 111002.
[165] A.M. Gheitaghy, A. Samimi, H. Saffari, Surface structuring with inclined minichannels for pool boiling improvement, Appl. Therm. Eng. 126 (2017) 892–902.
[166] A.K. Das, P.K. Das, P. Saha, Performance of different structured surfaces in nucleate pool boiling, Appl. Therm. Eng. 29 (2009) 3643–3653.
[167] A.K. Das, P.K. Das, P. Saha, Some investigations on the enhancement of boiling heat transfer from planer surface embedded with continuous open tunnels, Exp. Therm. Fluid Sci. 34 (2010) 1422–1431.
[168] S.G. Kandlikar, Controlling bubble motion over heated surface through evaporation momentum force to enhance pool boiling heat transfer, Appl. Phys. Lett. 102 (2013) 051611.
[169] M.M. Rahman, J. Pollack, M. McCarthy, Increasing boiling heat transfer using low conductivity materials, Sci. Rep. 5 (2015) 13145.
[170] A. Jaikumar, S.G. Kandlikar, Pool boiling enhancement through bubble induced convective liquid flow in feeder microchannels, Appl. Phys. Lett. 108 (2016) 041604.
[171] A.E. Bergles, M.C. Chyu, Characteristics of nucleate pool boiling from porous metallic coatings, J. Heat Transfer 104 (1982) 279–285.
[172] V.I. Borzenko, S.P. Malyshenko, Mechanisms of phase exchange under conditions of boiling on surfaces with porous coatings, High Temp. 39 (2001) 714–721.
[173] S.G. Liter, M. Kaviany, Pool-boiling CHF enhancement by modulated porous-layer coating: theory and experiment, Int. J. Heat Mass Transfer 44 (2001) 4287–4311.
[174] S.M. You, T.W. Simon, A. Bar-Cohen, A technique for enhancing boiling heat transfer with application to cooling of electronic equipment, IEEE Trans. Compon. Hybrid Manuf. Technol. 15 (1992) 823–831.
[175] J.P. O'Connor, S.M. You, A painting technique to enhance pool boiling heat transfer in saturated FC-72, J. Heat Transfer 117 (1995) 387–393.
[176] J.P. O'Connor, S.M. You, D.C. Price, A dielectric surface coating technique to enhance boiling heat transfer from high power microelectronics, IEEE Trans. Compon. Packag. Manuf. Technol. Part A 18 (1995) 656–663.
[177] J.Y. Chang, S.M. You, Heater orientation effects on pool boiling of micro-porous-enhanced surfaces in saturated FC-72, J. Heat Transfer 118 (1996) 937–943.
[178] K.N. Rainey, S.M. You, Effects of heater size and orientation on pool boiling heat transfer from microporous coated surfaces, Int. J. Heat Mass Transfer 44 (2001) 2589–2599.
[179] J.Y. Chang, S.M. You, Enhanced boiling heat transfer from microporous surfaces: effects of a coating composition and method, Int. J. Heat Mass Transfer 40 (1997) 4449–4460.
[180] K.N. Rainey, S.M. You, S. Lee, Effect of pressure, subcooling, and dissolved gas on pool boiling heat transfer from microporous surfaces in FC-72, J. Heat Transfer 125 (2003) 75–83.
[181] J.H. Kim, K.N. Rainey, S.M. You, J.Y. Pak, Mechanism of nucleate boiling heat transfer enhancement from microporous surfaces in saturated FC-72, J. Heat Transfer 124 (2002) 500–506.

[182] J.H. Kim, A. Gurung, M. Amaya, S.M. Kwark, S.M. You, Microporous coatings to maximize pool boiling heat transfer of saturated R-123 and water, J. Heat Transfer 137 (2015) 081501.

[183] S. Jun, J. Kim, D. Son, H.Y. Kim, S.M. You, Enhancement of pool boiling heat transfer in water using sintered copper microporous coatings, Nucl. Eng. Technol. 48 (2016) 932–940.

[184] S. Jun, J. Kim, S.M. You, H.Y. Kim, Effect of heater orientation on pool boiling heat transfer from sintered copper microporous coating in saturated water, Int. J. Heat Mass Transfer 103 (2016) 277–284.

[185] S. Jun, H. Wi, A. Gurung, M. Amaya, S.M. You, Pool boiling heat transfer enhancement of water using brazed copper microporous coatings, J. Heat Transfer 138 (2016) 071502.

[186] G.-S. Hwang, M. Kaviany, Critical heat flux in thin, uniform particle coatings, Int. J. Heat Mass Transfer 49 (2006) 844–849.

[187] J.Y. Chang, S.M. You, Boiling heat transfer phenomena from microporous and porous surfaces in saturated FC-72, Int. J. Heat Mass Transfer 40 (1997) 4437–4447.

[188] R.L. Webb, Nucleate boiling on porous coated surfaces, Heat Transfer Eng. 4 (1983) 71–82.

[189] S. Sarangi, J.A. Weibel, S.V. Garimella, Effect of particle size on surface-coating enhancement of pool boiling heat transfer, Int. J. Heat Mass Transfer 81 (2015) 103–113.

[190] S. Sarangi, J.A. Weibel, S.V. Garimella, Quantitative evaluation of the dependence of pool boiling heat transfer enhancement on sintered particle coating characteristics, J. Heat Transfer 139 (2017) 021502.

[191] R.G. Scurlock, Enhanced boiling heat transfer surfaces, Cryogenics 35 (1995) 233–237.

[192] S.J. Thiagarajan, R. Yang, C. King, S. Narumanchi, Bubble dynamics and nucleate pool boiling heat transfer on microporous copper surfaces, Int. J. Heat Mass Transfer 89 (2015) 1297–1315.

[193] G. Moreno, S. Narumanchi, C. King, Pool boiling heat transfer characteristics of HFO-1234yf on plain and microporous-enhanced surfaces, J. Heat Transfer 135 (2013) 111014.

[194] C. Byon, S. Choi, S.J. Kim, Critical heat flux of bi-porous sintered copper coatings in FC-72, Int. J. Heat Mass Transfer 65 (2013) 655–661.

[195] K. Nishikawa, T. Ito, Augmentation of nucleate boiling heat transfer by prepared surfaces, in: T. Mizushina, W.J. Yang (Eds.), Heat Transfer in Energy Problems, Hemisphere, Washington, D.C., 1980, pp. 111–118.

[196] P.S. O'Neill, C.F. Gottzmann, J.W. Terbot, Novel heat exchanger increases cascade cycle efficiency for natural gas liquefaction, in: K.D. Timmerhaus (Ed.), Advances in Cryogenic Engineering, Springer, New York, 1972, pp. 420–437.

[197] A.M. Czikk, P.S. O'Neill, Correlation of nucleate boiling from porous metal films, in: J.M. Chenoweth, J. Kaellis, J.W. Michel, S. Shenkman (Eds.), Advances in Enhanced Heat Transfer, ASME, New York, 1979, pp. 103–113.

[198] S.M. Lu, R.H. Chang, Pool boiling from a surface with a porous layer, AIChE J. 33 (1987) 1813–1828.

[199] N.H. Afgan, L.A. Jovic, S.A. Kovalev, V.A. Lenykov, Boiling heat transfer from surfaces with porous layers, Int. J. Heat Mass Transfer 28 (1985) 415–422.

[200] D.H. Min, G.S. Hwang, Y. Usta, O.N. Cora, M. Koc, M. Kaviany, 2-D and 3-D modulated porous coatings for enhanced pool boiling, Int. J. Heat Mass Transfer 52 (2009) 2607–2613.

[201] Ö.N. Cora, D. Min, M. Koç, M. Kaviany, Microscale-modulated porous coatings: fabrication and pool-boiling heat transfer performance, J. Micromech. Microeng. 20 (2010) 035020.

[202] X. Ji, J. Xu, Z. Zhao, W. Yang, Pool boiling heat transfer on uniform and non-uniform porous coating surfaces, Exp. Therm. Fluid Sci. 48 (2013) 198–212.

[203] C.H. Li, T. Li, P. Hodgins, C.N. Hunter, A.A. Voevodin, J.G. Jones, G.P. Peterson, Comparison study of liquid replenishing impacts on critical heat flux and heat transfer coefficient of nucleate pool boiling on multiscale modulated porous structures, Int. J. Heat Mass Transfer 54 (2011) 3146–3155.

[204] C. Li, G.P. Peterson, Experimental study of enhanced nucleate boiling heat transfer on uniform and modulated porous structures, Front. Heat Mass Transfer 1 (2010) 023007.

[205] C.H. Li, Nucleate boiling heat transfer on sintered copper porous structure module cone surfaces, J. Thermophys. Heat Transfer 25 (2011) 186–191.

[206] J.T. Cieśliński, Nucleate pool boiling on porous metallic coatings, Exp. Therm. Fluid Sci. 25 (2002) 557–564.

[207] A. Jaikumar, A. Rishi, A. Gupta, S.G. Kandlikar, Microscale morphology effects of copper–graphene oxide coatings on pool boiling characteristics, J. Heat Transfer 139 (2017) 111509.

[208] Z. Protich, K.S.V. Santhanam, A. Jaikumar, S.G. Kandlikar, P. Wong, Electrochemical deposition of copper in graphene quantum dot bath: Pool boiling enhancement, J. Electrochem. Soc. 163 (2016) E166–E172.

[209] A. Jaikumar, S.G. Kandlikar, Ultra-high pool boiling performance and effect of channel width with selectively coated open microchannels, Int. J. Heat Mass Transfer 95 (2016) 795–805.

[210] A. Jaikumar, S.G. Kandlikar, Pool boiling inversion through bubble induced macroconvection, Appl. Phys. Lett. 110 (2017) 094107.

[211] C. Kruse, A. Tsubaki, C. Zuhlke, T. Anderson, D. Alexander, G. Gogos, S. Ndao, Secondary pool boiling effects, Appl. Phys. Lett. 108 (2016) 051602.

[212] C.M. Kruse, T. Anderson, C. Wilson, C. Zuhlke, D. Alexander, G. Gogos, S. Ndao, Enhanced pool-boiling heat transfer and critical heat flux on femtosecond laser processed stainless steel surfaces, Int. J. Heat Mass Transfer 82 (2015) 109–116.

[213] C. Li, G.P. Peterson, Parametric study of pool boiling on horizontal highly conductive microporous coated surfaces, J. Heat Transfer 129 (2007) 1465–1475.

[214] C. Li, G.P. Peterson, Geometric effects on critical heat flux on horizontal microporous coatings, J. Thermophys. Heat Transfer 24 (2010) 449–455.

[215] C. Li, G.P. Peterson, Y. Wang, Evaporation/boiling in thin capillary wicks (I)—wick thickness effects, J. Heat Transfer 128 (2006) 1312–1319.

[216] C. Li, G.P. Peterson, Evaporation/boiling in thin capillary wicks (II)—effects of volumetric porosity and mesh size, J. Heat Transfer 128 (2006) 1320–1328.

[217] Y. Chen, L.S. Melvin, M.M. Weislogel, R.M. Jenson, S. Dhuey, P.F. Nealey, Design, fabrication, and testing of microporous wicking structure, Microelectron. Eng. 85 (2008) 1027–1030.

[218] D.S. Jung, J.E.S. Venart, A.C.M. Sousa, Effects of enhanced surfaces and surface orientation on nucleate and film boiling heat transfer in R-11, Int. J. Heat Mass Transfer 30 (1987) 2627–2639.

[219] H. Kubo, H. Takamatsu, H. Honda, Effects of size and number density of micro-reentrant cavities on boiling heat transfer from a silicon chip immersed in degassed and gas-dissolved FC-72, J. Enhanced Heat Transfer 6 (1999) 151–160.

[220] W. Nakayama, T. Daikoku, T. Nakajima, Effects of pore diameters and system pressure on saturated pool nucleate boiling heat transfer from porous surfaces, J. Heat Transfer 104 (1982) 286–291.

[221] W. Nakayama, T. Daikoku, H. Kuwahara, T. Nakajima, Dynamic model of enhanced boiling heat transfer on porous surfaces—Part II: analytical modeling, J. Heat Transfer 102 (1980) 451–456.

[222] W. Nakayama, T. Daikoku, H. Kuwahara, T. Nakajima, Dynamic model of enhanced boiling heat transfer on porous surfaces—Part I: experimental investigation, J. Heat Transfer 102 (1980) 445–450.

[223] L.-H. Chien, R.L. Webb, A nucleate boiling model for structured enhanced surfaces, Int. J. Heat Mass Transfer 41 (1998) 2183–2195.

[224] A.K. Das, P.K. Das, S. Bhattacharyya, P. Saha, Nucleate boiling heat transfer from a structured surface–effect of liquid intake, Int. J. Heat Mass Transfer 50 (2007) 1577–1591.

[225] Y.Y. Jiang, W.C. Wang, D. Wang, B.X. Wang, Boiling heat transfer on machined porous surfaces with structural optimization, Int. J. Heat Mass Transfer 44 (2001) 443–456.

[226] S. Murthy, Y. Joshi, S. Gurrum, W. Nakayama, Enhanced boiling heat transfer simulation from structured surfaces: semi-analytical model, Int. J. Heat Mass Transfer 49 (2006) 1885–1895.

[227] L.-H. Chien, R.L. Webb, Measurement of bubble dynamics on an enhanced boiling surface, Exp. Therm. Fluid Sci. 16 (1998) 177–186.

[228] L.-H. Chien, R.L. Webb, Visualization of pool boiling on enhanced surfaces, Exp. Therm. Fluid Sci. 16 (1998) 332–341.

[229] J. Arshad, J.R. Thome, Enhanced boiling surfaces: heat transfer mechanism and mixture boiling, Proceedings of ASME-JSME Thermal Engineering Joint Conference, JSME, Honolulu, USA, 1983, pp. 191–197.

[230] L.-H. Chien, R.L. Webb, A parametric study of nucleate boiling on structured surfaces, Part I: effect of tunnel dimensions, J. Heat Transfer 120 (1998) 1042–1048.

[231] L.-H. Chien, R.L. Webb, A parametric study of nucleate boiling on structured surfaces, Part II: effect of pore diameter and pore pitch, J. Heat Transfer 120 (1998) 1049–1054.

[232] C. Ramaswamy, Y. Joshi, W. Nakayama, W.B. Johnson, High-speed visualization of boiling from an enhanced structure, Int. J. Heat Mass Transfer 45 (2002) 4761–4771.

[233] C. Ramaswamy, Y. Joshi, W. Nakayama, W.B. Johnson, Semi-analytical model for boiling from enhanced structures, Int. J. Heat Mass Transfer 46 (2003) 4257–4269.

[234] C.-D. Ghiu, Y.K. Joshi, Boiling performance of single-layered enhanced structures, J. Heat Transfer 127 (2005) 675–683.

[235] C.-D. Ghiu, Y.K. Joshi, Visualization study of pool boiling from thin confined enhanced structures, Int. J. Heat Mass Transfer 48 (2005) 4287–4299.

[236] C. Ramaswamy, Y. Joshi, W. Nakayama, W.B. Johnson, Effects of varying geometrical parameters on boiling from microfabricated enhanced structures, J. Heat Transfer 125 (2003) 103–109.

[237] T. Wang, Y.-Y. Jiang, H.-C. Jiang, C. Guo, C.-H. Guo, D.-W. Tang, L.-J. Rong, Surface with recoverable mini structures made of shape-memory alloys for adaptive-control of boiling heat transfer, Appl. Phys. Lett. 107 (2015) 023904.

[238] W. Hao, T. Wang, Y.-Y. Jiang, C. Guo, C.-H. Guo, Pool boiling heat transfer on deformable structures made of shape-memory-alloys, Int. J. Heat Mass Transfer 112 (2017) 236–247.

[239] N.K. Phadke, S.H. Bhavnani, A. Goyal, R.C. Jaeger, J.S. Goodling, Re-entrant cavity surface enhancements for immersion cooling of silicon multichip packages, IEEE Trans. Compon. Hybrid Manuf. Technol. 15 (1992) 815–822.

[240] N.D. Nimkar, S.H. Bhavnani, R.C. Jaeger, Effect of nucleation site spacing on the pool boiling characteristics of a structured surface, Int. J. Heat Mass Transfer 49 (2006) 2829–2839.

[241] L. Zhang, M. Shoji, Nucleation site interaction in pool boiling on the artificial surface, Int. J. Heat Mass Transfer 46 (2003) 513–522.

[242] A. Calka, R.L. Judd, Some aspects of the interaction among nucleation sites during saturated nucleate boiling, Int. J. Heat Mass Transfer 28 (1985) 2331–2342.

[243] S. Chatpun, M. Watanabe, M. Shoji, Experimental study on characteristics of nucleate pool boiling by the effects of cavity arrangement, Exp. Therm. Fluid Sci. 29 (2004) 33–40.

[244] A.S. Moita, E. Teodori, A.L.N. Moreira, Influence of surface topography in the boiling mechanisms, Int. J. Heat Fluid Flow 52 (2015) 50–63.
[245] E. Teodori, A.S. Moita, A.L.N. Moreira, Characterization of pool boiling mechanisms over micro-patterned surfaces using PIV, Int. J. Heat Mass Transfer 66 (2013) 261–270.
[246] C.K. Yu, D.C. Lu, T.C. Cheng, Pool boiling heat transfer on artificial micro-cavity surfaces in dielectric fluid FC-72, J. Micromech. Microeng. 16 (2006) 2092–2099.
[247] A.D. Messina, E.L. Park, Effects of precise arrays of pits on nucleate boiling, Int. J. Heat Mass Transfer 24 (1981) 141–145.
[248] A.K. Das, P.K. Das, P. Saha, Nucleate boiling of water from plain and structured surfaces, Exp. Therm. Fluid Sci. 31 (2007) 967–977.
[249] C. Hutter, D.B.R. Kenning, K. Sefiane, T.G. Karayiannis, H. Lin, G. Cummins, A.J. Walton, Experimental pool boiling investigations of FC-72 on silicon with artificial cavities and integrated temperature microsensors, Exp. Therm. Fluid Sci. 34 (2010) 422–433.
[250] Y. Fukada, I. Haze, M. Osakabe, The effect of fouling on nucleate pool boiling of small wires, Heat Transfer Asian Res. 33 (2004) 316–329.
[251] S. Li, R. Furberg, M.S. Toprak, B. Palm, M. Muhammed, Nature-inspired boiling enhancement by novel nanostructured macroporous surfaces, Adv. Funct. Mater. 18 (2008) 2215–2220.
[252] R. Furberg, B. Palm, Boiling heat transfer on a dendritic and micro-porous surface in R134a and FC-72, Appl. Therm. Eng. 31 (2011) 3595–3603.
[253] C.M. Patil, K.S.V. Santhanam, S.G. Kandlikar, Development of a two-step electrodeposition process for enhancing pool boiling, Int. J. Heat Mass Transfer 79 (2014) 989–1001.
[254] A.M. Gheitaghy, H. Saffari, D. Ghasimi, A. Ghasemi, Effect of electrolyte temperature on porous electrodeposited copper for pool boiling enhancement, Appl. Therm. Eng. 113 (2017) 1097–1106.
[255] P. Xu, Q. Li, Y. Xuan, Enhanced boiling heat transfer on composite porous surface, Int. J. Heat Mass Transfer 80 (2015) 107–114.
[256] M.S. El-Genk, A.F. Ali, Subcooled boiling of PF-5060 dielectric liquid on microporous surfaces, J. Heat Transfer 133 (2011) 081503.
[257] M.S. El-Genk, A.F. Ali, Enhancement of saturation boiling of PF-5060 on microporous copper dendrite surfaces, J. Heat Transfer 132 (2010) 071501.
[258] A.F. Ali, M.S. El-Genk, Effect of inclination on saturation boiling of PF-5060 dielectric liquid on 80-and 137-μm thick copper micro-porous surfaces, Int. J. Therm. Sci. 53 (2012) 42–48.
[259] M.S. El-Genk, Nucleate boiling enhancements on porous graphite and microporous and macro–finned copper surfaces, Heat Transfer Eng. 33 (2012) 175–204.
[260] M.S. El-Genk, A.F. Ali, Enhanced nucleate boiling on copper micro-porous surfaces, Int. J. Multiphase Flow 36 (2010) 780–792.
[261] N. Wright, B. Gebhart, Enhanced boiling on microconfigured surfaces, J. Electron. Packag. 111 (1989) 112–120.
[262] B. Gebhart, N. Wright, Boiling enhancement on microconfigured-surfaces, Int. Commun. Heat Mass Transfer 15 (1988) 141–149.
[263] W.J. Miller, B. Gebhart, N.T. Wright, Effects of boiling history on a microconfigured surface in a dielectric liquid, Int. Commun. Heat Mass Transfer 17 (1990) 389–398.
[264] M.S. El-Genk, A. Suszko, Effects of inclination angle and liquid subcooling on nucleate boiling on dimpled copper surfaces, Int. J. Heat Mass Transfer 95 (2016) 650–661.
[265] R. Holguin, K. Kota, S. Wootton, R.-H. Chen, S. Ross, Enhanced boiling heat transfer on binary surfaces, Int. J. Heat Mass Transfer 114 (2017) 1105–1113.
[266] M.S. El-Genk, J.L. Parker, Enhanced boiling of HFE-7100 dielectric liquid on porous graphite, Energy Convers. Manage. 46 (2005) 2455–2481.
[267] J.L. Parker, M.S. El-Genk, Enhanced saturation and subcooled boiling of FC-72 dielectric liquid, Int. J. Heat Mass Transfer 48 (2005) 3736–3752.
[268] J.L. Parker, M.S. El-Genk, Effect of surface orientation on nucleate boiling of FC-72 on porous graphite, J. Heat Transfer 128 (2006) 1159–1175.
[269] M.S. El-Genk, J.L. Parker, Nucleate boiling of FC-72 and HFE-7100 on porous graphite at different orientations and liquid subcooling, Energy Convers. Manage. 49 (2008) 733–750.
[270] H. Seo, J.H. Chu, S.-Y. Kwon, I.C. Bang, Pool boiling CHF of reduced graphene oxide, graphene, and SiC-coated surfaces under highly wettable FC-72, Int. J. Heat Mass Transfer 82 (2015) 490–502.
[271] A. Jaikumar, S.G. Kandlikar, A. Gupta, Pool boiling enhancement through graphene and graphene oxide coatings, Heat Transfer Eng. 38 (2017) 1274–1284.
[272] A. Jaikumar, A. Gupta, S.G. Kandlikar, C.-Y. Yang, C.-Y. Su, Scale effects of graphene and graphene oxide coatings on pool boiling enhancement mechanisms, Int. J. Heat Mass Transfer 109 (2017) 357–366.
[273] S. Ujereh, T. Fisher, I. Mudawar, Effects of carbon nanotube arrays on nucleate pool boiling, Int. J. Heat Mass Transfer 50 (2007) 4023–4038.
[274] M. Dharmendra, S. Suresh, C.S.S. Kumar, Q. Yang, Pool boiling heat transfer enhancement using vertically aligned carbon nanotube coatings on a copper substrate, Appl. Therm. Eng. 99 (2016) 61–71.
[275] H.S. Ahn, N. Sinha, M. Zhang, D. Banerjee, S. Fang, R.H. Baughman, Pool boiling experiments on multiwalled carbon nanotube (MWCNT) forests, J. Heat Transfer 128 (2006) 1335–1342.
[276] H.S. Ahn, V. Sathyamurthi, D. Banerjee, Pool boiling experiments on a nano-structured surface, IEEE Trans. Compon. Packag. Technol. 32 (2009) 156–165.
[277] V. Sathyamurthi, H.S. Ahn, D. Banerjee, S.C. Lau, Subcooled pool boiling experiments on horizontal heaters coated with carbon nanotubes, J. Heat Transfer 131 (2009) 071501.
[278] R. Bertossi, N. Caney, J.A. Gruss, J. Dijon, A. Fournier, P. Marty, Influence of carbon nanotubes on deionized water pool boiling performances, Exp. Therm. Fluid Sci. 61 (2015) 187–193.
[279] J.Y. Ho, K.C. Leong, C. Yang, Saturated pool boiling from carbon nanotube coated surfaces at different orientations, Int. J. Heat Mass Transfer 79 (2014) 893–904.
[280] G.H. Seo, H. Hwang, J. Yoon, T. Yeo, H.H. Son, U. Jeong, G. Jeun, W. Choi, S.J. Kim, Enhanced critical heat flux with single-walled carbon nanotubes bonded on metal surfaces, Exp. Therm. Fluid Sci. 60 (2015) 138–147.
[281] G.H. Seo, U. Jeong, H.H. Son, D. Shin, S.J. Kim, Effects of layer-by-layer assembled PEI/MWCNT surfaces on enhanced pool boiling critical heat flux, Int. J. Heat Mass Transfer 109 (2017) 564–576.
[282] S. Lee, G.H. Seo, S. Lee, U. Jeong, S.J. Lee, S.J. Kim, W. Choi, Layer-by-layer carbon nanotube coatings for enhanced pool boiling heat transfer on metal surfaces, Carbon 107 (2016) 607–618.
[283] B.J. Zhang, R. Ganguly, K.J. Kim, C.Y. Lee, Control of pool boiling heat transfer through photo-induced wettability change of titania nanotube arrayed surface, Int. Commun. Heat Mass Transfer 81 (2017) 124–130.
[284] Y. Chen, D. Mo, H. Zhao, N. Ding, S. Lu, Pool boiling on the superhydrophilic surface with TiO2 nanotube arrays, Sci. China Ser. E Technol. Sci. 52 (2009) 1596–1600.
[285] R. Chen, M.-C. Lu, V. Srinivasan, Z. Wang, H.H. Cho, A. Majumdar, Nanowires for enhanced boiling heat transfer, Nano Lett. 9 (2009) 548–553.
[286] R.P. Sahu, S. Sinha-Ray, S. Sinha-Ray, A.L. Yarin, Pool boiling on nano-textured surfaces comprised of electrically-assisted supersonically solution-blown, copper-plated nanofibers: experiments and theory, Int. J. Heat Mass Transfer 87 (2015) 521–535.
[287] M.-C. Lu, R. Chen, V. Srinivasan, V.P. Carey, A. Majumdar, Critical heat flux of pool boiling on Si nanowire array-coated surfaces, Int. J. Heat Mass Transfer 54 (2011) 5359–5367.
[288] B.S. Kim, S. Shin, D. Lee, G. Choi, H. Lee, K.M. Kim, H.H. Cho, Stable and uniform heat dissipation by nucleate-catalytic nanowires for boiling heat transfer, Int. J. Heat Mass Transfer 70 (2014) 23–32.
[289] B.S. Kim, H. Lee, S. Shin, G. Choi, H.H. Cho, Interfacial wicking dynamics and its impact on critical heat flux of boiling heat transfer, Appl. Phys. Lett. 105 (2014) 191601.
[290] D.I. Shim, G. Choi, N. Lee, T. Kim, B.S. Kim, H.H. Cho, Enhancement of pool boiling heat transfer using aligned silicon nanowires array, ACS Appl. Mater. Interfaces 9 (2017) 17595–17602.
[291] E. Demir, T. Izci, A.S. Alagoz, T. Karabacak, A. Koşar, Effect of silicon nanorod length on horizontal nanostructured plates in pool boiling heat transfer with water, Int. J. Therm. Sci. 82 (2014) 111–121.
[292] H.S. Jo, M.-W. Kim, K. Kim, S. An, Y.I. Kim, S.C. James, J. Choi, S.S. Yoon, Effects of capillarity on pool boiling using nano-textured surfaces through electrosprayed BiVO4 nano-pillars, Chem. Eng. Sci. 171 (2017) 360–367.
[293] Z. Yao, Y.-W. Lu, S.G. Kandlikar, Effects of nanowire height on pool boiling performance of water on silicon chips, Int. J. Therm. Sci. 50 (2011) 2084–2090.
[294] Z. Yao, Y.-W. Lu, S.G. Kandlikar, Direct growth of copper nanowires on a substrate for boiling applications, Micro Nano Lett. 6 (2011) 563–566.
[295] B. Shi, Y.-B. Wang, K. Chen, Pool boiling heat transfer enhancement with copper nanowire arrays, Appl. Therm. Eng. 75 (2015) 115–121.
[296] Y. Im, Y. Joshi, C. Dietz, S.S. Lee, Enhanced boiling of a dielectric liquid on copper nanowire surfaces, Int. J. Micro-Nano Scale Transp. 1 (2010) 79–95.
[297] U. Kumar, S. Suresh, M.R. Thansekhar, D. Babu, Effect of diameter of metal nanowires on pool boiling heat transfer with FC-72, Appl. Surf. Sci. 423 (2017) 509–520.
[298] C. Li, Z. Wang, P. Wang, Y. Peles, N. Koratkar, G.P. Peterson, Nanostructured copper interfaces for enhanced boiling, Small 4 (2008) 1084–1088.
[299] R. Wen, Q. Li, W. Wang, B. Latour, C.H. Li, C. Li, Y.-C. Lee, R. Yang, Enhanced bubble nucleation and liquid rewetting for highly efficient boiling heat transfer on two-level hierarchical surfaces with patterned copper nanowire arrays, Nano Energy 38 (2017) 59–65.
[300] S. Shin, B. Seok Kim, G. Choi, H. Lee, H. Hee Cho, Double-templated electrodeposition: Simple fabrication of micro-nano hybrid structure by electrodeposition for efficient boiling heat transfer, Appl. Phys. Lett. 101 (2012) 251909.
[301] M. Ray, S. Deb, S. Bhaumik, Pool boiling heat transfer of refrigerant R-134a on TiO2 nano wire arrays surface, Appl. Therm. Eng. 107 (2016) 1294–1303.
[302] D. Lee, T. Kim, S. Park, S.S. Lee, S.H. Ko, Zinc oxide nanowire forest for pool boiling heat transfer, Jpn. J. Appl. Phys. 51 (2012) 11PE11.
[303] S. Jun, S. Sinha-Ray, A.L. Yarin, Pool boiling on nano-textured surfaces, Int. J. Heat Mass Transfer 62 (2013) 99–111.
[304] R.P. Sahu, S. Sinha-Ray, S. Sinha-Ray, A.L. Yarin, Pool boiling of Novec 7300 and self-rewetting fluids on electrically-assisted supersonically solution-blown, copper-plated nanofibers, Int. J. Heat Mass Transfer 95 (2016) 83–93.
[305] S. Sinha-Ray, W. Zhang, R.P. Sahu, S. Sinha-Ray, A.L. Yarin, Pool boiling of Novec 7300 and DI water on nano-textured heater covered with supersonically-blown or electrospun polymer nanofibers, Int. J. Heat Mass Transfer 106 (2017) 482–490.
[306] B.J. Zhang, K.J. Kim, Effect of liquid uptake on critical heat flux utilizing a three dimensional, interconnected alumina nano porous surfaces, Appl. Phys. Lett. 101 (2012) 054104.
[307] B.J. Zhang, J. Park, K.J. Kim, Augmented boiling heat transfer on the wetting-modified three dimensionally-interconnected alumina nano porous surfaces

in aqueous polymeric surfactants, Int. J. Heat Mass Transfer 63 (2013) 224–232.
[308] B.J. Zhang, K.J. Kim, H. Yoon, Enhanced heat transfer performance of alumina sponge-like nano-porous structures through surface wettability control in nucleate pool boiling, Int. J. Heat Mass Transfer 55 (2012) 7487–7498.
[309] B.J. Zhang, K.J. Kim, Nucleate pool boiling heat transfer augmentation on hydrophobic self-assembly mono-layered alumina nano-porous surfaces, Int. J. Heat Mass Transfer 73 (2014) 551–561.
[310] C.Y. Lee, B.J. Zhang, K.J. Kim, Morphological change of plain and nano-porous surfaces during boiling and its effect on nucleate pool boiling heat transfer, Exp. Therm. Fluid Sci. 40 (2012) 150–158.
[311] H. Hu, C. Xu, Y. Zhao, K.J. Ziegler, J.N. Chung, Boiling and quenching heat transfer advancement by nanoscale surface modification, Sci. Rep. 7 (2017) 6117.
[312] M. Arya, S. Khandekar, D. Pratap, S.A. Ramakrishna, Pool boiling of water on nano-structured micro wires at sub-atmospheric conditions, Heat Mass Transfer 52 (2016) 1725–1737.
[313] A. Nazari, S. Saedodin, Porous anodic alumina coating for optimisation of pool-boiling performance, Surf. Eng. 33 (2017) 753–759.
[314] S. Vemuri, K.J. Kim, Pool boiling of saturated FC-72 on nano-porous surface, Int. Commun. Heat Mass Transfer 32 (2005) 27–31.
[315] M.M. Rahman, E. Ölçeroğlu, M. McCarthy, Scalable nanomanufacturing of virus-templated coatings for enhanced boiling, Adv. Mater. Interfaces 1 (2014) 1300107.
[316] Y. Tang, B. Tang, J. Qing, Q. Li, L. Lu, Nanoporous metallic surface: facile fabrication and enhancement of boiling heat transfer, Appl. Surf. Sci. 258 (2012) 8747–8751.
[317] Y. Tang, B. Tang, Q. Li, J. Qing, L. Lu, K. Chen, Pool-boiling enhancement by novel metallic nanoporous surface, Exp. Therm. Fluid Sci. 44 (2013) 194–198.
[318] L. Lu, T. Fu, Y. Tang, T. Tang, B. Tang, Z. Wan, A novel in-situ nanostructure forming route and its application in pool-boiling enhancement, Exp. Therm. Fluid Sci. 72 (2016) 140–148.
[319] B. Tang, R. Zhou, L. Lu, G. Zhou, Augmented boiling heat transfer on a copper nanoporous surface and the stability of nano-porosity in a hydrothermal environment, Int. J. Heat Mass Transfer 90 (2015) 979–985.
[320] J. Gao, L.-S. Lu, J.-W. Sun, X.-K. Liu, B. Tang, Enhanced boiling performance of a nanoporous copper surface by electrodeposition and heat treatment, Heat Mass Transfer 53 (2017) 947–958.
[321] T.J. Hendricks, S. Krishnan, C. Choi, C.-H. Chang, B. Paul, Enhancement of pool-boiling heat transfer using nanostructured surfaces on aluminum and copper, Int. J. Heat Mass Transfer 53 (2010) 3357–3365.
[322] H.S. Jo, S. An, H.G. Park, M.-W. Kim, S.S. Al-Deyab, S.C. James, J. Choi, S.S. Yoon, Enhancement of critical heat flux and superheat through controlled wettability of cuprous-oxide fractal-like nanotextured surfaces in pool boiling, Int. J. Heat Mass Transfer 107 (2017) 105–111.
[323] S. Kalaiselvam, M.S. Gugan, E. Kuraloviyan, R. Meganathan, A.N. Priyan, M.R. Swaminathan, Experimental investigation of anodized/spray pyrolysed nanoporous structure on heat transfer augmentation, J. Therm. Sci. 18 (2009) 358–363.
[324] E.J.T. Pialago, O.K. Kwon, C.W. Park, Nucleate boiling heat transfer of R134a on cold sprayed CNT–Cu composite coatings, Appl. Therm. Eng. 56 (2013) 112–119.
[325] E.J.T. Pialago, O.K. Kwon, J.S. Jin, C.W. Park, Nucleate pool boiling of R134a on cold sprayed Cu–CNT–SiC and Cu–CNT–AlN composite coatings, Appl. Therm. Eng. 103 (2016) 684–694.
[326] X. Zheng, C.W. Park, Experimental study of the sintered multi-walled carbon nanotube/copper microstructures for boiling heat transfer, Appl. Therm. Eng. 86 (2015) 14–26.
[327] S.-S. Park, Y.H. Kim, Y.H. Jeon, M.T. Hyun, N.-J. Kim, Effects of spray-deposited oxidized multi-wall carbon nanotubes and graphene on pool-boiling critical heat flux enhancement, J. Ind. Eng. Chem. 24 (2015) 276–283.
[328] A.K. Sadaghiani, A.R. Motezakker, A.V. Özpınar, G.Ö. İnce, A. Koşar, Pool boiling heat transfer characteristics of inclined pHEMA-coated surfaces, J. Heat Transfer 139 (2017) 111501.
[329] P.R. Jones, A.R. Elliott, N.A. Patankar, Sustaining superheated liquid within hydrophilic surface texture, Langmuir 32 (2016) 12947–12953.
[330] C.Y. Lee, M.M.H. Bhuiya, K.J. Kim, Pool boiling heat transfer with nano-porous surface, Int. J. Heat Mass Transfer 53 (2010) 4274–4279.
[331] E. Forrest, E. Williamson, J. Buongiorno, L.-W. Hu, M. Rubner, R. Cohen, Augmentation of nucleate boiling heat transfer and critical heat flux using nanoparticle thin-film coatings, Int. J. Heat Mass Transfer 53 (2010) 58–67.
[332] S. An, D.-Y. Kim, J.-G. Lee, H.S. Jo, M.-W. Kim, S.S. Al-Deyab, J. Choi, S.S. Yoon, Supersonically sprayed reduced graphene oxide film to enhance critical heat flux in pool boiling, Int. J. Heat Mass Transfer 98 (2016) 124–130.
[333] B. Feng, K. Weaver, G.P. Peterson, Enhancement of critical heat flux in pool boiling using atomic layer deposition of alumina, Appl. Phys. Lett. 100 (2012) 053120.
[334] H. Seo, H.D. Yun, S.-Y. Kwon, I.C. Bang, Hybrid graphene and single-walled carbon nanotube films for enhanced phase-change heat transfer, Nano Lett. 16 (2016) 932–938.
[335] H. Yeom, K. Sridharan, L.M. Corradini, Bubble dynamics in pool boiling on nanoparticle-coated surfaces, Heat Transfer Eng. 36 (2015) 1013–1027.
[336] G. Stange, H. Yeom, B. Semerau, K. Sridharan, M. Corradini, A study of nanoparticle surface modification effects on pool boiling critical heat flux, Nucl. Technol. 182 (2013) 286–301.
[337] H.H. Son, G.H. Seo, U. Jeong, S.J. Kim, Capillary wicking effect of a Cr-sputtered superhydrophilic surface on enhancement of pool boiling critical heat flux, Int. J. Heat Mass Transfer 113 (2017) 115–128.
[338] D.H. Kam, J.H. Lee, T. Lee, Y.H. Jeong, Critical heat flux for SiC-and Cr-coated plates under atmospheric condition, Ann. Nucl. Energy 76 (2015) 335–342.
[339] G.H. Seo, G. Jeun, S.J. Kim, Enhanced pool boiling critical heat flux with a FeCrAl layer fabricated by DC sputtering, Int. J. Heat Mass Transfer 102 (2016) 1293–1307.
[340] S. Das, D.S. Kumar, S. Bhaumik, Experimental study of nucleate pool boiling heat transfer of water on silicon oxide nanoparticle coated copper heating surface, Appl. Therm. Eng. 96 (2016) 555–567.
[341] S. Das, B. Saha, S. Bhaumik, Experimental study of nucleate pool boiling heat transfer of water by surface functionalization with SiO2 nanostructure, Exp. Therm. Fluid Sci. 81 (2017) 454–465.
[342] S. Das, S.D. Kumar, S. Bhowmik, Enhancement of nucleate pool boiling heat transfer on silicon oxide thin film surface, Procedia Eng. 90 (2014) 530–537.
[343] S. Das, B. Saha, S. Bhaumik, Experimental study of nucleate pool boiling heat transfer of water by surface functionalization with crystalline TiO2 nanostructure, Appl. Therm. Eng. 113 (2017) 1345–1357.
[344] A. Zou, S.C. Maroo, Critical height of micro/nano structures for pool boiling heat transfer enhancement, Appl. Phys. Lett. 103 (2013) 221602.
[345] A. Zou, D.P. Singh, S.C. Maroo, Early evaporation of microlayer for boiling heat transfer enhancement, Langmuir 32 (2016) 10808–10814.
[346] S.C. Maroo, J.N. Chung, A possible role of nanostructured ridges on boiling heat transfer enhancement, J. Heat Transfer 135 (2013) 041501.
[347] Y.-Y. Li, Z.-H. Liu, B.-C. Zheng, Experimental study on the saturated pool boiling heat transfer on nano-scale modification surface, Int. J. Heat Mass Transfer 84 (2015) 550–561.
[348] H.S. Ahn, C. Lee, H. Kim, H. Jo, S. Kang, J. Kim, J. Shin, M.H. Kim, Pool boiling CHF enhancement by micro/nanoscale modification of zircaloy-4 surface, Nucl. Eng. Des. 240 (2010) 3350–3360.
[349] H.S. Ahn, H.J. Jo, S.H. Kang, M.H. Kim, Effect of liquid spreading due to nano/microstructures on the critical heat flux during pool boiling, Appl. Phys. Lett. 98 (2011) 071908.
[350] H.S. Ahn, C. Lee, J. Kim, M.H. Kim, The effect of capillary wicking action of micro/nano structures on pool boiling critical heat flux, Int. J. Heat Mass Transfer 55 (2012) 89–92.
[351] H.S. Ahn, G. Park, J.M. Kim, J. Kim, M.H. Kim, The effect of water absorption on critical heat flux enhancement during pool boiling, Exp. Therm. Fluid Sci. 42 (2012) 187–195.
[352] D. Saeidi, A.A. Alemrajabi, Experimental investigation of pool boiling heat transfer and critical heat flux of nanostructured surfaces, Int. J. Heat Mass Transfer 60 (2013) 440–449.
[353] D. Saeidi, A.A. Alemrajabi, N. Saeidi, Experimental study of pool boiling characteristic of an aluminized copper surface, Int. J. Heat Mass Transfer 85 (2015) 239–246.
[354] S.D. Park, S.B. Moon, I.C. Bang, Effects of thickness of boiling-induced nanoparticle deposition on the saturation of critical heat flux enhancement, Int. J. Heat Mass Transfer 78 (2014) 506–514.
[355] S.M. Kwark, G. Moreno, R. Kumar, H. Moon, S.M. You, Nanocoating characterization in pool boiling heat transfer of pure water, Int. J. Heat Mass Transfer 53 (2010) 4579–4587.
[356] M. Amaya, S.M. Kwark, A. Gurung, S.M. You, Pool boiling heat transfer of borated (H3BO3) water on a nanoporous surface, J. Heat Transfer 135 (2013) 091302.
[357] S.M. Kwark, M. Amaya, R. Kumar, G. Moreno, S.M. You, Effects of pressure, orientation, and heater size on pool boiling of water with nanocoated heaters, Int. J. Heat Mass Transfer 53 (2010) 5199–5208.
[358] C.-K. Huang, C.-W. Lee, C.-K. Wang, Boiling enhancement by TiO_2 nanoparticle deposition, Int. J. Heat Mass Transfer 54 (2011) 4895–4903.
[359] R.N. Hegde, S.S. Rao, R.P. Reddy, Investigations on boiling-induced nanoparticle coating, transient characteristics, and effect of pressure in pool boiling heat transfer on a cylindrical surface, Exp. Heat Transfer 25 (2012) 323–340.
[360] S. Kim, H.D. Kim, H. Kim, H.S. Ahn, H. Jo, J. Kim, M.H. Kim, Effects of nano-fluid and surfaces with nano structure on the increase of CHF, Exp. Therm. Fluid Sci. 34 (2010) 487–495.
[361] I.S. Kiyomura, L.L. Manetti, A.P. da Cunha, G. Ribatski, E.M. Cardoso, An analysis of the effects of nanoparticles deposition on characteristics of the heating surface and ON pool boiling of water, Int. J. Heat Mass Transfer 106 (2017) 666–674.
[362] R.R. Souza, J.C. Passos, E.M. Cardoso, Influence of nanoparticle size and gap size on nucleate boiling using HFE7100, Exp. Therm. Fluid Sci. 59 (2014) 195–201.
[363] L.V. Heitich, J.C. Passos, E.M. Cardoso, M.F. da Silva, A.N. Klein, Nucleate boiling of water using nanostructured surfaces, J. Braz. Soc. Mech. Sci. Eng. 36 (2014) 181–192.
[364] B. Stutz, C.H.S. Morceli, M.D.F. Da Silva, S. Cioulachtjian, J. Bonjour, Influence of nanoparticle surface coating on pool boiling, Exp. Therm. Fluid Sci. 35 (2011) 1239–1249.
[365] H. Sakashita, CHF and near-wall boiling behaviors in pool boiling of water on a heating surface coated with nanoparticles, Int. J. Heat Mass Transfer 55 (2012) 7312–7320.
[366] K.N. Rainey, S.M. You, S. Lee, Effect of pressure, subcooling, and dissolved gas on pool boiling heat transfer from microporous, square pin-finned surfaces in FC-72, Int. J. Heat Mass Transfer 46 (2003) 23–35.

[367] J.Y. Chang, S.M. You, Enhanced boiling heat transfer from micro-porous cylindrical surfaces in saturated FC-87 and R-123, J. Heat Transfer 119 (1997) 319–325.
[368] R. Pastuszko, T.M. Wójcik, Experimental investigations and a simplified model for pool boiling on micro-fins with sintered perforated foil, Exp. Therm. Fluid Sci. 63 (2015) 34–44.
[369] R. Pastuszko, Boiling heat transfer enhancement in subsurface horizontal and vertical tunnels, Exp. Therm. Fluid Sci. 32 (2008) 1564–1577.
[370] R. Pastuszko, Pool boiling for extended surfaces with narrow tunnels–visualization and a simplified model, Exp. Therm. Fluid Sci. 38 (2012) 149–164.
[371] R. Pastuszko, M.E. Poniewski, Semi-analytical approach to boiling heat fluxes calculation in subsurface horizontal and vertical tunnels, Int. J. Therm. Sci. 47 (2008) 1169–1183.
[372] R. Pastuszko, Pool boiling on micro-fin array with wire mesh structures, Int. J. Therm. Sci. 49 (2010) 2289–2298.
[373] T. Halon, B. Zajaczkowski, S. Michaie, R. Rulliere, J. Bonjour, Experimental study of low pressure pool boiling of water from narrow tunnel surfaces, Int. J. Therm. Sci. 121 (2017) 348–357.
[374] R.P. Rioux, E.C. Nolan, C.H. Li, A systematic study of pool boiling heat transfer on structured porous surfaces: from nanoscale through microscale to macroscale, AIP Adv. 4 (2014) 117133.
[375] C.H. Li, R.P. Rioux, Independent and collective roles of surface structures at different length scales on pool boiling heat transfer, Sci. Rep. 6 (2016) 37044.
[376] D. Deng, J. Feng, Q. Huang, Y. Tang, Y. Lian, Pool boiling heat transfer of porous structures with reentrant cavities, Int. J. Heat Mass Transfer 99 (2016) 556–568.
[377] M. Misale, G. Guglielmini, M. Frogheri, A.E. Bergles, FC-72 pool boiling from finned surfaces placed in a narrow channel: preliminary results, Heat Mass Transfer 34 (1999) 449–452.
[378] D. Deng, W. Wan, J. Feng, Q. Huang, Y. Qin, Y. Xie, Comparative experimental study on pool boiling performance of porous coating and solid structures with reentrant channels, Appl. Therm. Eng. 107 (2016) 420–430.
[379] A.K. Stubos, J.-M. Buchlin, Enhanced cooling via boiling in porous layers: the effect of vapor channels, J. Heat Transfer 121 (1999) 205–210.
[380] W. Wu, J.-H. Du, X.-J. Hu, B.-X. Wang, Pool boiling heat transfer and simplified one-dimensional model for prediction on coated porous surfaces with vapor channels, Int. J. Heat Mass Transfer 45 (2002) 1117–1125.
[381] Y. Tang, J. Zeng, S. Zhang, C. Chen, J. Chen, Effect of structural parameters on pool boiling heat transfer for porous interconnected microchannel nets, Int. J. Heat Mass Transfer 93 (2016) 906–917.
[382] S. Zhang, Y. Tang, J. Zeng, W. Yuan, J. Chen, C. Chen, Pool boiling heat transfer enhancement by porous interconnected microchannel nets at different liquid subcooling, Appl. Therm. Eng. 93 (2016) 1135–1144.
[383] Y. Sun, G. Chen, S. Zhang, Y. Tang, J. Zeng, W. Yuan, Pool boiling performance and bubble dynamics on microgrooved surfaces with reentrant cavities, Appl. Therm. Eng. 125 (2017) 432–442.
[384] L. Dong, X. Quan, P. Cheng, An experimental investigation of enhanced pool boiling heat transfer from surfaces with micro/nano-structures, Int. J. Heat Mass Transfer 71 (2014) 189–196.
[385] K.-H. Chu, Y. Soo Joung, R. Enright, C.R. Buie, E.N. Wang, Hierarchically structured surfaces for boiling critical heat flux enhancement, Appl. Phys. Lett. 102 (2013) 151602.
[386] Y.-Q. Wang, S.-S. Lyu, J.-L. Luo, Z.-Y. Luo, Y.-X. Fu, Y. Heng, J.-H. Zhang, D.-C. Mo, Copper vertical micro dendrite fin arrays and their superior boiling heat transfer capability, Appl. Surf. Sci. 422 (2017) 388–393.
[387] H.S. Jo, J.-G. Lee, S. An, T.G. Kim, S.C. James, J. Choi, S.S. Yoon, Supersonically sprayed, triangular copper lines for pool boiling enhancement, Int. J. Heat Mass Transfer 113 (2017) 210–216.
[388] M.M. Rahman, E. Olceroglu, M. McCarthy, Role of wickability on the critical heat flux of structured superhydrophilic surfaces, Langmuir 30 (2014) 11225–11234.
[389] M.M. Rahman, M. McCarthy, Effect of length scales on the boiling enhancement of structured copper surfaces, J. Heat Transfer 139 (2017) 111508.
[390] M.M. Rahman, M. McCarthy, Boiling enhancement on nanostructured surfaces with engineered variations in wettability and thermal conductivity, Heat Transfer Eng. 38 (2017) 1285–1295.
[391] J.P. McHale, S.V. Garimella, T.S. Fisher, G.A. Powell, Pool boiling performance comparison of smooth and sintered copper surfaces with and without carbon nanotubes, Nanoscale Microscale Thermophys. Eng. 15 (2011) 133–150.
[392] N.S. Dhillon, J. Buongiorno, K.K. Varanasi, Critical heat flux maxima during boiling crisis on textured surfaces, Nat. Commun. 6 (2015) 8247.
[393] H.W. Moon, Y.J. Yoon, J.H. Park, B.-S. Myung, D.E. Kim, Dynamic wetting and boiling characteristics on micro-structured and micro/nano hierarchically structured surfaces, Exp. Therm. Fluid Sci. 74 (2016) 19–26.
[394] S. Mori, S.M. Aznam, K. Okuyama, Enhancement of the critical heat flux in saturated pool boiling of water by nanoparticle-coating and a honeycomb porous plate, Int. J. Heat Mass Transfer 80 (2015) 1–6.
[395] S.M. Aznam, S. Mori, A. Ogoshi, K. Okuyama, CHF enhancement of a large heated surface by a honeycomb porous plate and a gridded metal structure in a saturated pool boiling of nanofluid, Int. J. Heat Mass Transfer 115 (2017) 969–980.
[396] Z. Yao, Y.-W. Lu, S.G. Kandlikar, Fabrication of nanowires on orthogonal surfaces of microchannels and their effect on pool boiling, J. Micromech. Microeng. 22 (2012) 115005.
[397] Z. Yao, Y.-W. Lu, S.G. Kandlikar, Pool boiling heat transfer enhancement through nanostructures on silicon microchannels, J. Nanotechnol. Eng. Med. 3 (2012) 031002.
[398] Y. Im, C. Dietz, S.S. Lee, Y. Joshi, Flower-like CuO nanostructures for enhanced boiling, Nanoscale Microscale Thermophys. Eng. 16 (2012) 145–153.
[399] A. Sathyanarayana, P. Warrier, Y. Im, Y. Joshi, A.S. Teja, Pool boiling of HFE 7200–$C_4H_4F_6O$ mixture on hybrid micro-nanostructured surface, J. Nanotechnol. Eng. Med. 3 (2012) 041004.
[400] C.M. Patil, S.G. Kandlikar, Pool boiling enhancement through microporous coatings selectively electrodeposited on fin tops of open microchannels, Int. J. Heat Mass Transfer 79 (2014) 816–828.
[401] A. Jaikumar, S.G. Kandlikar, Enhanced pool boiling for electronics cooling using porous fin tops on open microchannels with FC-87, Appl. Therm. Eng. 91 (2015) 426–433.
[402] A. Jaikumar, S.G. Kandlikar, Enhanced pool boiling heat transfer mechanisms for selectively sintered open microchannels, Int. J. Heat Mass Transfer 88 (2015) 652–661.
[403] S.G. Kandlikar, Enhanced macroconvection mechanism with separate liquid–vapor pathways to Iimprove pool poiling performance, J. Heat Transfer 139 (2017) 051501.
[404] A.M. Gheitaghy, H. Saffari, M. Mohebbi, Investigation pool boiling heat transfer in U-shaped mesochannel with electrodeposited porous coating, Exp. Therm. Fluid Sci. 76 (2016) 87–97.
[405] E. Akbari, A.M. Gheitaghy, H. Saffari, S.M. Hosseinalipour, Effect of silver nanoparticle deposition in re-entrant inclined minichannel on bubble dynamics for pool boiling enhancement, Exp. Therm. Fluid Sci. 82 (2017) 390–401.
[406] L. Bai, L. Zhang, G. Lin, G.P. Peterson, Pool boiling with high heat flux enabled by a porous artery structure, Appl. Phys. Lett. 108 (2016) 233901.
[407] L. Bai, L. Zhang, J. Guo, G. Lin, X. Bu, D. Wen, Evaporation/boiling heat transfer characteristics in an artery porous structure, Appl. Therm. Eng. 104 (2016) 587–595.
[408] I.L. Pioro, W. Rohsenow, S.S. Doerffer, Nucleate pool-boiling heat transfer. I: review of parametric effects of boiling surface, Int. J. Heat Mass Transfer 47 (2004) 5033–5044.
[409] I.L. Pioro, W. Rohsenow, S.S. Doerffer, Nucleate pool-boiling heat transfer. II: assessment of prediction methods, Int. J. Heat Mass Transfer 47 (2004) 5045–5057.
[410] G. Liang, I. Mudawar, Pool boiling critical heat flux (CHF)–Part 2: Assessment of models and correlations, Int. J. Heat Mass Transfer 117 (2018) 1368–1383.
[411] B. Bourdon, P. Di Marco, R. Riobóo, M. Marengo, J. De Coninck, Enhancing the onset of pool boiling by wettability modification on nanometrically smooth surfaces, Int. Commun. Heat Mass Transfer 45 (2013) 11–15.
[412] B. Bourdon, R. Rioboo, M. Marengo, E. Gosselin, J. De Coninck, Influence of the wettability on the boiling onset, Langmuir 28 (2012) 1618–1624.
[413] B. Bourdon, E. Bertrand, P. Di Marco, M. Marengo, R. Rioboo, J. De Coninck, Wettability influence on the onset temperature of pool boiling: experimental evidence onto ultra-smooth surfaces, Adv. Colloid Interface Sci. 221 (2015) 34–40.
[414] H.J. Jo, H. Kim, H.S. Ahn, S. Kim, S.H. Kang, J. Kim, M.H. Kim, Experimental study of boiling phenomena by micro/milli hydrophobic dot on the silicon surface in pool boiling, Proceedings of the ASME 2009 7th International Conference on Nanochannels, Microchannels and Minichannels, ASME, Pohang, South Korea, 2009, pp. 93–97.
[415] H. Jo, S. Kim, H. Kim, J. Kim, M.H. Kim, Nucleate boiling performance on nano/microstructures with different wetting surfaces, Nanoscale Res. Lett. 7 (2012) 242.
[416] S. Kim, H. Kim, H.D. Kim, H.S. Ahn, M.H. Kim, J. Kim, G.-C. Park, Experimental investigation of critical heat flux enhancement by micro/nanoscale surface modification in pool boiling, Proceedings of the 6th International ASME Conference on Nanochannels, Microchannels and Minichannels, ASME, Darmstadt, Germany, 2008, pp. 669–675.
[417] H.T. Phan, N. Caney, P. Marty, S. Colasson, J. Gavillet, Surface wettability control by nanocoating: the effects on pool boiling heat transfer and nucleation mechanism, Int. J. Heat Mass Transfer 52 (2009) 5459–5471.
[418] H.T. Phan, N. Caney, P. Marty, S. Colasson, J. Gavillet, How does surface wettability influence nucleate boiling?, CR. Mec. 337 (2009) 251–259.
[419] R.-D. Sun, A. Nakajima, A. Fujishima, T. Watanabe, K. Hashimoto, Photoinduced surface wettability conversion of ZnO and TiO2 thin films, J. Phys. Chem. B 105 (2001) 1984–1990.
[420] Y. Takata, S. Hidaka, J.M. Cao, T. Nakamura, H. Yamamoto, M. Masuda, T. Ito, Effect of surface wettability on boiling and evaporation, Energy 30 (2005) 209–220.
[421] Y. Takata, S. Hidaka, M. Masuda, T. Ito, Pool boiling on a superhydrophilic surface, Int. J. Energy Res. 27 (2003) 111–119.
[422] S.P. Liaw, V.K. Dhir, Void fraction measurements during saturated pool boiling of water on partially wetted vertical surfaces, J. Heat Transfer 111 (1989) 731–738.
[423] Y.H. Maeng, S.L. Song, J.Y. Lee, Unaffectedness of improved wettability on critical heat flux enhancement with TiO2 sputtered surface, Appl. Phys. Lett. 108 (2016) 074101.
[424] Y. Wang, L.-L. Wang, M.-Y. Liu, Antifouling and enhancing pool boiling by TiO2 coating surface in nanometer scale thickness, AIChE J. 53 (2007) 3062–3076.
[425] S. Das, S. Bhaumik, Enhancement of nucleate pool boiling heat transfer on titanium oxide thin film surface, Arab. J. Sci. Eng. 39 (2014) 7385–7395.

[426] W. Wu, H. Bostanci, L.C. Chow, Y. Hong, M. Su, J.P. Kizito, Nucleate boiling heat transfer enhancement for water and FC-72 on titanium oxide and silicon oxide surfaces, Int. J. Heat Mass Transfer 53 (2010) 1773–1777.
[427] J.M. Kim, D.I. Yu, H.S. Park, K. Moriyama, M.H. Kim, Smart surface in pool boiling: thermally-induced wetting transition, Int. J. Heat Mass Transfer 109 (2017) 231–241.
[428] J.M. Kim, T. Kim, D.I. Yu, M.H. Kim, K. Moriyama, H.S. Park, Time effect on wetting transition of smart surface and prediction of the wetting transition for critical heat flux in pool boiling, Int. J. Heat Mass Transfer 114 (2017) 735–742.
[429] N.A. Patankar, Supernucleating surfaces for nucleate boiling and dropwise condensation heat transfer, Soft Matter 6 (2010) 1613–1620.
[430] H. Jo, H.S. Ahn, S. Kang, M.H. Kim, A study of nucleate boiling heat transfer on hydrophilic, hydrophobic and heterogeneous wetting surfaces, Int. J. Heat Mass Transfer 54 (2011) 5643–5652.
[431] H. Jo, M. Kaviany, S.H. Kim, M.H. Kim, Heterogeneous bubble nucleation on ideally-smooth horizontal heated surface, Int. J. Heat Mass Transfer 71 (2014) 149–157.
[432] H. Jo, S. Kim, H.S. Park, M.H. Kim, Critical heat flux and nucleate boiling on several heterogeneous wetting surfaces: controlled hydrophobic patterns on a hydrophilic substrate, Int. J. Multiphase Flow 62 (2014) 101–109.
[433] H. Jo, D.I. Yu, H. Noh, H.S. Park, M.H. Kim, Boiling on spatially controlled heterogeneous surfaces: wettability patterns on microstructures, Appl. Phys. Lett. 106 (2015) 181602.
[434] A.R. Betz, J. Xu, H. Qiu, D. Attinger, Do surfaces with mixed hydrophilic and hydrophobic areas enhance pool boiling?, Appl Phys. Lett. 97 (2010) 141909.
[435] A.R. Betz, J. Jenkins, D. Attinger, Boiling heat transfer on superhydrophilic, superhydrophobic, and superbiphilic surfaces, Int. J. Heat Mass Transfer 57 (2013) 733–741.
[436] C.-C. Hsu, M.-R. Lee, C.-H. Wu, P.-H. Chen, Effect of interlaced wettability on horizontal copper cylinders in nucleate pool boiling, Appl. Therm. Eng. 112 (2017) 1187–1194.
[437] C.C. Hsu, W.C. Chiu, L.S. Kuo, P.H. Chen, Reversed boiling curve phenomenon on surfaces with interlaced wettability, AIP Adv. 4 (2014) 107110.
[438] C.-C. Hsu, T.-W. Su, P.-H. Chen, Pool boiling of nanoparticle-modified surface with interlaced wettability, Nanoscale Res. Lett. 7 (2012) 259.
[439] S. Gong, P. Cheng, Numerical simulation of pool boiling heat transfer on smooth surfaces with mixed wettability by lattice Boltzmann method, Int. J. Heat Mass Transfer 80 (2015) 206–216.
[440] Z. Zhao, J. Zhang, D. Jia, K. Zhao, X. Zhang, P. Jiang, Thermal performance analysis of pool boiling on an enhanced surface modified by the combination of microstructures and wetting properties, Appl. Therm. Eng. 117 (2017) 417–426.
[441] C.-H. Choi, M. David, Z. Gao, A. Chang, M. Allen, H. Wang, C.-H. Chang, Large-scale generation of patterned bubble arrays on printed bi-functional boiling surfaces, Sci. Rep. 6 (2016) 23760.
[442] B.J. Suroto, M. Tashiro, S. Hirabayashi, S. Hidaka, M. Kohno, Y. Takata, Effects of hydrophobic-spot periphery and subcooling on nucleate pool boiling from a mixed-wettability surface, J. Therm. Sci. Technol. 8 (2013) 294–308.
[443] H. Noh, J.-O. Kim, D.-H. Kim, H.S. Park, Y.-H. Hwang, M.H. Kim, D.-P. Kim, Enhanced boiling heat transfer performance on microstructured silicate glass surfaces derived from inorganic polymer-based soft lithography, Adv. Mater. Interfaces 3 (2016) 1600507.
[444] M. Zupančič, M. Steinbücher, P. Gregorčič, I. Golobič, Enhanced pool-boiling heat transfer on laser-made hydrophobic/superhydrophilic polydimethylsiloxane-silica patterned surfaces, Appl. Therm. Eng. 91 (2015) 288–297.
[445] M. Zupančič, M. Može, P. Gregorčič, I. Golobič, Nanosecond laser texturing of uniformly and non-uniformly wettable micro structured metal surfaces for enhanced boiling heat transfer, Appl. Surf. Sci. 399 (2017) 480–490.
[446] X. Dai, X. Huang, F. Yang, X. Li, J. Sightler, Y. Yang, C. Li, Enhanced nucleate boiling on horizontal hydrophobic-hydrophilic carbon nanotube coatings, Appl. Phys. Lett. 102 (2013) 161605.
[447] J.S. Lee, J.S. Lee, Critical heat flux enhancement of pool boiling with adaptive fraction control of patterned wettability, Int. J. Heat Mass Transfer 96 (2016) 504–512.
[448] R. Bertossi, N. Caney, J.A. Gruss, O. Poncelet, Pool boiling enhancement using switchable polymers coating, Appl. Therm. Eng. 77 (2015) 121–126.
[449] S.-M. Kim, I. Mudawar, Universal approach to predicting two-phase frictional pressure drop for mini/micro-channel saturated flow boiling, Int. J. Heat Mass Transfer 58 (2013) 718–734.
[450] S.-M. Kim, I. Mudawar, Review of databases and predictive methods for pressure drop in adiabatic, condensing and boiling mini/micro-channel flows, Int. J. Heat Mass Transfer 77 (2014) 74–97.
[451] S.-M. Kim, I. Mudawar, Review of databases and predictive methods for heat transfer in condensing and boiling mini/micro-channel flows, Int. J. Heat Mass Transfer 77 (2014) 627–652.